Structure-function studies on *Vibrio parahaemolyticus* thermostable direct hemolysin

A thesis submitted by

Nidhi Kundu

in partial fulfillment of the requirements for the degree of

Doctor of Philosophy

Indian Institute of Science Education and Research (IISER)

Mohali

Knowledge city, Sector 81, Manauli PO,
Sahibzada Ajit Singh Nagar,
Punjab 140306

August 2018

Dedicated to the path of knowledge…

Declaration

The work presented in this thesis has been carried out by me under the guidance of Dr. Kausik Chattopadhyay at Indian Institute of Science Education and Research Mohali. This work has not been submitted in part or in full for a degree, diploma or a fellowship to any other University or Institute. Whenever contributions of others are involved, every effort has been made to indicate this clearly, with due acknowledgment of collaborative research and discussions. This thesis is a bonafide record of original work done by me and all sources listed within have been detailed in the bibliography.

Nidhi Kundu

Place:

Date:

In my capacity as the supervisor of the candidate's Ph.D. thesis work, I certify that the above statements by the candidate are true to the best of my knowledge.

Dr. Kausik Chattopadhyay

Associate Professor,

Department of Biological Sciences,

Indian Institute of Science Education and Research Mohali.

Place:

Date:

:

Acknowledgements

I would like to express my deepest gratitude to my supervisor Dr. Kausik Chattopadhyay for his constant support and guidance during all these years. I feel very fortunate to get training from him in terms of doing research enthusiastically and accepting the challenging questions. I really thank him for his all-time motivation and encouragement showered on me whenever I felt low both professionally and personally.

I would like to thank my doctoral committee members Prof. Anand K. Bachhawat and Prof. Purnananda Guptasarma for evaluating my research progress time to time and giving me experimental suggestions to improvise my research work. I also thank Dr. Shashi Bhushan Pandit and Mr. Swapnil Tichkule for their collaboration. I thank Dr. Arunika Mukhopadhaya for helping me with all FACS based experiments and allowing me to work in her cell culture lab for my experiments. I also thank Dr. Arunika Mukhopadhaya's lab members for helping me learning cell-based experiments.

I express my sincere thanks to my previous lab members, Dr. Anand Rai, Dr. Barkha Khilwani, Dr. Kusum Lata and Dr. Karan Paul. I especially thank Dr. Anand Rai for helping me in learning all lab experiments and in utilizing instrumentation facility for my research work. Dr. Anand Rai has been the best possible senior whose presence will be acknowledged forever. I feel so happy to thank my present lab members Ms. Amritha, Mr. Anish, Ms. Reema, Ms. Pratima and Mr. Abhinav for providing me a friendly and joyful atmosphere in the lab. I especially thank Ms. Amritha for her constant support and care during all these years. I feel delighted to thank Mr. Ravinder Gulia and Mr. Rohan Sharma for their help and suggestions. I would also like to thank Mrs. Harleen Kaur, my batchmate, who has been with me during all ups and downs of my life. Her presence next to my hostel room has always made me feel relaxed and comfortable.

A special thanks go to my family members for their constant love, support, and encouragement. Last, but not the least, I thank Almighty for giving me the courage and dedication to accomplish this journey.

Nidhi Kundu

:

List of publications

1) **Kundu, N**., Tichkule, S., Pandit, S. B., & Chattopadhyay, K. (2017). Disulphide bond restrains the C-terminal region of thermostable direct hemolysin during folding to promote oligomerization. *Biochemical Journal*, *474*(2), 317-331.

2) **Kundu, N**., Verma, P., Dhar, V., & Chattopadhyay, K. (2018). Intrinsically disordered N-terminal region of *Vibrio parahaemolyticus* thermostable direct hemolysin regulates the membrane-damaging action of the pore-forming toxin. (manuscript is in communication).

:

Table of Contents

:

Chapter 2

:

Chapter 3

:

:

List of figures

:

:

:

:

:

List of tables

:

Glossary

(CD) Circular dichroism

(CDC) Cholesterol dependent cytolysin

(ClyA) Cytolysin A protein

(DNA) Deoxyribonucleic acid

(EDTA) Ethylenediaminetetraacetic acid

(FITC) Fluorescein isothiocyanate

(HCl) Hydrochloric acid

(HEPES) 4-(2-hydroxyethyl)-1-piperazineethanesulfonic acid

(HRP) Horseradish peroxidase

(IPTG) Isopropyl β-D-1-thiogalactopyranoside

(kDa) Kilo Dalton

(LB) Luria Broth

(LDH) Lactate Dehydrogenase

(NaOH) Sodium hydroxide

(DTT) Dithiothreitol

(TCEP) Tris(2-carboxyethyl)phosphine hydrochloride

(NCBI) National Centre for Biotechnology Information

(Ni-NTA) Nitrilotriacetic acid

(POC) Phosphocholine

(OD) Optical density

(PCR) Polymerase chain reaction

(PC) Phosphatidylcholine

(PMSF) Phenylmethylsulfonyl fluoride

(SDS-PAGE) Sodium dodecyl sulfate polyacrylamide gel electrophoresis

(SPR) Surface Plasmon Resonance

(UV) Ultraviolet

(PFT) Pore-forming toxin

:

(PFO) Perfringolysin O

(LLO) Listeriolysin O

(VCC) *Vibrio cholerae* cytolysin

(EqtII) Equinatoxin II

(StnII) Sticholysin II

(FraC) Fragaceatoxin C

(TDH) Thermostable direct hemolysin

(CTR) C-terminal region

(NTR) N-terminal region

:

Chapter 1

Introduction and literature review

:

Chapter 1

Introduction and Literature Review

1.0 Introduction

In 1972, the Fluid-Mosaic Membrane Model of biological cell membrane structure was introduced, and it proposed the plasma membrane as a fluid-matrix consisting of a bilayer of phospholipids embedded with the integral membrane proteins [1]. With time, great advancements and knowledge have been gained and the model has been improved in terms of explaining the mobility of phospholipids, diffusion of membrane components, cohesive forces which act to maintain the membrane-structures, and the introduction of lipid-rafts [2-4]. Plasma membrane acts as an important structural component of a cell in terms of protecting the cell from extracellular environment and it compartmentalize the cellular cytoplasm from the extracellular matrix [5]. Plasma membrane also acts as a bridge in conveying the extracellular signals to intracellular milieu and helps in generating cytoplasmic responses via various integral membrane protein complexes [6, 7]. In a higher organism, approximately 30% of genes code for membrane proteins and they play crucial roles in transport of ions, nutrients and waste across the cell membranes [8, 9]. The plasma membrane is selectively permeable to ions and macromolecules, thereby functioning towards maintaining the survival of the living cells [10, 11]. With evolution, many bacterial pathogens have understood the eukaryotic plasma membrane structures and have evolved with the strategies to destroy this plasma membrane integrity. Apart from bacterial species, various eukaryotic species like sea anemones and earthworms secrete toxins which can perturb the plasma membrane integrity as a part of their defense, invasion and toxicity mechanism. The size of the toxins can vary from a small peptides to large macromolecular protein complexes, all released to destroy the plasma membrane integrity [12-14]. The largest class of bacterial toxins are such pore-forming toxins (PFTs), which represent ~30% of all known bacterial toxins.

The present thesis work describes the structure-function mechanism of action of thermostable direct hemolysin (TDH), a major pore-forming toxin produced by the Gram-negative pathogenic bacteria, *Vibrio parahaemolyticus*, which is the causative agent of gastro-enteric diseases in humans.

:

1.1 Pore-forming toxins

Pore-forming toxins (PFTs) are the largest class of bacterial protein toxins that form pores in the membranes of target host cells and cause colloid-osmotic lysis of the cells [15]. Apart from bacteria, PFTs are also produced by higher organisms like cnidaria [16], sea anemones [17], earthworm [18], and plants [19]. Even higher organisms, like mammals, use the mechanism of membrane pore-formation to kill the pathogens and the pathogen-infected cells by employing specialized PFTs (Membrane Attack Complex of the complement cascade pathway and perforin) as the component of the innate and adaptive immune defense [20]. The mechanism of pore-formation across the different species is so well conserved that it is considered to be the ancient form of the cell-killing action, used by different organisms [21]. PFTs are secreted in the form of water-soluble molecules, which after binding to the target cell membrane undergo various structural rearrangements thereby converting to a transmembrane protein. This feature of converting from the water-soluble state to the transmembrane protein, from the same primary amino acid sequence, is a unique feature of PFTs [14, 22]. The general mechanism of pore-formation by the PFTs involves distinct steps like (i) secretion of the toxin as water-soluble molecule, (ii) binding of the toxin to the surface of the target cell membrane, (iii) self assembly of the toxin on the membranes to form oligomeric species, (iv) formation of membrane pore by the toxin [14, 21, 22]. Due to the membrane pore formation, free diffusion of ions and water takes place across the cell membrane, and as a result, the turgor pressure on the membrane increases which leads to colloid-osmotic lysis (bursting) of the cells. Depending upon the number of the protomers that participate in oligomer formation, the sizes of the pores formed on the membrane may vary from 2 nm to 50 nm [21]. In response to the pore-formation, the cells may respond in multiple ways to survive the stress generated due to the membrane pore formation. The decrease in the cellular potassium ion concentration may lead to the activation of stress- and mitogen-activated protein kinases (MAPK) along with the release of calcium ions from the cell storage [23, 24]. In addition, membrane repair mechanism pathway may get activated either by shedding the vesicles or endocytosis of the pore structure [14, 25].

:

1.1.1 Structural classification of pore-forming toxins:

The most acceptable classification of PFTs is on the basis of the type of secondary structure used for forming the transmembrane pore: α-PFTs use α-helices to span the membrane and β-PFTs utilize β-strands to form the β-barrel transmembrane pore. On the basis of the secondary structure used for membrane insertion few PFTs are mentioned below (Table1):

PFT	Organism	No. of protomers	Type of PFT
Melittin	*Apis mellifera* bee venom	1-3 and 3.5-4.5	α-helix
α-Latrotoxin	*Latrodectus tredecimguttatus* spider venom	2.5	α-helix
Equinatoxin II	*Actinia equina* sea anemone venom	3-4	α-helix
Sticholysin II	*Stichodactyla helianthus* Sea anemone venom	3-4	α-helix
Magainin	*Xenopus laevis* clawed frog skin	4-7	α-helix
Protegrin	Porcine leukocytes	8-10	β-sheet
Human perforin	Human lymphocytes	20	β-sheet
Colicin E1	Enterobacteria	1	α-helix
Diphtheria toxin	*Corynebacterium diphtheriae*	4	α-helix
VacA	*Helicobacter pylori*	6	α-helix
α-Hemolysin	*Escherichia coli*	1	α-helix
Pneumolysin	*Streptococcus pneumoniae*	44	β-sheet
α-Hemolysin	*Staphylococcus aureus*	7	β-sheet
Hemolysin II	*Bacillus cereus*	6-8	β-sheet
Aerolysin	*Aeromonas hydrophila*	7	β-sheet
α-Toxin	*Clostridium septicum*	6	β-sheet
VCC	*Vibrio cholerae*	7	β-sheet
Leucocidin	*Staphylococcus aureus*	8	β-sheet
γ-Hemolysin	*Staphylococcus aureus*	7	β-sheet

:

Hemolysin E	*Escherichia coli*	8	β-sheet
Protective Antigen (Anthrax toxin)	*Bacillus anthracis*	7	β-sheet
Nisin	*Lactococcus lactis*	5-8	cyclic
Viroporin p7	Hepatitis C virus	7	α-helix
Listeriolysin O	*Listeria monocytogenes*	?	β-sheet
Hemolysin ShlA	*Serratia marcescens*	?	α-helix
Defensin	Animals and plants	?	β-sheet, α-helix
Cardiotoxin CTX A3	Taiwan cobra venom	?	β-sheet
Pardaxin	*Pardachirus marmoratus* ish mucous glands	?	α-helix
Toxin A-III	*Cerebratulus lacteus* marine worm-nemertine	?	α-helix
Pandinin 2	*Pandinus imperator* african scorpion venom	?	α-helix
Oxyopinin 1	*Oxyopes kitabensis* spider venom	?	α-helix
Lycotoxin I	*Lycosa carolinensis* wolf spider venom	?	α-helix
Cecropin A	*Hyalophora cecropia* moth hemolymph	.2	α-helix
TDH	*Vibrio parahaemolyticus*	4	?

Table 1: Classification of the pore-forming toxins on the basis of the secondary structure element used for pore formation on the membranes of the target cells from different organisms. '?' indicates that the number of protomers involved in oligomerization and pore-formation remains unknown (Adapted from Andreeva *et.al.*, Biochemistry, 2008) [26-81].

:

1.1.2 α-Pore-Forming Toxins:

The α-PFTs are known to form pores in the membranes of the target cells by utilizing α-helices. These PFTs are rich in α-helical structures and their pore-forming domain usually consists of a three-layer structure of up to ten α-helices. The membrane-spanning domain sandwiches a hydrophobic helical hairpin in the middle of the structure which undergoes partial unfolding and inserts into the membrane [82].

After membrane binding, the toxins generally oligomerizes on the membrane to form the transmembrane pores which allow free diffusion of ions. This class of PFTs is barely understood in detail so far, and the exact mechanism of the pore formation still remains unclear [21]. Some of the structurally characterized α-PFTs are discussed below:

1.1.2.1

Cytolysin A (ClyA)

Cytolysin A (ClyA), also known as Hemolysin E, is a 34 kDa α-PFT produced by bacteria like *Escherichia coli* and *Salmonella enterica* [83]. Apart from the hemolytic activity of bacteria against human erythrocytes, ClyA can also kill cultured macrophages and tumor cells [84-86]. The soluble monomeric ClyA consists of two domains: (i) a large tail domain with four long α-helices and one short α-helix (residues 1-159 and 206-303), along with two conserved cysteine residues (Cys 87 and Cys 285) that form a disulphide bond, (ii) a small head domain consisting of a central hydrophobic β-hairpin (the β-tongue, residues 185-195), which is surrounded by two short α-helices (residues 160-205) (Fig. 1.1A). The solution monomeric toxin undergoes several structural rearrangements to form the final dodecameric pore complex in the membranes of the target cells [87-89]. The transition of monomer to dodecameric pore involves following steps: (i) membrane binding of ClyA with the hydrophobic β-tongue present in the head domain; membrane binding triggers the rearrangements of the head domain along with the neighboring helices, (ii) this is followed by swinging-up movement of the N-terminal helix by 180^{o}, (iii) formation of inter-subunit interface by rearrangements of the helices present in the tail domain, (iv) penetration of the N-terminal region (residues 1-34) from all protomers to form a transmembrane pore with the inner diameter of 3.5 nm (Fig. 1.1B) [90].

:

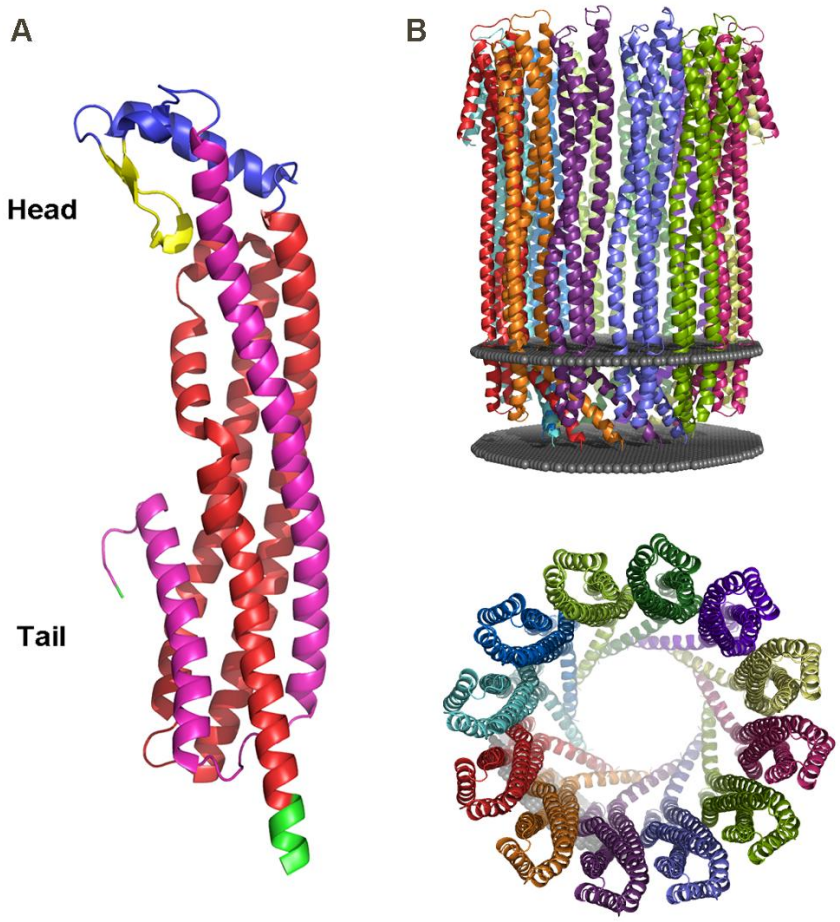

Fig. 1.1: (A) Crystal structure of Cytolysin A monomer (PDB ID: 1QOY). Representation of (i) tail domain consisting of four long α-helices and one short α-helix (residues 1-159 red; 206-303 magenta), (ii) head domain consisting of a central hydrophobic β-hairpin (the β-tongue, residues 185-195, yellow) surrounded by two short α-helices (residues 160-205 blue). (B) Oligomeric assembly of ClyA monomers into dodecameric pore structure highlighting membrane inserted region (PDB ID 2WCD) (Side view and top view) [90].

1.1.2.2

Colicin Ia

Colicin Ia is an elongated 210 Å long structure with a molecular weight of 69 kDa. It is an α-helical PFT produced by the bacteria *Escherichia coli* to kill other competing bacteria like *Escherichia coli* and *Shigella sonnei* [91, 92]. It shares structural and functional similarities to Colicins A, E1, and N [93-95]. The elongated structure of this toxin is prominently due to a long coiled-coil region from residues 176-282 and 359-467 (marked red in Fig. 1.2). The protein consists of three domains with three distinct functions: (i) the receptor domain (R), which binds to the outer membrane protein receptor, ‘Cir receptor’ (Colicin Ia receptor)

:

present on the target cells, (ii) the N-terminal translocation domain (T), consists of 'TonB box' which helps in traversing the outer membrane and periplasmic space, as part of an antiparallel helix bundle to deliver the (iii) C-terminal pore-forming domain (C) to the bacterial inner membrane (Fig. 1.2). The C domain then undergoes conformational changes and forms a voltage-gated ion channel in the plasma membrane resulting in the efflux of ions that depletes the cellular energy and leads to the cell death [96-98]. The single monomer forms the channel with the pore size of 2-3 nm.

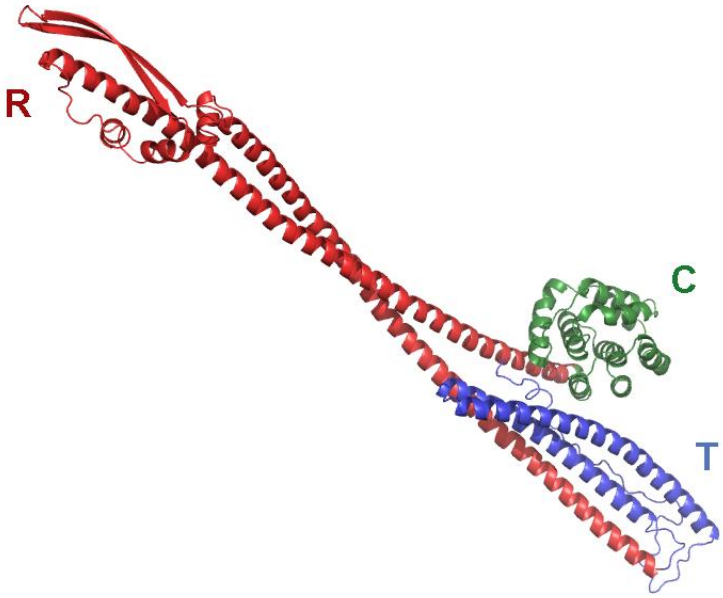

Fig. 1.2: Crystal structure of Colicin Ia (PDB ID 1CII) highlighting all structural and functional domains. (i) the receptor (R) domain, marked in red, (ii) N-terminal, translocating domain (T), marked blue, (iii) C-terminal channel-forming domain (C), marked in green [98].

1.1.2.3 CryIA

Bacillus thuringiensis (Bt) is a ubiquitous Gram-positive bacterium that produces insecticidal proteins like Cry proteins during its sporulation phase. It is widely used as a biopesticide, and when ingested by the insects it kills the insects by affecting their gut [99]. The major effect is mediated via Cry proteins which are stored inside the cells in the crystal forms (protoxin), and gets activated once they reach the gut of the insects by certain proteases. After activation, Cry toxin (CryIA) binds specifically to the midgut epithelial cells of the insects, and forms channel in the membrane of these cells. As a result, the cell swells up and ultimately burst thereby killing the insect [100, 101]. The lepidopteran specific CryIA(a) is a 65 kDa toxin (active

:

form). One model of the membrane pore-formation suggests the following steps: (i) low-affinity binding of the activated form of the toxin to the aminopeptidase N or alkaline phosphatase receptors that are present on the cell membranes, (ii) high-affinity interaction with the cadherin receptor that facilitates (iii) cleavage of N-terminal end of the toxin thereby facilitating oligomerization of the toxin, which further facilitates strong interaction with aminopeptidase receptor, and (iv) insertion of the pre-pore into the target cell membranes forming the functional channel [102-105]. Another model of pore formation suggests that after binding to cadherin receptors the toxin inserts first into the membrane followed by oligomerization and functional pore-formation [106]. The crystal structure of CryIA suggests that it is a globular protein consisting of three different domains. The N-terminal domain I (residue 33-253, red) is hydrophobic, rich in α-helical structures, consists of 8 α-helices, and are responsible for membrane-insertion and pore-formation. Domain II consists of three anti-parallel β-sheets and two short α-helices (residues 265-461, blue). Domain III (463-609, green) contains two highly twisted anti-parallel β-sheets (Fig. 1.3). Domain II and III are involved in receptor recognition and binding of the toxin to the target cell membranes (Fig. 1.3) [107, 108].

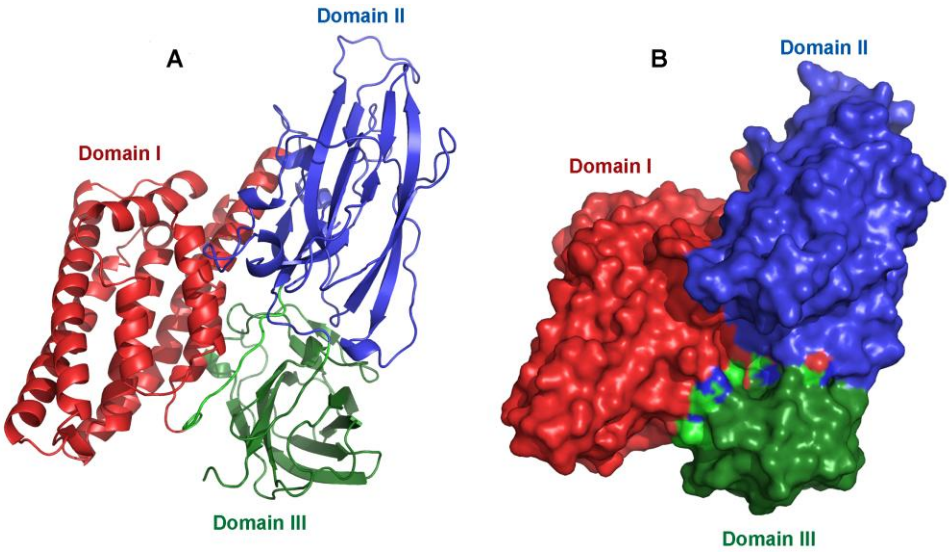

Fig. 1.3: Crystal structure of CryIA toxin (PDB ID 1CIY) highlighting all the structural domains. Domain I consists of N-terminal residues from 33-253 (colored in red) forms the channel, domain II is from residues 265-461(colored in blue), domain III contains residues 463-609 (colored in green). Domain II and III are involved in binding of the toxin to the receptor present on the target cells [107, 108].

:

1.1.3 β-barrel pore-forming toxins:

Like all PFTs**,** β-barrel PFTs (β-PFTs) are water-soluble proteins secreted by different classes of bacteria, as well as by many higher organisms. These toxins insert into the membrane lipid bilayer of the target cells and form the pores by using β-barrel architecture. Such β-barrel motifs are amphipathic in nature, and the pore architecture is composed of hydrophilic residues which line the inner opening of the pore and hydrophobic residues facing the membrane lipid bilayer. The general mechanism of pore formation is similar in this family of toxins involving secretion of the toxin as a monomer, binding of the toxin as a monomer to the target cell membranes, oligomerization and formation of pre-pore complex followed by membrane perforation and pore formation. As compared to α-PFTs, β-PFTs are more well-studied in terms of structural characterization and pore-formation mechanism. Few examples are discussed below.

1.1.3.1

***Staphylococcus aureus* α-hemolysin**:

Staphylococcus aureus α-hemolysin (α-HL) is a water-soluble toxin with a molecular weight of 33.3 kDa. It has been known to cause toxicity in various type of human cells like human erythrocytes, human platelets, epithelial cells, endothelial cells, and an array of other hematopoietic-lineage cells including T cells, monocytes, macrophages, and neutrophils [109-112]. After binding to the target cell membrane as a monomer, the toxin oligomerizes and makes the transition from pre-pore to final pore structure in which 7 protomers participate, and makes a β-barrel-like heptameric pore structure in the membrane with the pore diameter of 1.5 nm (Fig. 1.4). The final membrane-inserted heptameric pore structure resembles a mushroom-like structure and has three distinct domain, (i) the cap domain, present on the extracellular face of the membrane-inserted toxin, is a hydrophilic domain which is exposed to aqueous environment; (ii) the rim domain, is present in the close proximity of the outer leaflet of host cell membrane; and (iii) the stem domain, constituted from 14 β-strands (2 from each protomer) thus generating β-barrel pore that forms the membrane-perforating region (Fig. 1.4) [113-115].

:

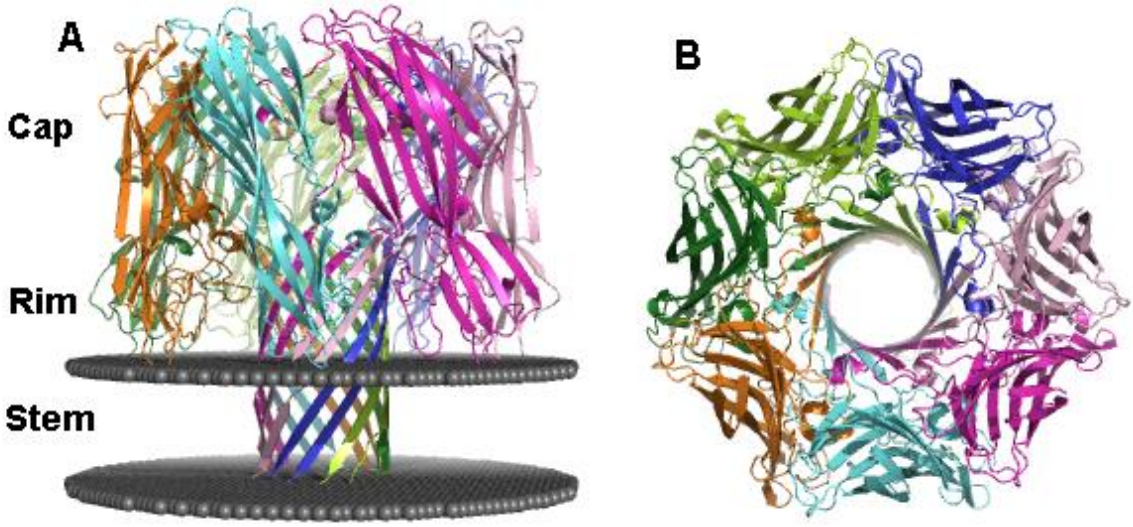

Fig. 1.4: Crystal structure of α-Hemolysin toxin (PDB ID 7AHL) highlighting all structural domains: Cap domain, Rim domain and Stem domain [114].

1.1.3.2

Aerolysin:

Aerolysin is a water-soluble 52 kDa (monomer) PFT secreted by the bacterium *Aeromonas hydrophila*. The toxin is initially secreted as an inactive precursor called proaerolysin. Aerolysin is known to cause gastroenteritis, sepsis and wound infections in humans [116]. The protein is present as a homodimer and the monomer-monomer interactions are mostly hydrophobic interactions. The crystal structure of the monomeric toxin suggests that it has four domains. The N-terminal domain I and II play important role in binding of the toxin to *N*-glycosylated glycosylphosphatidylinositol (GPI)-anchored proteins, which are known to be the receptor of aerolysin [117]. Domain III contains five stranded β-sheets and prestem loop, which plays a critical role in insertion of the β-barrel in the membrane. Domain IV is an extended structure of domain III and contains C-terminal peptide (CTP) (Fig. 1.5). In its precursor proaerolysin form, it contains CTP in domain IV which prevents nonspecific oligomerization of the toxin. The steps involved in mechanism of pore-formation are as follows: (i) secretion of toxin as proaerolysin via type II secretion system by the bacteria, (ii) binding of monomeric proaerolysin to the target GPI-anchored protein receptors present on the target cell membranes, (iii) conversion of proaerolysin to aerolysin via certain proteases

:

like bacterial gut protease (trypsin or α-chymotrypsin), or mammalian cell-surface proteases like furin, which removes C-terminal peptide (CTP), the last 40 amino-acids from the toxin, (iv) removal of CTP triggers conformational changes in the toxin which promotes process of oligomerization and membrane insertion. The final heptameric pore structures formed on the membrane are voltage-gated channels of 1 nm in diameter [118-120]. Cryo-EM analysis of the structure of aerolysin suggested that during pore-formation, domain III and domain IV undergoes various conformational rearrangements [121]. The amphipathic hairpins move away from the toxin core towards the lipid bilayer and associates with hairpins of another protomer to form the final transmembrane β-barrel architecture (Fig. 1.5).

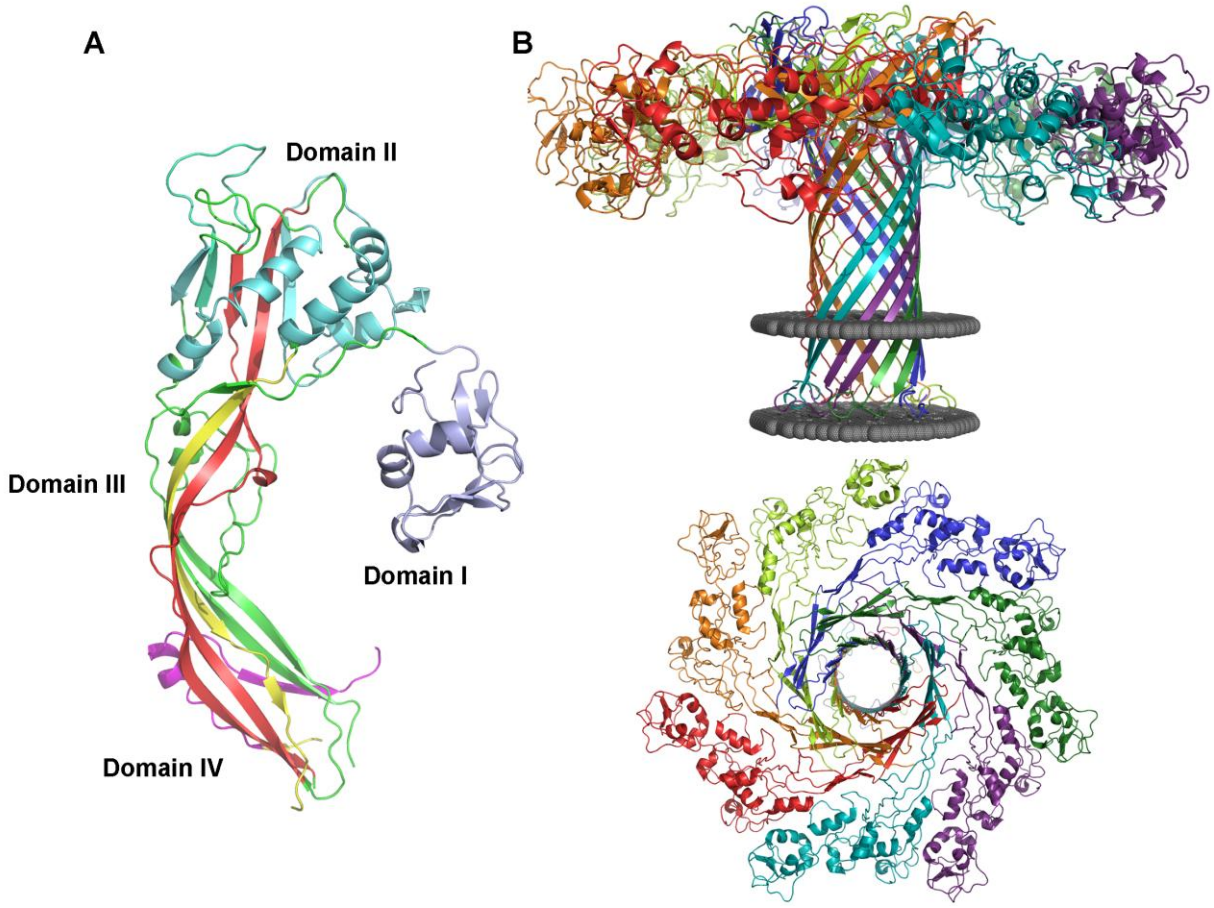

Fig. 1.5: (A) Crystal structure of proaerolysin monomer highlighting four different domains (PDB ID 1PRE), (B) CryoEM structure of transmembrane aerolysin oligomer (PDB ID 5JZT) highlighting the heptameric pore structure (side view and top view) [119].

:

1.1.3.3

***Vibrio cholerae* cytolysin (VCC):**

VCC is a pore-forming toxin secreted by the Gram-negative bacteria *Vibrio cholerae*, the causative agent of the diarrheal disease cholera in humans. The bacterial genome consists of *hlyA* gene which codes for an inactive, 80 kDa pro-toxin [69, 122-124]. The crystal structure of water-soluble VCC monomer is a cross-shaped structure highlighting four different domains: (i) Pro-domain: an N-terminal domain which has homology to the chaperone proteins like Hsp90 family (Fig. 1.6). This domain plays a critical role in proper secretion and folding of the VCC molecule. Following the pro-domain is a 15 amino acid long linker which acts as a cleavage site for various proteases like trypsin, α-chymotrypsin, subtilisin, HA protease, papain. Proteolytic cleavage at this site releases pro-domain and the toxin converts from pro-toxin to mature toxin (active form) [125]. (ii) Cytolysin domain: following the pro-domain and proteolytic cleavage site, is the 325 amino acids long cytolysin domain. This domain is the structural and functional core of VCC molecule with structural similarity to Staphylococcal LukF and α-hemolysin (β-barrel PFTs). Cytolysin domain contains 42 amino acids long pre-stem loop which forms the transmembrane region in the final pore structure. In the water-soluble state, the pre-stem is folded and is associated with the cytolysin domain, but during pore-formation, the pre-stem loop moves away from the cytolysin domain, towards the lipid bilayer, and associates with pre-stem loops of six other protomers to form a heptameric β-barrel transmembrane structure. The cytolysin domain also contains a membrane-proximal rim-domain, which mediates protein:lipid interaction present on the target cell membranes. (iii) β-trefoil lectin-like domain: following the cytolysin domain are two different domains with lectin-like folds. The first domain is β-trefoil lectin-like domain which has structural similarity to carbohydrate-binding B domain of plant toxin ricin. It also has two disulphide bonds and a β-trefoil fold. This domain is the topmost domain and might play important role in binding of the toxin to carbohydrates present on the membranes of target cells. (iv) β-prism lectin-like domain: is a 15 kDa domain present at the C-terminal end of VCC. It has structural similarity with the β-prism lectins, like plant lectin jacalin, *Maclura pomifera* agglutinin (MPA), and possesses a carbohydrate-binding pocket. This domain is exclusively present in

:

VCC and is absent in any other β-PFT including those from *Vibrio vulnificus* and *Aeromonas hydrophila*. It plays important role in membrane-binding and assembly of the toxin. During pore-formation mechanism, β-prism domain undergoes various structural rearrangements. In the pro-VCC, β-prism domain is present opposite to the pro-domain and masks pre-stem loop, but during pore formation on the membrane, it moves 180^{o} and comes to the position of pro-domain thereby facilitating oligomerization and insertion of pre-stem loop into the membrane to form the transmembrane pore structure (Fig. 1.6) [69, 125-132].

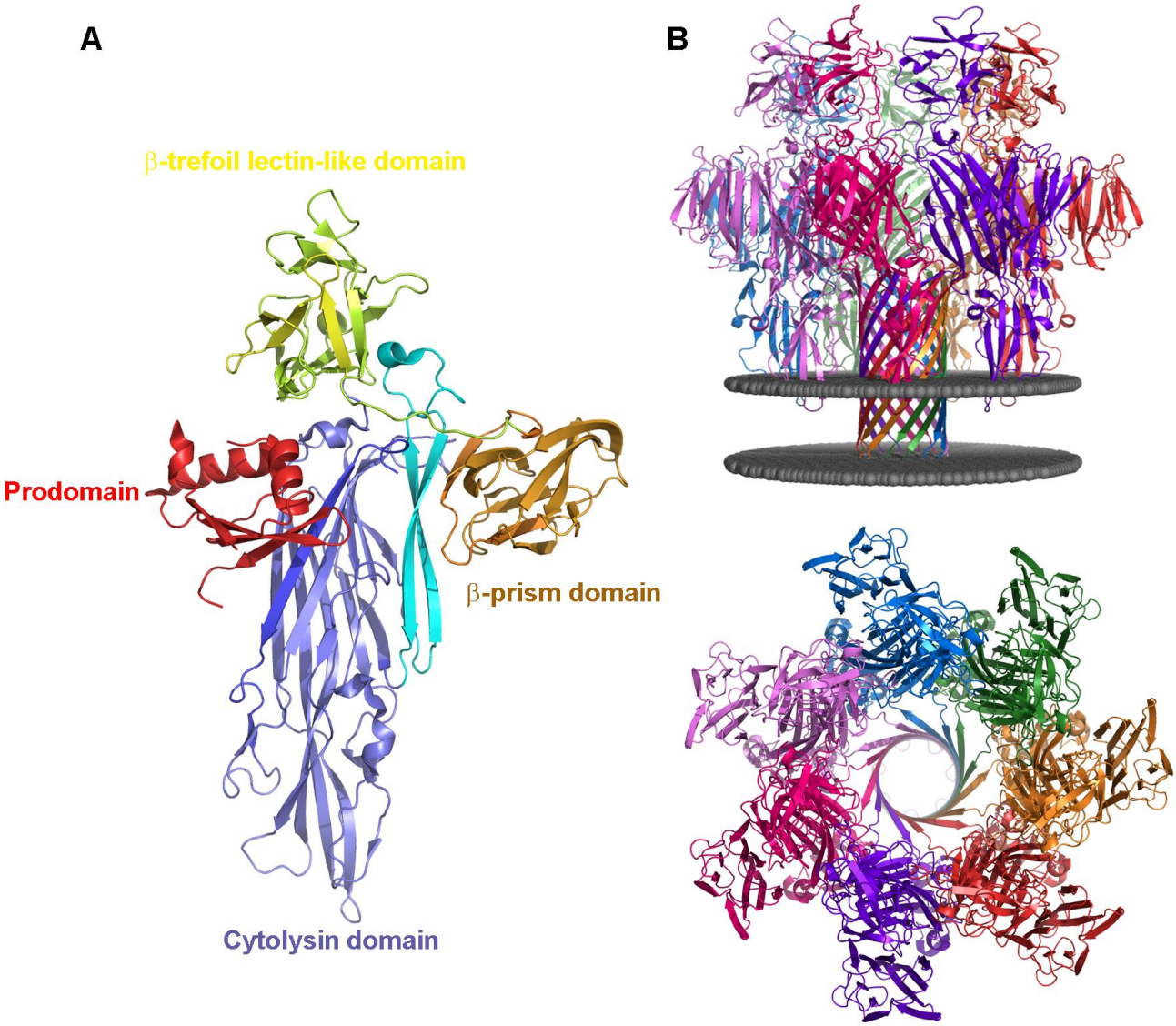

Fig. 1.6: (A) Crystal structure of VCC monomer highlighting four different domains (PDB ID 1XEZ), (B) Crystal structure of transmembrane VCC oligomer (PDB ID 3O44) highlighting the heptameric pore structure (side view and top view) [69].

:

1.1.4 Cholesterol-dependent cytolysins (CDCs):

There is another subclass of β-PFTs known as cholesterol-dependent cytolysins (CDCs) that show the obligatory requirement of cholesterol for membrane pore formation. The size of the pores formed by the CDCs, and the number of protomers used for pore formation are much larger than the conventional β-PFTs.

CDCs are widely distributed PFTs across five different Gram-positive bacteria like *Clostridium, Bacillus, Streptococcus, Listeria, and Arcanobacterium*. The members of the CDC family show high sequence similarities (40%-80%) suggesting similar activities and similar structure. CDCs exhibit various unique features like the requirement of cholesterol in the target cell membranes, the involvement of a large number of protomers to form the pore, and formation of large oligomeric transmembrane pore, greater than 150 Å in diameter. There can be involvement of up to 50 monomers, each contributing two β-hairpins thereby generating a 200-strand β-barrel pore structure, hence forming very large pores [21, 22, 133]. The large size of CDC pores can allow translocation of fully folded proteins across the membrane, and they have been widely used in cell biology to generate semi-permeabilized cell systems [134]. The structural studies of different CDCs have suggested that there is a conserved undecapeptide sequence (ECTGLAWEWWR) present near the C-terminal region which is important for membrane-binding of the toxin. The mechanism of membrane insertion and membrane permeabilization is used either to kill the target cell or to transfer the secreted proteins produced by the bacteria into the host cells [135, 136].

1.1.4.1 Perfringolysin O (PFO):

PFO is a 52.5 kDa water-soluble toxin, secreted by the Gram-positive bacterium *Clostridium perfringens*. PFO is the first CDC whose crystal structure was solved in 1997 and it revealed that PFO is a long rod-shaped molecule consisting of four different domains and is rich in β-sheets (Fig. 1.7) [137]. Domain I: the N-terminal domain and present at the top of the PFO molecule. It has an α-β topology with the β-sheet core surrounded by α-helices. It is the only domain in PFO molecule which does not undergo various structural rearrangements. Domain

:

II: it is the central domain in the elongated molecule and consists of a pair of anti-parallel β-sheet which connects top end to the bottom end of the PFO molecule. During pore formation, it collapses vertically to allow the insertion of β-hairpins to form the transmembrane pore [58, 138, 139]. Domain III: consists of β-sheets that play important role in oligomerization of the toxin and also it contains six short α-helices that transform into two amphipathic β-hairpins to form the β-barrel pore [140-142]. Domain IV: a β-sandwich structure, present at the distal tip of the PFO molecule. It contains a conserved Trp-rich motif which helps in generating a hydrophobic surface in domain IV (Fig. 1.7). This domain is important for recognizing cholesterol on the target cell membranes as well as binding of the toxin to the target cells [143, 144].

The mechanism of pore-formation by PFO involves (i) binding of the toxin to cholesterol-rich membranes via domain IV, which facilitates the flipping out movement of the hydrophobic Trp-rich loop, and penetrates into the membrane partially and anchors the toxin onto the membrane. This results in (ii) bringing the domain III in proximity to the membrane surface, which further facilitates the oligomerization of the toxin and formation of the pre-pore complex [145-147].

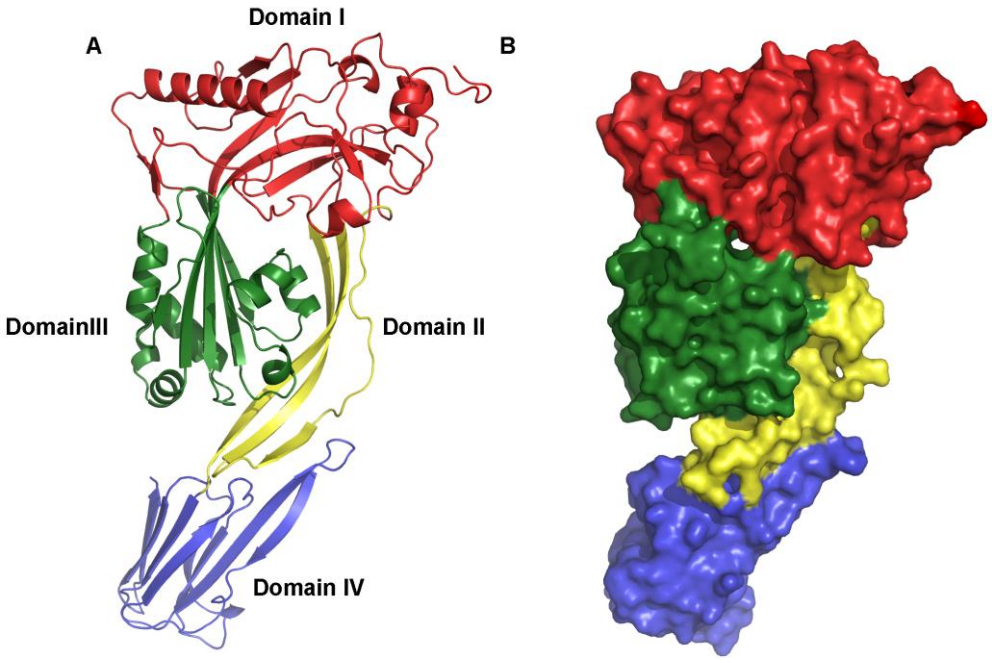

Fig. 1.7: (A) Crystal structure of perfringolysin O (PFO) highlighting four different domains (PDB ID 1PFO), (B) Surface view of PFO molecule [137].

(iii) The formation of oligomers triggers a conformational change in domain IV which moves

:

away from the long axis of the molecule, and domain III moves away from the molecule, towards the membrane and transforms from transmembrane α-helices to β-hairpins. The β-hairpins from all the monomers then insert into the membrane and to form the large transmembrane β-barrel structure [148, 149].

1.1.4.2 Listeriolysin O (LLO):

Pathogens like *Listeria monocytogenes* produce CDC both extracellularly and intracellularly (when phagocytosed by the cell). LLO is a 56 kDa, water-soluble toxin, produced by *Listeria monocytogenes*, the causative agent of listeriosis [150]. LLO form pores in the phagosomal membrane and gets released from phagosomes to the cytoplasm of the host cells. Generally, CDCs are known to act on cholesterol-rich cell membranes, but LLO gets activated at low pH and shows higher activity at low pH when compared with the high pH. This is logical because the pH of the phagosomes is low which is suitable for LLO to act on phagosomal membranes thereby translocate *L. monocytogenes* from phagosomes to the cytoplasm to enhance intracellular growth [151-155].

LLO is long elongated molecule consisting of four different domains similar to present in PFO. LLO monomer binds to the membranes which are rich in cholesterol [151]. After binding to the target cell membranes, LLO oligomerizes and forms a pre-pore complex, which undergoes major conformational changes to allow membrane insertion and pore-formation. As discussed above, LLO is unique and different from other CDCs because of its low pH activity and stability [59, 156, 157]. After ingestion of contaminated food, *Listeria monocytogenes* enters the human gut where it is phagocytosed by the cells. In the phagosomes, pH is low as compared to the cytosol, at this low pH, LLO gets activated and forms pores in the membranes of phagosomes and hence releases the *L. monocytogenes* from phagosomes to cytosol [158-160]. In the cytosol, the bacteria grow and modulate cellular processes like changes in gene expression and intracellular ca^{2+} oscillations. Domain I has an α/β topology with five β-sheets surrounded by six α-helices (Fig. 1.8). Domain II connects domain I (top end) to domain IV (bottom end) and also consists of α/β topology with four β-stands forming three-stranded antiparallel β-sheet structure. Domain III is made up of five-stranded antiparallel β-sheet surrounded by six α-helices in a α/β/α fold. Domain I and III play role in oligomerization of the toxin. Domain I, II and III are clustered together, domain IV on the

:

other hand, forms a separate and independent folding unit. Domain IV is compact β-sandwich structure and plays important role in membrane binding and receptor recognition. Within domain IV various tryptophan residues are present which play a crucial role in membrane interaction (W512) and oligomerization of the toxin (W189 and W489) [161].

Another unique feature in LLO is a PEST-like sequence (marked in blue in domain I) present in domain I. This sequence contains six proline residues and forms a polyproline type II helix (PPII). It is known to play important role in compartmentalization of the toxin and regulation of pore-forming activity, limiting it to vacuole of the host cells (Fig. 1.8) [162].

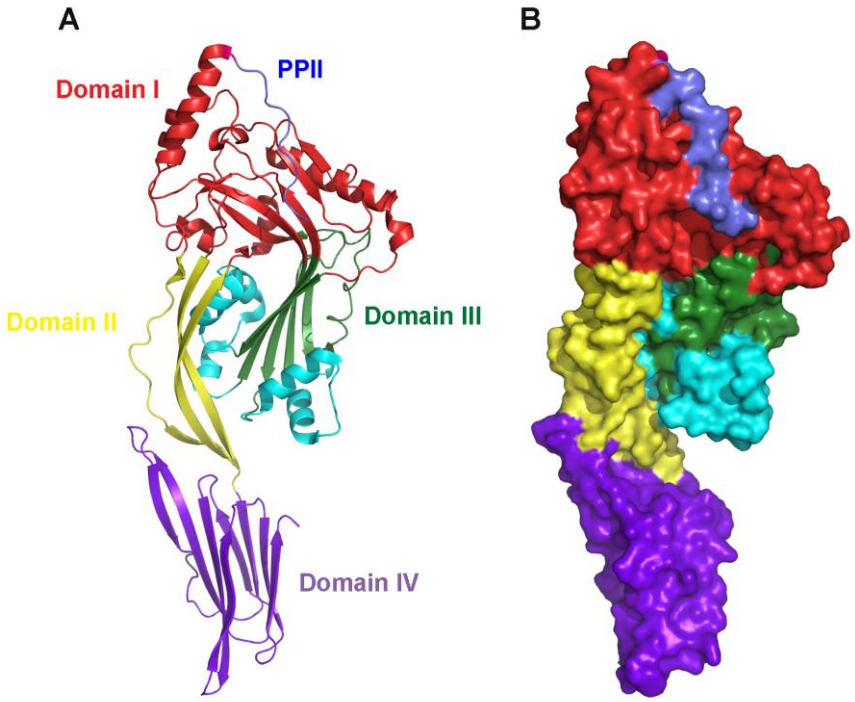

Fig. 1.8: (A) Crystal structure of Listeriolysin O (LLO) highlighting four different domains (PDB ID 4CDB), PPII sequence in domain I (marked blue); (B) Surface view of LLO molecule [162].

1.1.5 Actinoporins:

There is another unique class of eukaryotic PFTs, named as actinoporins, that are secreted by the sea anemones. Actinoporins are present in the nematocysts of the sea anemones [163]. The physical contact of the tentacles of sea anemones with their prey releases these toxins and inject the toxin into the prey thereby generating a noxious effect in the target [164]. Actinoporins produced by different sea anemones show common structural and functional features: (i) they are all produced as single polypeptide chain of around 175 amino acids; (ii)

:

they have compact β-sandwich structure surrounded by short α–helices; (iii) they lack cysteine residues; (iv) they have basic isoelectric point; (v) they all act as α-PFTs, i.e they use α-helices to form transmembrane channel; (vi) form pore having size of around 1-2 nm in diameter; (vii) require presence of phosphocholine/sphingomyelin for binding on the target cell membranes [165-172]. Actinoporins are water-soluble protein toxins and show high sequence similarity (60-80%) and structural similarity. The well-studied actinoporins are equinatoxin II (EqtII) from *Actinia equina* and sticholysin II (StnII) from *Stichodactyla helianthus* [173, 174]. Apart from EqtII and StnII, the crystal structure of Fragaceatoxin C (FraC) has also been determined [175]. They all have a compact β-sandwich core domain of 10-12 β-strands which are flanked by two α-helices, present at both sides of β-sandwich domain. The N-terminal region consists of the first, long helix, which is composed of almost 30 amino acids [173-176]. The N-terminal helix is amphipathic in nature and undergoes various structural rearrangements to form the final α-helical transmembrane channel [33]. There are different structural regions present in actinoporins which might play a functional role in the pore-formation mechanisms like (i) phosphocholine (POC) binding pocket, (ii) cluster of aromatic residues, and (iii) stretch of basic amino acid residues. It is known that all these three features play important role in membrane binding ability of the toxin [177, 178]. The crystal structural of Stn II has been solved with the bound POC and is discussed in further sections. The mechanism of channel formation in actinoporins proceeds via (i) binding of the toxin to sphingomyelin on the target cell membrane by using aromatic amino acids and POC binding pocket, (ii) oligomerization of the toxin and (iii) insertion of the α-helices from the protomers into the membrane to form the transmembrane α-helical pore.

1.1.5.1 Equinatoxin II:

Equinatoxin II is a water-soluble, 179 amino acid containing toxin with a molecular weight of ~20 kDa. It is a eukaryotic PFT secreted by sea anemone *Actinia equina [166]*. The protein adopts a 12 β-stranded folded structure with α-helices on each end of the toxin (Fig. 1.9). It contains a unique region of ‘aromatic amino acid cluster’ made up of residues Trp112, Tyr113, Trp116, Tyr133, Tyr137 and Tyr 138 (marked red in Fig. 1.9), that play a crucial role in membrane binding of the toxin. The N-terminal helix consisting of 30 amino acid residues

:

(marked blue in Fig 1.9), moves away from the core β-sandwich domain, towards the membrane and partitions itself into the membrane by inserting into the bilayer to form transmembrane α-helical pore [33]. The N-terminal α-helix from 3-4 monomers insert into the membrane to form a cation-selective pore with the diameter of 20 Å [179].

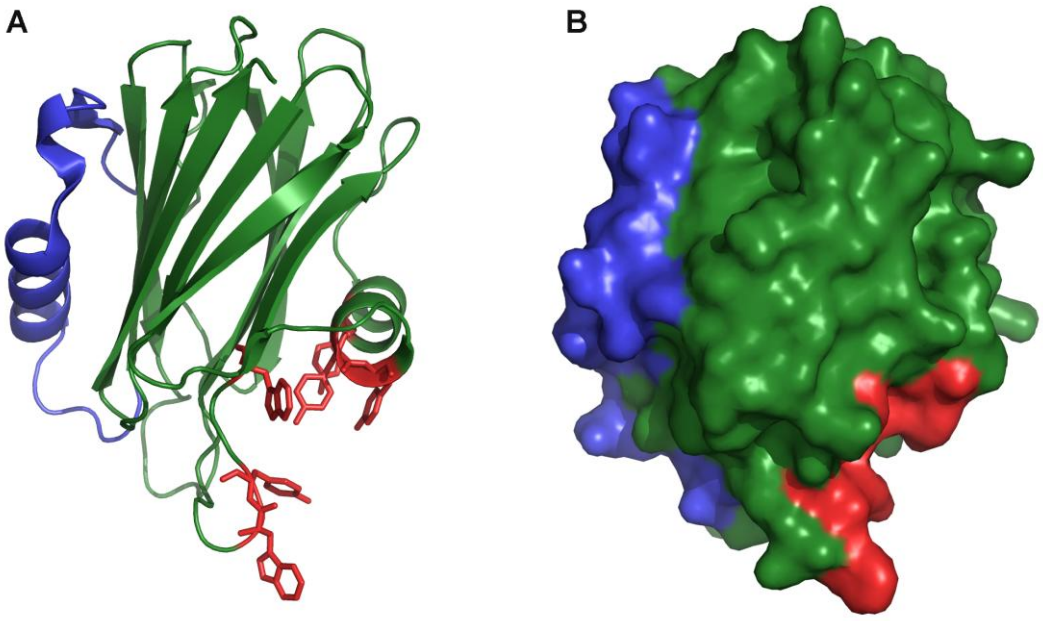

Fig. 1.9: (A) Crystal structure of Equinatoxin II highlighting N-terminal transmembrane region (in blue) and a cluster of aromatic amino acid residues (in red) (PDB ID 1IAZ), (B) Surface view of Equinatoxin II molecule [173].

1.1.5.2 Sticholysin II

Sticholysin II (StnII) is an α-PFT secreted by a sea anemone *Stichodactyla helianthus.* It is a water-soluble toxin of molecular weight around 20 kDa. There is a high structural similarity between StnII and EqtII, with a similar β-sandwich topology flanked by two α-helices (Fig. 1.10) [174]. The N-terminal α-helix is amphipathic (marked in purple, Fig. 1.10 A), and consists of 30 amino acid residues which form the transmembrane region of the final pore structure. The unique lipid (POC) binding pocket of StnII has been resolved by solving the crystal structure with phosphocholine. The POC binding site is partly hydrophobic (made with the side chains of Val-85, Pro-105, Tyr-111 and Tyr-135) and partly hydrophilic (made with the side chains of Ser-52 and Ser-103, Tyr-131, Tyr-135 and Tyr-136) (shown in yellow in Fig. 1.10A). Few residues which are present in POC binding pocket are also part of the conserved cluster of aromatic amino acid residues (side chains of Phe-106, Trp-110, Tyr-111, Trp-114,

:

Tyr-131, Tyr-135, and Tyr-136) (marked green in Fig. 1.10 A). Both POC-binding pocket and clustered aromatic amino acid residues play important role in binding of the toxin to phosphocholine/sphingomyelin present on the target cell membranes. Analysis of the structural comparison of StnII with EqtII suggests that StnII consists of a region rich in basic amino acid residues (shown in blue, Fig. 1.10 C). It is proposed that these basic residues mediate the initial interaction of StnII with the negatively charged lipid groups on the membrane [170, 171, 180].

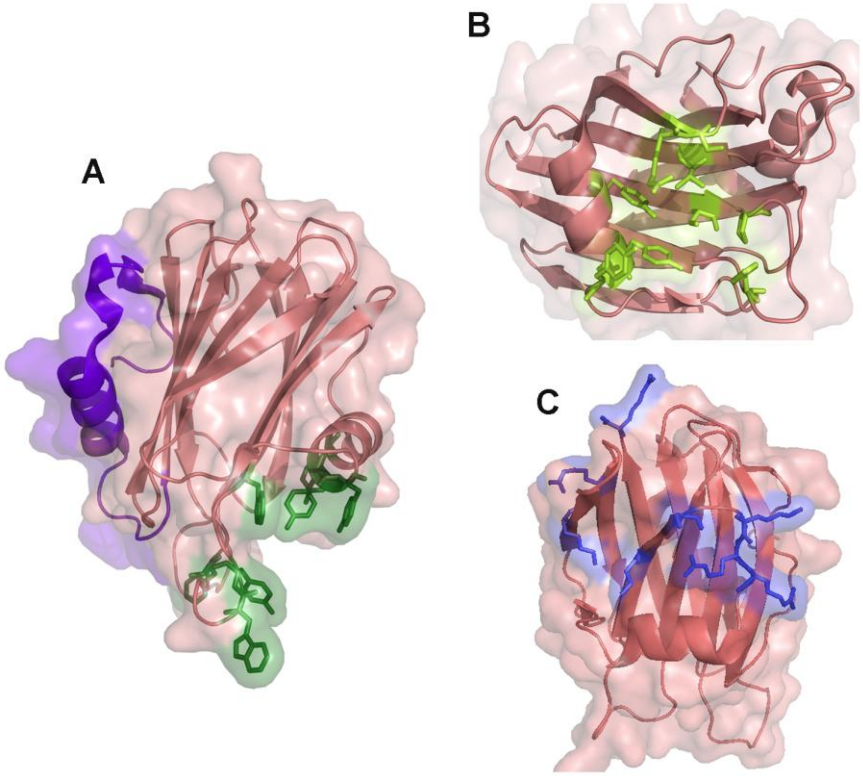

Fig. 1.10: (A) Crystal structure of Sticholysin II highlighting N-terminal region (in violet) and cluster of aromatic amino acid residues (in green; Fig. 1.10 A) (PDB ID 1GWY), (B) Surface view of Stn II highlighting POC binding pocket (in yellow; Fig 1.10 B), (C) Surface view of Stn II highlighting basic amino acid residues (in blue; Fig 1.10 C) [174].

1.1.5.3 Fragaceatoxin C (Fra C):

Fra C is a potent hemolysin from a sea anemone *Actinia fragacea,* with a molecular weight of ~20 kDa. Transmembrane pore structure of Fra C has been solved showing that it forms oligomeric α-helical transmembrane pore. Fra C forms a symmetrical and funnel-shaped pore comprising of eight protomers with a diameter of 110 Å and height of 70 Å (Fig. 1.11). It is known that sphingomyelin act as the receptor for actinoporins and critical for pore-formation.

:

The initial interaction of Fra C with the phosphate groups present on the lipid bilayer is mediated by electrostatic interactions. Along with electrostatic interactions, various non-covalent interactions like Hydrogen bonding and cation- π interactions play important role in membrane binding of the toxin. From the analysis of transmembrane oligomeric pore structure, it is known that the N-terminal residues (4-29 amino acids) move more than 50 Å as compared to the monomeric water-soluble structure, and can span the entire membrane. During pore-formation, the helices align perpendicular to the membrane plane, and the hydrophilic residues are oriented towards the lumen while the hydrophobic residues are faced towards the membrane lipids. The lumen of the pore is comprised of negatively charged residues suggesting it forms a cation-selective pore [168, 170, 171]. The oligomeric pore structure is stabilized by protein-protein and protein-lipid interactions [181].

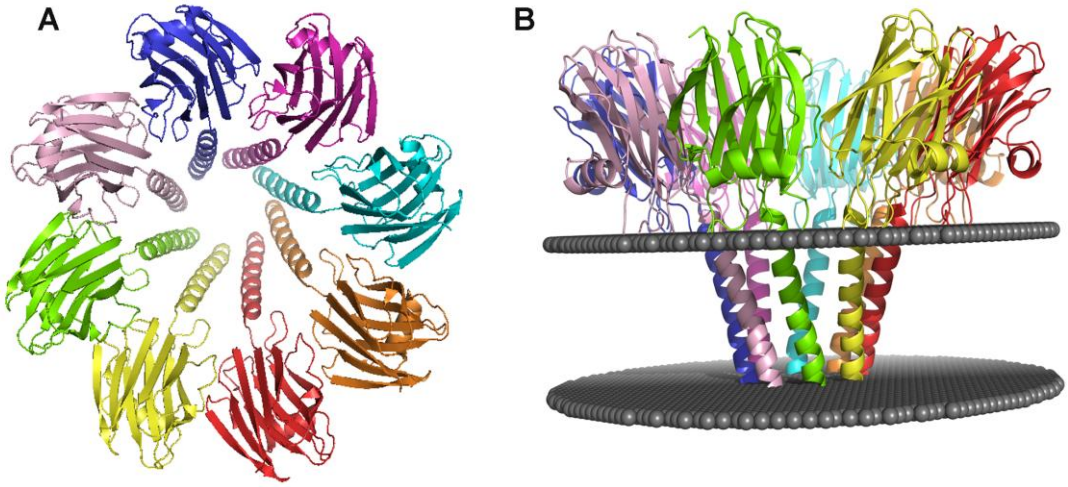

Fig. 1.11: (A) The crystal structure of Fragaceatoxin C (PDB ID 4TSY) transmembrane pore, top view (B) side view of the α-helices inserted into the lipid [181].

1.2: *Vibrio parahaemolyticus*

1.2.1 Microbiology:

Vibrio parahaemolyticus is a member of *Vibrio* species from the Vibrionaceae family. *Vibrio parahaemolyticus* was discovered by Tsunesaburo Fujino in 1950 as a causative agent of foodborne disease that led to an outbreak in Japan, causing illnesses in 272 individuals with 20 deaths after consumption of *shirasu* [182]. *V. parahaemolyticus* is a Gram-negative halophilic bacterium that is distributed across estuarine, marine and coastal surroundings [183, 184]. *V. parahaemolyticus* can be classified depending on the antigenic properties of

:

the somatic (O) and capsular (K) antigen produced in different environmental conditions [185]. Depending on the environmental conditions, *V. parahaemolyticus* can produce a capsule with more than 70 different K antigens found in many strains. Most of the pathogenic strains are of serotype O3:K6, while other reported serotypes are O4:K12 and O4:K68.

1.2.2 Disease:

V. parahaemolyticus cause three distinct pathophysiological effects: gastroenteritis, wound infections, and septicemia. Acute gastroenteritis shows symptoms like abdominal cramping, diarrhea, nausea, vomiting, low-grade fever, headache and occasional bloody diarrhea. After consumption of contaminated sea food, infection results after 4 to 96 hours, and lasts up to three days [186, 187]. When *V. parahaemolyticus* enters the blood stream of the patient, it spreads across the body and causes septicemia. This results in activation of immune responses leading to inflammation and increased vascular permeability, which might further result in hypovolemic shock, multisystem organ failure, and may ultimately lead to death [188].

1.2.3 Pathogenicity associated with *Vibrio parahaemolyticus*:

V. parahaemolyticus harbor several virulence factors like adhesins, thermostable direct hemolysin (TDH) and TDH related hemolysin (TRH), as well as two type III secretion systems, T3SS1 and T3SS2 [189]. In addition to Type III secretion systems and TDH/TRH, *V. parahaemolyticus* contain two different types of flagella for two different functions like swimming and swarming (Fig. 1.12). It also has an ability to produce a capsule surrounding the entire bacteria. These factors collectively mediate the pathogenicity caused by *V. parahaemolyticus* and help the bacteria to survive in different environmental conditions as well as in colonization within the human host [190].

1.2.3.1 Adhesion to host cells

The first and critical step in *V. parahaemolyticus* pathogenesis is initial interaction with the host cells. Bacterial adhesion factors like MAM7 (multivalent adhesion molecule 7), present at the bacterial cell surface, forms contact with the host cell surface followed by secretion of

:

effectors and toxin proteins. The N-terminal region of MAM7 consists of 44 hydrophobic amino acid residues, which play a critical role in accurate localization and anchoring of the bacteria onto the host cells (Fig. 1.12) [191]. The binding of MAM7 to fibronectin and phosphatidic acid present on the host cells lead to the up-regulation of other pathogen-specific and host cell-specific adhesion and virulence factors [192].

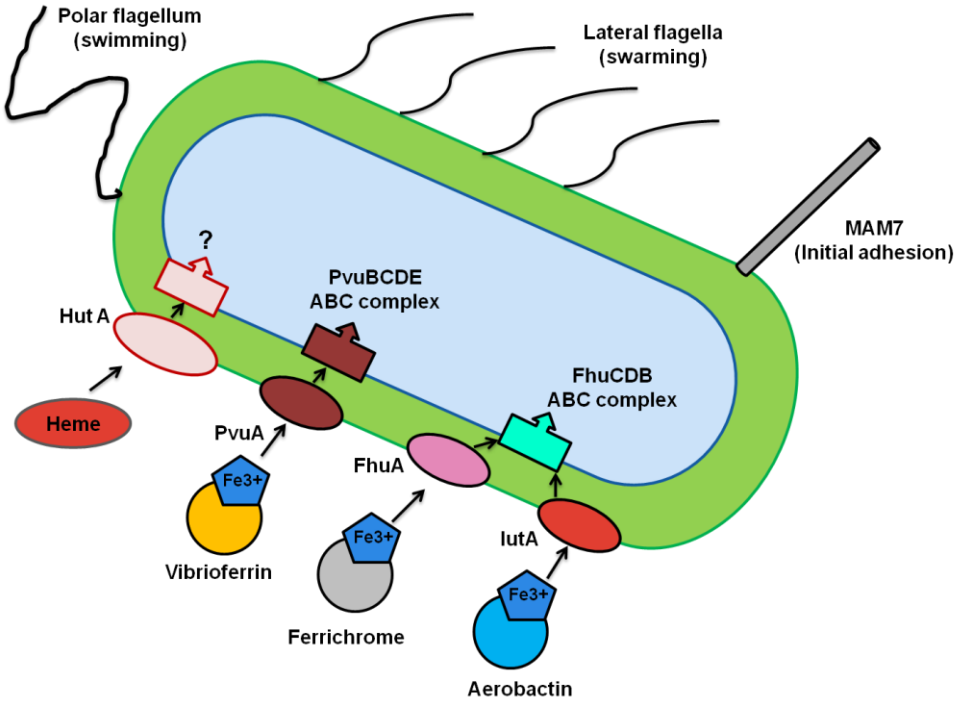

Fig. 1.12: Virulence factors associated with *V. parahaemolyticus:* A single flagellum is present that is required for swimming motility of the bacteria. Lateral flagella are needed for swarming. MAM7 is responsible for mediating the binding of the bacteria to fibronectin and phosphatidic acid, and mediates initial attachment to host cells. *V. parahaemolyticus* contains siderophores like, vibrioferrin, ferrichrome, and aerobactin, along with heme, to extract iron from the external environment, which is required for bacterial growth.

1.2.3.2 Iron acquisition

V. parahaemolyticus require iron for its growth and survival. Inside the host, the bacteria utilize several strategies to acquire iron. In humans, iron is associated with the complexes like transferrin, lactoferrin and hemoglobin [193]. During infection, bacteria use iron chelators called siderophores to scavenge iron from such complexes. Different siderophores are acquired with the help of siderophores membrane receptors. For example, vibrioferrin is acquired with the help of receptor PvuA, ferrichrome by FhuA, and aerobactin by IutA receptors. The

:

ATP-binding cassette (ABC) transporters like pvuBCDE and FhuCDB ABC complexes are required for transporting siderophores across the inner membrane (Fig. 1.12) [194, 195].

1.2.3.3 Toxins

Most of the *V. parahaemolyticus* strains isolated from the patients show the presence of two effector protein toxins, thermostable direct hemolysin (TDH) and TDH-related hemolysin (TRH) (Fig. 1.13). In *V. parahaemolyticus*, TDH and TRH are the two virulence factors which display hemolytic and cytotoxic activity [190]. TDH and TRH-containing bacteria are able to lyse human erythrocytes when plated on high-salt containing media called Wagatsuma agar, a process known as Kanagawa phenomenon (KP). The KP test is used to screen the pathogenic strains of *V. parahaemolyticus*.

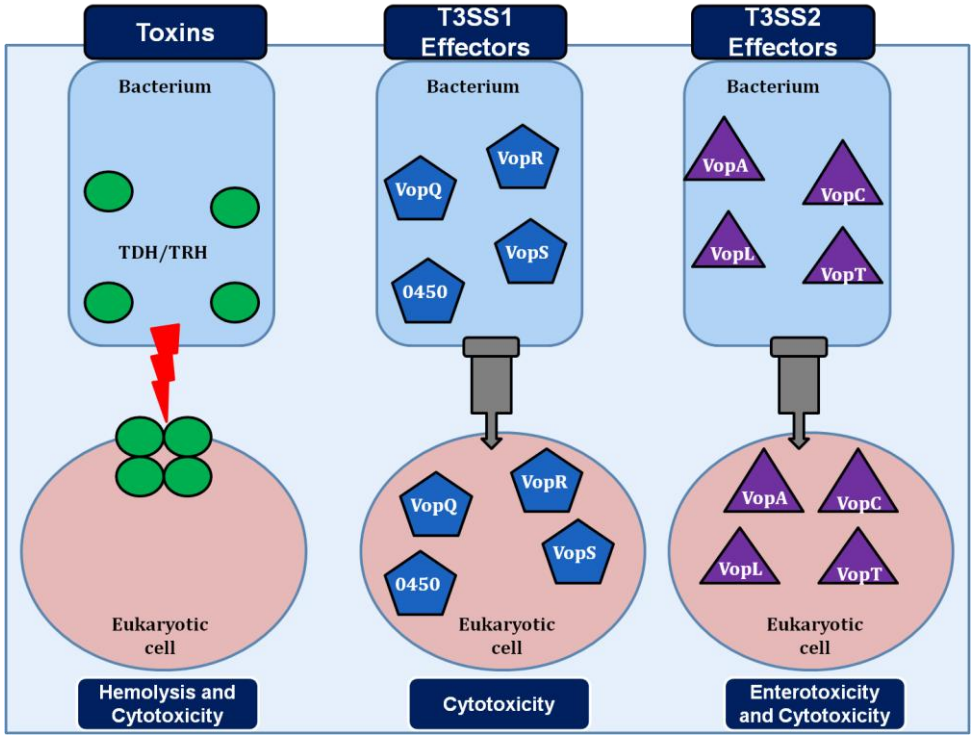

Fig. 1.13: Major toxins and type 3 secreted effector proteins of *V. parahaemolyticus*:
TDH is a secretory toxin which forms pores in the target host cell membrane, leading to hemolysis or cytotoxicity (left panel). Different T3SS1 effector proteins of the bacteria (VopQ, VopR, VopS, and VPA0450) are known to show cytotoxicity in various cell types (middle panel). T3SS2 effector proteins (VopA, VopC, VopL, and VopT) also cause cytotoxicity and enterotoxicity in the host cells (right panel).

:

The *tdh* gene is encoded and co-regulated with the genes of T3SS2 [196]. In *V. parahaemolyticus* RIMD 2210633 (scientific name), there are two copies of the gene for the TDH toxin, vpa1314 (*tdhA*) and vpa1378 (*tdhS*) emphasizing on the importance of TDH on the pathogenicity caused by the bacteria [189]. TDH binds to the cholesterol and sphingomyelin-containing lipid rafts [197]. Disruption of lipid rafts abrogates the cytotoxicity in nucleated cells, but not the hemolytic activity again erythrocytes suggesting two distinct mechanisms for such activities of this toxin [198]. The analysis of the crystal structure of TDH suggests that it forms a tetramer with a central pore of 23 Å in diameter and 50 Å in depth, which allows water and ions to pass through the membrane channel [199]. The mechanism of channel formation results in the colloid-osmotic lysis of the cells. TRH and thermolabile hemolysin (TLH) are also the pore-forming toxins from *V. parahaemolyticus* showing similar cell-killing property like TDH (Fig. 1.13).

1.2.3.4 Type III secretion systems (T3SS) of *Vibrio parahaemolyticus*:

The T3SS of *V. parahaemolyticus* is a complex bacterial organelle, made up of 20-30 different proteins, and it is used to deliver effector proteins directly from the cytoplasm of the bacteria into the cytoplasm of the host cells. The secretion apparatus is a needle-like structure which has a basal body spanning the inner and outer bacterial membranes, an elongated rod-like structure that acts as a channel between the bacterial and eukaryotic cell, and a pore that is inserted in the host cell membrane (Fig. 1.13) [190, 200, 201].

1.2.3.4.1 T3SS1:

T3SS1 is present in all strains of *V. parahaemolyticus* and is one of the major effector systems utilized by the bacteria [202]. During infection, T3SS1 causes cytotoxicity in human cells, but does not cause enterotoxicity as confirmed by rabbit ileal loop model [203]. The major effectors of T3SS1 are VopQ, VopS, and VPA0450 that induce autophagy, membrane blebbing, cell rounding, followed by cell lysis (Fig. 1.14). The different actions of T3SS1 effectors are shown in Fig. 1.14, and are also discussed in Table 2. VopQ induces autophagy in the infected cells, and also prevents phagocytosis of the bacteria. VPA0450 disrupts the cellular integrity by detaching the plasma membranes from the actin cytoskeleton.

:

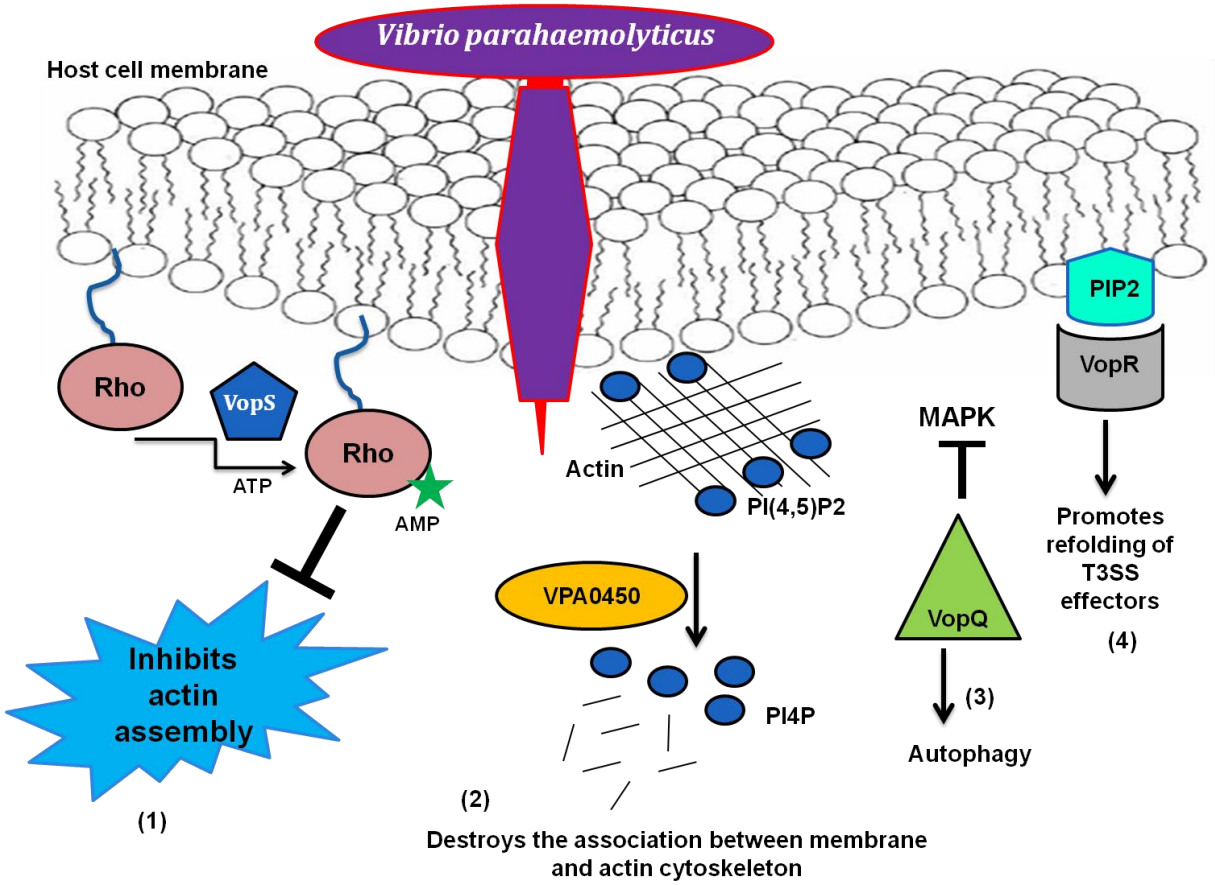

Fig. 1.14 Toxicity of T3SS1 effectors of *V. parahaemolyticus*: VopS effector inhibits Rho protein, thereby causing cell rounding and invasion of phagocytes (1). VPA0450 hydrolyzes phosphatidylinositide (4, 5)-biphosphate to D5 phosphate and destroys the assembly of membrane and active cytoskeleton, thereby causing membrane blebbing (2). VopQ inhibits MAPK pathway and promotes autophagy (3), VopR binds to PIP2 present in the membrane, thus promoting the refolding of the T3SS effectors (4).

VopS prevents actin assembly and destabilizes the actin cytoskeleton, leading to cell rounding and cell shrinkage, which eventually kill the infected cells.

Effectors	Gene	Biological activity	Effects on host cells
Toxins			
TDH	*tdh*	Forms pores on cells	Cytotoxicity and enterotoxicity
TRH	*trh*	Forms pores on cells	Cytotoxicity and enterotoxicity
TLH	*tlh*	Hemolysin activity or?	
T3SS1 effectors			
Vop Q	*vp1680*	Form pores and binds V-ATPase	Autophagy, cell lysis, MAPK activation, IL-8
Vop S	*vp1686*	Inhibition of Rho by AMPylation	Cells rounding, phagocytes invasion
VPA0450	*vpa0450*	Phosphatidylinositol phosphatase	Membrane blebbing, destabilization

:

Vop R	*vp1683*	Binds PIP2 in membrane	Promoting refolding of T3SS effectors
T3SS2 effectors			
Vop A/P	*vpa1346*	Inhibition of MAPK by acetylation of MKK	Blocking of phosphorylation and ATP binding
Vop T	*vpa1327*	Ras ADP-ribosylation	Cytotoxicity and yeast growth inhibition
Vop L	*vpa1370*	Actin nucleation	Stress fibres formation and cell shape changing
Vop C	*vpa1321*	Activation of Rac and CDC42 by deamidation	Invasion of non-phagocytic cells
Vop V	*vpa1357*	Actin-binding and bundling	Enterotoxicity and blunting of villi
Vop Z	*vpa1336*	Inhibition of TAK1 and downstream pathways	Enterotoxicity and colonization
VPA1380	*vpa1380*	Cysteine catalysis dependent on IP6	Toxicity in Yeast

Table 2: List of known virulence factors of V. parahaemolyticus (Adapted from Wang et.al., Frontiers in Microbiology, 2015)

1.2.3.4.2 T3SS2:

T3SS2 is a secretion system encoded by the pathogenicity island (*VP-PAL*) on chromosome II, and can be isolated from the patients infected by *V. parahaemolyticus* [204]. T3SS2 has been known to cause enterotoxicity in rabbit ileal loop, cytotoxicity in intestinal cell lines like CaCO-2 cells, and disruption of tight junction integrity in cultured cell monolayers [203-205]. The major effectors of T3SS2 are Vop C, Vop T, Vop Z, Vop A/P, Vop V, Vop L, and VPA1380. Vop A/P (VPA1346) inhibits cell division by blocking mitogen-activated protein kinase (MAPK) signaling pathway (Fig. 1.15) [206]. Vop L binds and accelerates the formation of polarized actin fibers. It also enhances the process of stress fibers formation independent of Rho GTPase [207]. Vop L also promotes the uptake and invasion of the bacteria by providing a favorable microenvironment for bacterial growth. Vop C disrupts the actin network and enhances bacterial invasion by deamidating glutamine 61 in both Rac and CDC42, resulting in constitutive activation of Rho family GTPases, thereby promoting the infected cells to engulf the bacteria (Fig. 1.15) [208, 209].

:

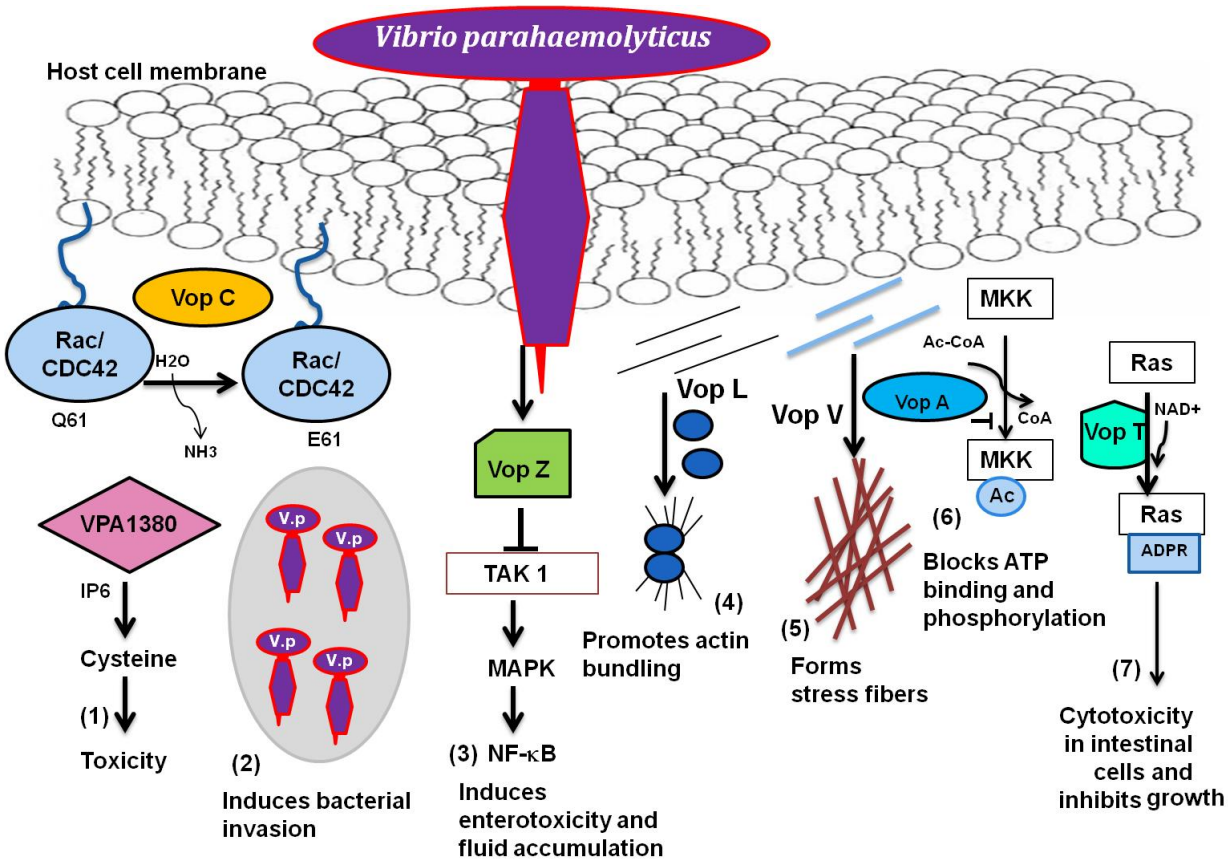

Fig. 1.15: Toxicity of T3SS2 effectors of V. parahaemolyticus: (1) VPA1380 catalyzes it targeted substrate. VopC promotes invasion of the bacteria (2). VopZ induces enterotoxicity and fluid accumulation (3). VopL promotes actin bundling (4). VopV binds to F-actin and promotes the stress fibers formation (5). VopA blocks the binding of ATP and phosphorylation (6). VopT induces cytotoxicity in intestinal cells of the host (7).

Vop T has been known to inhibit the yeast cell growth and shows cytotoxicity in human intestinal cultured cell lines [210]. Vop V promotes accumulation of F-actin filaments thereby facilitating enterotoxicity in rabbit ileal loop models [211]. Vop Z inhibits the activation of TAK1 kinase, which further inhibits the MAPK and NF-κB signaling pathways resulting in fluid accumulation, cellular detachment, and epithelial damage [212]. VPA1380 is a cysteine protease and is possibly involved in the invasion of the bacteria.

1.3 Thermostable direct hemolysin (TDH):

Thermostable direct hemolysin (TDH) is a major virulence factor of *Vibrio parahaemolyticus*, and is responsible for the biological activities like hemolytic activity, cardiotoxicity and enterotoxicity in humans [213-217]. TDH is a 165 amino acid-containing protein which forms

:

pores in the membranes of the target cells (Fig. 1.17A). Therefore, it is designated as a member in the family of pore-forming toxins (PFT). As discussed earlier, the general mechanism of action of PFTs involve the following critical steps: (i) PFTs usually exist as monomer in solution; (ii) binding of the monomeric unit of PFTs to the target host cell membrane via specific receptor; (iii) the conversion of membrane-bound monomeric toxins into oligomeric complexes; (iv) conformational changes in the oligomeric unit of PFTs, which drive membrane insertion of the toxins and transmembrane pore formation. Formation of such transmembrane pores on the host cell membranes leads to colloid-osmotic lysis of the cells. TDH deviates from this general scheme of pore-formation and follows a distinct and unique pathway of cell-killing. As suggested by earlier studies, TDH forms tetrameric assembly in aqueous solution [218]. Crystal structure of TDH also confirms tetrameric assembly of the toxin, which is indispensable for its hemolytic activity (Fig. 1.17B) [199]. The key inter-protomer interactions necessary for oligomerization have been identified: Arg46 is involved in multiple interactions at the oligomeric interface. The guanidium group of Arg46 forms an ion pair with both the carboxyl group of Glu138 and the C-terminal carboxyl group of Gln165 in the adjacent protomer. Also, the guanidium group of Arg46 forms a π-cation interaction with the aromatic ring of Tyr140 in the adjacent protomer [199]. The mechanism of pore-formation in TDH is different from general mode of action of the PFTs. The distinct steps of pore-formation of TDH are proposed to be as follows: (i) TDH exists as a tetramer in solution; (ii) as an oligomer, it binds to the target cell membranes; (iii) after binding, certain conformational changes (as yet unknown) in the toxin leads to membrane insertion and pore formation in the target cell membranes (Fig. 1.16) [218-220].

The identity of the receptor for TDH still remains controversial. There are some studies which suggest that gangliosides G_{T1} (present in neuronal cell membranes and endoplasmic reticulum) is the receptor of TDH. This has been challenged by other studies claiming that ganglioside asialo GM-2 is the most probable membrane receptor [221, 222].

:

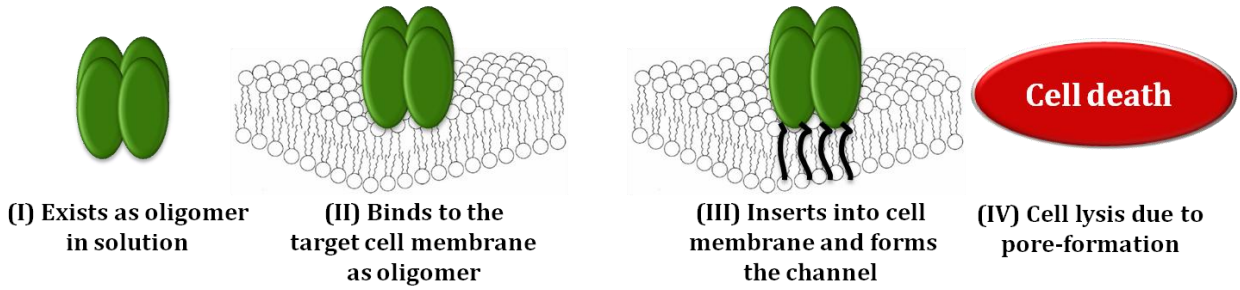

Fig. 1. 16: Steps Involved in pore-formation mechanism of TDH: TDH is present as a tetramer in solution (I); as an oligomer, it binds to the membranes of the target host cells (II); after binding, certain structural changes in the oligomeric assembly drives the membrane insertion and channel formation process (III); due to channel formation, water molecules and ions can pass across the channel leading to colloid-osmotic lysis of the cells (IV).

The functional pore-forming activity of TDH gets inhibited upon heating at 60 ^{o}C due to formation of β-sheets rich, amyloid-like structures [197]. However, it gets converted into unfolded states when heated at higher temperatures (80 ^{o}C), and regains its native structure with functional pore-forming activity, when refolded under fast cooling conditions. Such paradoxical responses to heat treatment is known as Arrhenius effect, and is documented in other toxins like α-hemolysin of *Staphylococcus aureus*, exotoxin of *Pseudomonas aeruginosa*, hemolysins of *Bacillus cereus* and *Klebsiella pneumoniae* [197, 223-226]. The crystal structure of TDH suggests that the mature toxin is rich in β-sheets secondary structure, and adopts a compact β-sandwich core structure (10 β-strands), with two short α-helices (α-1 and 3-$_{10}$ helix) flanking the core (Fig. 1.17A) [199]. The N-terminal region consisting of first 11 amino acid residues is absent in the crystal structure, possibly because of its tendency to adopt multiple conformations. The C-terminal region (CTR) of TDH forms a 3-$_{10}$ helix structure, and is held to the main β-sandwich core domain via a conserved disulphide bond (between C151 and C161 residues) (Fig. 1.17A). Each protomer of TDH faces the other protomer with its CTR present at the protomer:protomer interface, and forms a tetrameric assembly with a central pore of 23 Å in diameter and 50 Å in depth (Fig. 1.17B,C) [199].

:

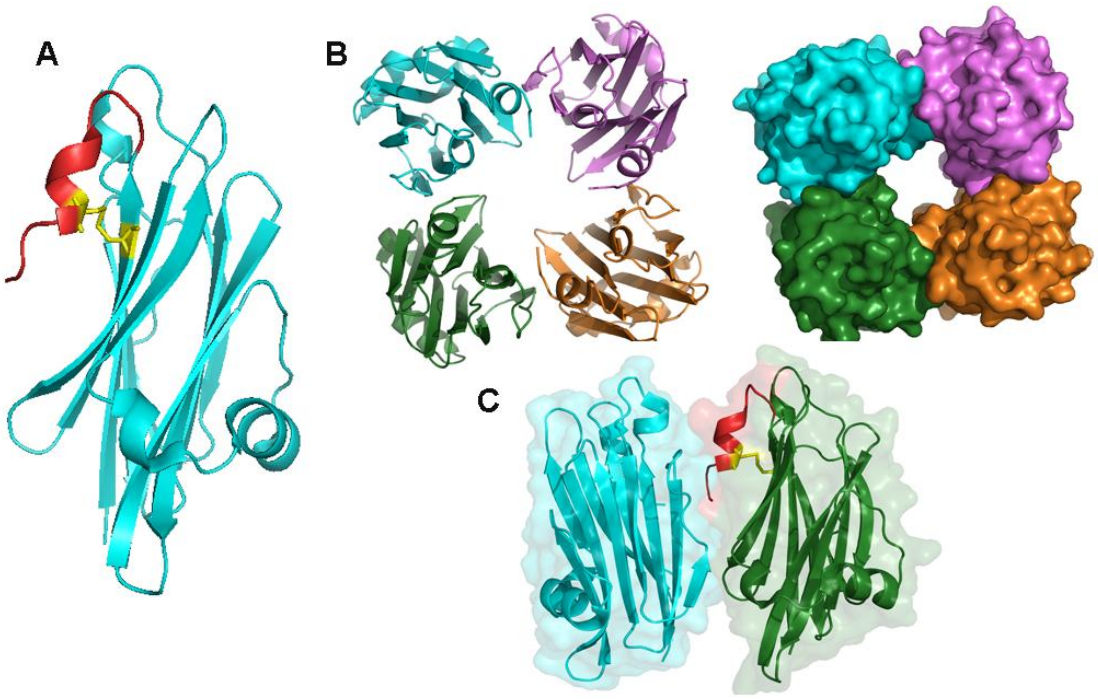

Fig. 1. 17: Structural model of TDH: (A) TDH monomer consisting of a β-sandwich core domain surrounded by short α-helices. The C-terminal region forms a 3_{-10} helix structure (in red) which is anchored to the main body via a disulphide bond (in yellow), (B) oligomeric assembly of TDH forming a central pore, (C) dimeric interface of TDH, each protomer faces other protomer and C-terminal region is present at the oligomeric interface [199].

A similar β-sandwich core domain has also been observed in the eukaryotic PFTs in the actionporin family that includes Equinatoxin II, Fragaceatoxin C, and Sticholysin II [173, 174, 181]. This structural similarity of bacterial PFT TDH, with the eukaryotic actinoporins is very unique (Fig. 1.18). However, despite such structural similarities, there are certain structural differences observed in TDH when compared to the actinoporins. For example: (i) presence of an extended C-terminal region which is absent in actinoporins; (ii) unlike actinoporins (which contains a long ~30-residue N-terminal region with α-helical signature), TDH has a shorter (11-residue long) N-terminal region which is absent in the crystal structure;

:

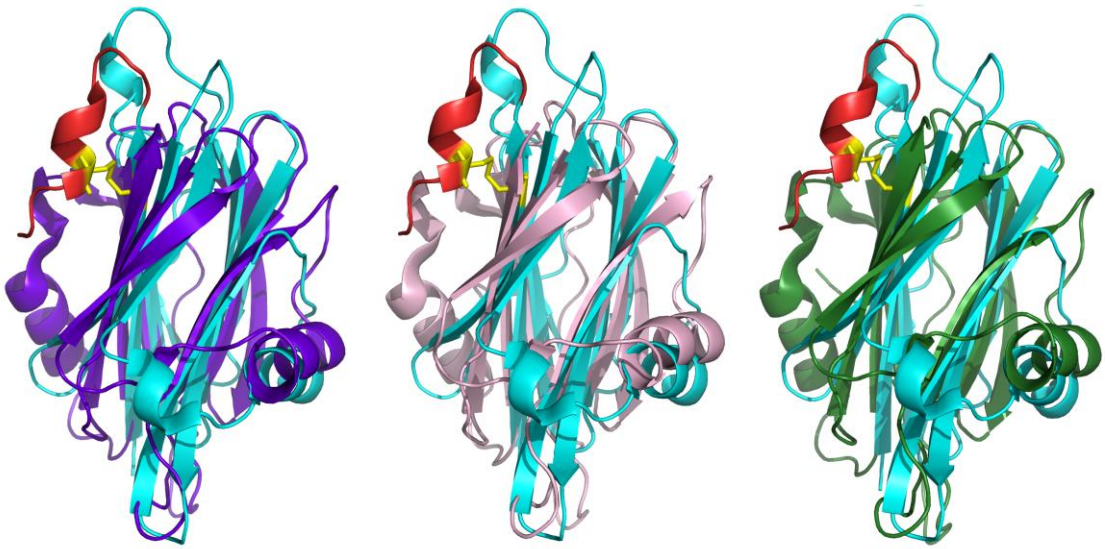

Fig. 1. 18: Structural superimposition of TDH with actinoporins using WinCoot: (A) TDH monomer (in cyan) overlapped with Equinatoxin II (in blue), (B) TDH monomer (in cyan) overlapped with Sticholysin II (light pink), (C) TDH monomer (in cyan) overlapped with Fragaceatoxin C (in green), the extended CTR (in red) and the disulphide bond (in yellow) are present in TDH but absent in actinoporins.

(iii) presence of a conserved disulphide bond between C151 and C161 residues, whereas actinoporins lack any cysteine residues. Also, the solution states of the actinoporins are of monomer, whereas TDH is present as a tetramer in solution.

The present thesis work aimed toward understanding the functional implications of the unique structural features present in TDH that are otherwise not documented in the structurally related PFTs. In particular, the present work intended to unravel the role of different structural motifs of TDH (like, flexible N-terminal region, and the unique C-terminal region) in the mode of action of TDH.

:

1.4 Specific objectives:

Toward determining the structure-function relationship of thermostable direct hemolysin (TDH), the present thesis work aimed to explore two specific objectives:

1. To elucidate the implications of the C-terminal region (CTR) of TDH in the structure-function mechanism of the toxin.

2. To explore the role of the N-terminal region (NTR) of TDH in the membrane-damaging activity of the toxin.

The present thesis work provided novel insights regarding the role of the CTR in regulating the oligomerization mechanism of TDH. Also, the present work elucidated the implications of the NTR for the membrane-damaging cell-killing action of TDH. Altogether, the present thesis work provided critical new insights regarding the functional implications of some of the unique structural features present in TDH for the mode of action of this atypical bacterial PFT.

:

Chapter 2

Implications of the C-terminal region (CTR) of TDH in the structure-function mechanism of the toxin*

***This part of the study has been published as: Kundu, N**., Tichkule, S., Pandit, S. B., & Chattopadhyay, K. (2017). Disulphide bond restrains the C-terminal region of thermostable direct hemolysin during folding to promote oligomerization. *Biochemical Journal*, *474*(2), 317-331.

:

Chapter 2

Implications of the C-terminal region (CTR) of TDH in the structure-function mechanism of the toxin

2.1 Abstract

Pore-forming toxins (PFTs) are typically produced as water-soluble monomers, which upon interacting with target cells assemble into transmembrane oligomeric pores. *Vibrio parahaemolyticus* thermostable direct hemolysin (TDH) is an atypical PFT that exists as a tetramer in solution, prior to membrane binding. The TDH structure highlights a core β-sandwich domain similar to those found in the eukaryotic actinoporin family of PFTs. However, the TDH structure harbors an extended C-terminal region (CTR) that is not documented in the actinoporins. This CTR remains tethered to the β-sandwich domain through an intra-molecular disulphide bond. Part of the CTR is positioned at the interprotomer interface in the TDH tetramer. Here we show that the truncation, as well as mutation, of the CTR compromise tetrameric assembly, and the membrane-damaging activity of TDH. Our study also reveals that intra-protomer disulphide bond formation during the folding/assembly process of TDH restrains the CTR to mediate its participation in the formation of inter-protomer contact, thus facilitating TDH oligomerization. However, once tetramerization is achieved, disruption of the disulphide bond does not affect oligomeric assembly. Our study provides critical insights regarding the regulation of the oligomerization mechanism of TDH, which has not been previously documented in the PFT family.

:

2.2 Introduction

Thermostable direct hemolysin (TDH) is a major virulence factor of *Vibrio parahaemolyticus*. During the course of *V. parahaemolyticus* infection, TDH is secreted by the bacteria and causes cell death by generating pores onto the target cell membranes [215-217]. TDH shows multiple distinct biological activities that include enterotoxicity, cardiotoxicity and hemolytic activity [186, 214, 217, 218, 227]. TDH shows structural similarity with the eukaryotic pore-forming toxins (PFTs) in the actinoporin family, i.e., Equinatoxin II, Fragaceatoxin C, and Sticholysin II [173, 174, 181, 199]. Previous structure-function studies suggest that TDH follows a distinct mechanism of action within the PFT family. The general steps in the pore-formation mechanism of the PFTs are as follows: (i) secretion of the toxin as a monomeric molecule, (ii) binding of the monomeric toxin onto the surface of the plasma membrane of the target cells, (iii) oligomerization of the toxin on the plasma membrane of cells, and (iv) insertion of the specific structural motif from the toxin oligomers into the cell membrane to form the transmembrane pores thereby causing the cell death [58, 61, 120, 127-129, 143, 145]. In contrast to this generalized mode of action, TDH appears to follow distinct mechanism of action. TDH forms a terameric assembly in solution that subsequently binds to the target cell membrane [218]. PFTs in the actinoporin family, which show structural similarity to TDH, exist as monomer in solution, and form functional oligomers only upon binding to the target cell membrane [171]. The mechanism that regulates the oligomerization mechanism of TDH in solution has remained unclear. Previous studies highlighted key interacting residues at the oligomerization surface of TDH, the mutation of which has been found to disrupt the tetrameric assembly of the toxin in solution [199]. However, implications of the additional structural motifs, that might be operational in the regulation of the tetrameric assembly of TDH, have remained obscure.

Crystal structure of TDH shows a tetrameric assembly of the toxin, where each of the toxin protomer is composed of a core β-sandwich domain [199]. Crystal structure of TDH also shows presence of an extended C-terminal region (CTR) at the C-terminal end of the β-sandwich domain. This CTR (157SFFECKHQQ165) forms a 3_{10}-helix structure, and it is not an integral part of its β-sandwich core [199]**.** The CTR of each protomer is positioned at the inter-protomer interface of

:

the tetrameric assembly of TDH. Also, several amino acid residues within the CTR appear to participate in making the interactions with the neighboring protomer. However, it remains unknown whether the CTR indeed plays any role in the oligomerization process of TDH. From the crystal structure, it is also observed that the CTR of each of the TDH protomer is tethered against the core β-sandwich domain via an intra-protomer disulphide bond formed between the two Cys residues (C151 and C161). Implication of such "disulphide-locked" structural disposition of CTR of TDH also remains unexplored. Notably, such extended CTR, and the presence of the intra-protomer disulphide bond that tethers the CTR against the main body if the toxin core, are absent in the structurally related actionoporin family of PFTs. Therefore, in this part of the present study, we examined the implications of the CTR for the structure-function mechanism of TDH.

2.3 Material and methods

2.3.1 PCR amplification and cloning of the nucleotide constructs of the TDH variants into the pET-14b vector

Nucleotide sequences encoding the TDH variants were amplified by polymerase chain reaction (PCR)-based approach using the wild-type construct as the template. The PCR cycle conditions used were as follows:

1) Initial denaturation for 5 min at 94 °C

2) Denaturation for 30 sec at 94 °C
3) Annealing for 30 sec at 54 °C
4) Amplification for 1.30 min at 68 °C
} 30 X

5) Final extension for 7 min at 68 °C

The PCR-amplified product was digested with Xho1 and BamH1 restriction enzymes for 3 h at 37 °C followed by short heat inactivation step at 80 °C for 5 min. The digested PCR product was separated on 1% agarose gel by electrophoresis and the band corresponding to the amplified product was extracted (using the Gel Extraction Kit; Qiagen). The ligation reaction of the digested product was set by using 50 ng of pET-14b vector (digested) with 27 ng of the insert (digested PCR product) for 1 h at 25 °C. The ligated product was transformed into TOP10 cells (Novagen) and the recombinants were screened on Ampicillin (50

:

μg/ml)-containing plate. The positive colonies containing the gene of interest were confirmed by colony PCR, and the recombinant plasmid was isolated from the respective colony grown in an overnight culture. The DNA sequence of the recombinant construct was confirmed by DNA sequencing.

	Primer	Sequence (5'-3')
1	TDH FW 5'	ATATTGCTCGAGATGTTTGAGCTTCCATCTGTCCC
2	TDH RC 3'	AACATTGGATCTTATTGTTGATGTTTACATTCAAAAAACGAT
3	Del 157-165_3'RC	AACTAAGGATCCTTATTCTTTGTTGGATATACACATTACCAATATATT
4	Q164A_3'RC	CGGGCTTTGTTAGCAGCCGGATCCTTATTGGGCATGTTTACATT
5	Q165A_3'RC	CGGGCTTTGTTAGCAGCCGGATCCTTAGGCTTGATGTTTACATT
6	Q164A-Q165A_3'RC	CGGGCTTTGTTAGCAGCCGGATCCTTAGGCGGCATGTTTACATT
7	F159A_3'RC	AACTAAGGATCCTTATTGTTGATGTTTACATTCGGCAAACGATTCTTT
8	Y53A_5'FW	TACAAAGATGTTGCCGGTCAATCAGTATTCACAACGTCAG
9	Y53A_3'RC	TACTGATTGACCGGCAACATCTTTGTACGGTTTTCTTTTT

2.3.2 Protein expression and purification

2.3.2.1 Protein purification from the soluble fraction of the bacterial cell lysate:

The nucleotide sequence coding for the wild-type *Vibrio parahaemolyticus* thermostable direct hemolysin (TDH) was cloned into the pET-14b expression vector (Novagen) between the Xho1 and BamH1 sites. All the constructs for the mutated/truncated variants of TDH were generated via the PCR-based approach as described above, and were also cloned in the pET-14b bacterial expression vector. The pET-14b expression vector allowed incorporation of $(His)_6$-tag at the N-terminal end of the recombinant proteins. Recombinant pET-14b vector harboring the constructs of the TDH variants were transformed into the *Escherichia coli* Origami B cells (Novagen) for protein expression. The transformed *E. coli* Origami cells were inoculated for a small-scale seed culture in LB medium supplemented with ampicillin (50 μg/ml), and were grown overnight at 37 °C with shaking at 180 rpm. The overnight seed culture was inoculated for large scale (1 liter) culture in LB broth medium (2% of LB medium volume) supplemented with ampicillin (50 μg/ml), at 37°C, until the mid-log growth phase

:

(corresponding to OD600 = 0.5) with continuous shaking at 180 rpm. Protein expression was induced with 1 mM IPTG (Isopropyl β-D-1-thiogalactopyranoside), and the culture was grown for additional three hours at 30 °C with continuous shaking. The bacterial cells were then harvested by centrifugation at 2700 x g for 30 minutes in a hanging bucket centrifuge, followed by resuspension in 10 ml of PBS [20 mM sodium phosphate buffer containing 150 mM NaCl (pH 7.5)], supplemented with bacterial protease inhibitor cocktail (Sigma). Cells were then lysed by ultrasonic disruption using a Mesonix Ultra-Sonicator with twenty pulses of thirty seconds, with ten seconds interval between each pulse, at amplitude of 20, followed by high-speed centrifugation at 18, 000 × g for 20 minutes at 4 °C. The supernatant (soluble) fraction of the cell lysate was collected, adjusted with 20 mM imidazole (prepared in PBS), was passed through Ni-NTA agarose column (Qiagen) pre-equilibrated with PBS. The loosely bound, non-specific proteins were removed by washing the Ni-NTA column with 50 ml of the 20 mM imidazole in PBS. The tightly bound His-tagged protein was eluted with 300 mM imidazole in PBS.

The eluted protein from Ni-NTA was diluted four-fold with 10 mM Tris-HCl buffer (pH 7.5) and subsequently was loaded onto Q Sepharose Fast Flow (GE Healthcare/Amersham) resin (pre-equilibrated with 10 mM Tris-HCl buffer (pH 7.5). The loosely bound non-specific proteins were removed by giving a wash with 10 mM Tris-HCl buffer containing 100 mM NaCl (pH 7.5). The specifically bound protein was eluted using 10 mM Tris-HCl buffer containing 500 mM NaCl (pH 7.5). Purified His-tagged protein was analyzed by SDS-PAGE/Coomassie staining.

2.3.2.2 Protein purification from inclusion bodies:

For purification of TDH via refolding from the inclusion body fraction, *E. coli* Origami B cells containing the constructs were grown till mid-log growth phase (corresponding to OD_{600} = 0.5), as described above. Protein expression was induced with 1 mM IPTG. In order to increase the yield of the inclusion body fraction, after the induction the cells were grown at 37 °C for 3 h in the presence of 1 mM IPTG. When TDH was recombinantly overexpressed in the heterologous expression system in *E. coli*, a significant part of the overexpressed protein was present in the form of insoluble inclusion bodies. Cells were lysed by ultrasonic disruption

:

followed by centrifugation at 18, 000 x g, and the pellet fraction containing the insoluble inclusion bodies was harvested. The pellet containing inclusion bodies was washed with the lysis buffer [10 mM Tris-HCl, 100 mM NaCl, 0.5% Triton X-100, 1 mM EDTA (pH 8)] with or without 10 mM DTT (dithiothreitol) to remove the unlysed cells. Finally, one wash was given with the same buffer without Triton X-100. The washed pellet fraction containing the inclusion bodies was solubilized under denaturing conditions in 8 M urea in 10 mM Tris-HCl buffer (pH 8), in the presence or absence of 10 mM DTT. The solubilized denatured protein was refolded by dialysis against the refolding buffer [10 mM Tris, 150 mM NaCl (pH 7.5)], with or without 10 mM DTT. Denatured protein extraction from the inclusion body followed by refolding in the presence of DTT would block formation of the intra-molecular disulphide bond in TDH, while absence of the reducing agent DTT would allow formation of the disulphide bond. High speed centrifugation at 16,000 × g for 15 min was done to remove the aggregated proteins generated during the refolding process, and the supernatant was passed through a 0.22 μm syringe filter. Finally, the purity of the refolded protein was confirmed by SDS-PAGE/ Coomassie staining analysis. Protein concentrations were determined by monitoring the absorbance at 280 nm, using the theoretical extinction coefficient based on the amino acid composition of the protein.

2.3.3 Removal of the His-Tag from the recombinant proteins:

Expression of the recombinant TDH variants from the pET-14b expression vector incorporated a tag of 6 Histidine residues at the N-terminal end of the recombinant protein. The N-terminal $(His)_6$-tag from the purified protein was removed by proteolysis with thrombin (Sigma-Aldrich). The $(His)_6$-tagged TDH variants were incubated with thrombin for 2 h at 37°C (1 unit thrombin/250 μg protein) and the reaction was stopped with 1 mM Phenyl Methyl Sulfonyl Fluoride (PMSF). The processed protein was further purified by passing through the Q Sepharose Fast Flow resin. Purity of the protein and the cleavage of His-tag was confirmed by monitoring the difference in the migration pattern of the corresponding protein bands by SDS-PAGE/ Coomassie staining. The protein concentration was estimated by monitoring the absorbance at 280 nm, using the theoretical extinction coefficient based on the amino acid composition of the protein.

:

2.3.4 Far-UV circular dichroism (CD) measurements

The important secondary structural information of proteins can be determined by far-UV circular dichroism (CD) spectroscopy. Far-UV CD spectra of the TDH variants were recorded on a Chirascan spectropolarimeter (Applied Photophysics, Leatherhead, Surrey, UK) equipped with a peltier-based temperature-controlled sample chamber, using a quartz cuvette of 5 mm pathlength. All the samples were dialysed for overnight with intermittent changes against 1 mM Tris-HCl buffer, pH 7.5. Far-UV CD spectra of the refolded proteins were taken in 1 mM Tris-HCl buffer, pH 7.5 with or without 0.1 mM TCEP [tris(2-carboxyethyl)phosphine hydrochloride]. The protein concentration used for collecting the spectra were in the range of 1 -3 μM. All the protein spectra were corrected for the baseline by subtracting with the corresponding buffer spectra.

2.3.5 Intrinsic tryptophan fluorescence emission measurements

Intrinsic tryptophan fluorescence spectra of the TDH variants (in 1 mM Tris-HCl buffer, pH 7.5) were recorded on a Fluoromax-4 spectrofluorimeter (Horiba Scientific, Edison, NJ) equipped with a peltier-based temperature controller. The spectra were collected upon excitation at 290 nm, and the tryptophan fluorescence emission spectra were recorded between 310-400 nm. The excitation and emission slit widths were 2.5 nm and 5 nm, respectively. The final concentration of the protein used for the measurement was 2 μM. For the refolded proteins, spectra were collected in 1 mM Tris-HCl buffer, pH 7.5, with or without 0.1 mM TCEP.

2.3.6 Hemolytic activity assay to monitor pore-forming activity of the TDH variants

The membrane-damaging pore-forming cytolytic activity of the TDH variants were determined against the human erythrocytes (suspended in PBS; corresponding to OD_{600} ~0.9) by measuring the release of hemoglobin (hemolytic activity assay), spectrophotometrically at 415 nm, over a period of 1 h at 37 °C [130]. The hemolytic activity plot was obtained by increasing concentration of toxin ranging from 0-1.5 μM incubated with human erythrocytes in a 100 μl reaction volume. Data represent the average ± standard deviation determined from the three

:

independent treatments. The pore-forming activity of TDH under reducing conditions was monitored in PBS containing 1 mM DTT. The presence of an equivalent quantity of DTT in the buffer without protein (control) did not cause any hemolysis indicating the lytic activity is not caused by DTT but by the protein toxin.

2.3.7 Sedimentation velocity analytical ultracentrifugation

WT-TDH exists as tetramer in-solution. Oligomerization of TDH is important for functional pore-formation. Different solution oligomerization states of wild type TDH and its variants were examined by sedimentation velocity analytical ultracentrifugation (AUC) on a Beckman Coulter ProteomeLab XL-I analytical ultracentrifuge equipped with an An-50 Ti 8-hole rotor. In the channels of a two-channel centerpiece (Epon charcoal-filled) with 12 mm path length, 380 µl of sample and 400 µl of the reference buffer (10 mM Tris-HCl, 500 mM NaCl, pH 7.5) were taken. Absorbance scans were collected while spinning the rotor at 42,000 or 40,000 rpm at 20 °C, using the continuous scan mode without any time delay between the scans. A total of 300 scans were taken. Data was analyzed using the continuous c(S) distribution model with the program SedFit. Data were presented using the plot of c(S) (sedimentation coefficient distribution) on Y-axis versus the sedimentation coefficient [S] on X-axis (expressed in the svedberg unit). Partial specific volume, buffer density, and viscosity values were determined using the Sednterp server available online (http://sednterp.unh.edu/) and were used during the data analysis in SedFit [228]. For assessing the sedimentation velocity AUC profile of TDH under reducing conditions, an experiment was performed in 10 mM Tris-HCl buffer, 500 mM NaCl, pH 7.5, containing 0.1 mM TCEP. TCEP does not absorb at 280 nm hence no false positive signals were obtained due to the presence of TCEP. Same buffer except the protein samples served as the blank.

2.3.8 Size exclusion chromatography

Size exclusion chromatography is one of the conventional techniques to determine the protein oligomerization states. Therefore, information related to the different oligomerization states of TDH and its mutant variants was confirmed by performing size exclusion chromatography using a XK16/40 column packed with Superdex 200 resin (GE Healthcare Life Sciences). Size

:

exclusion chromatography was performed on an AKTA Purifier platform (GE Healthcare). Superdex 200 resin allows the separation of proteins ranging from 10 kDa to 600 kDa. Superdex 200 column was equilibrated with the 10 mM Tris-HCl buffer (pH 7.5) with a flow rate of 0.5 ml/min. Each of the test proteins (TDH variants; 1 ml at a concentration of ~60 μM) was loaded onto the column, and was allowed to separate at a flow rate of 0.5 ml/min. The fractions (1 ml) were collected, and analyzed by SDS-PAGE/Coomassie staining to confirm the presence of the TDH variants in the different fractions. Assembly states of the TDH variants were estimated by monitoring their corresponding elution profile, as compared to the elution profile of the molecular weight markers. The column was calibrated with the following molecular weight markers: Blue Dextran 2000 [2000 kDa; eluting at the void volume (V_o) = 26.9 ml], aprotinin (6.5 kDa; eluting at 59.8 ml), and carbonic anhydrase (29 kDa; eluting at 50.6 ml).

2.3.9 Flow cytometry-based assay to monitor binding of the TDH variants with human erythrocytes:

Binding of the TDH variants to the human erythrocyte cell membrane was determined by a flow-cytometry-based assay [129, 229]. Human erythrocytes were washed multiple times with PBS, and the pellet was resuspended in PBS containing 10 mM dextran (average molecular weight of dextran was 9000–11000, Sigma-Aldrich). The cells were diluted and were counted on hemocytometer. Human erythrocytes (10^6 cells) were then treated with the TDH variants in PBS-dextran, pH 7.5, for 1 h at 37 °C. Final concentration of the toxin used for binding experiment was 1 μM. After incubation with the toxin, the cells were washed with PBS-dextran to remove unbound protein. Cells bound with the TDH variants were then treated with anti-TDH antibody (polyclonal antibody raised in rabbit) for 30 min at 37 °C. Unbound anti-TDH antibody was removed by giving three washes with PBS-dextran. The cells were then treated with FITC (fluorescein isothiocyanate)-conjugated goat anti-rabbit antibody for 30 min at 37 °C. Unbound FITC-conjugated antibody was removed by washing the cells three times with PBS-dextran. Cells were finally resuspended in PBS-dextran, and the extent of fluorescence was determined by acquiring the cells on a FACSCalibur (BD Biosciences) flow cytometer. The FITC fluorescence signal was directly correlated with the extent of binding of

:

the TDH variants with the human erythrocytes.

2.3.10 DTNB experiment:

The free sulfhydryl groups in the refolded form of the TDH variants were determined by using a water-soluble reagent 5, 5'-dithio-bis-(2-nitrobenzoic acid)(DTNB; Ellman's reagent). DTNB reacts with the free thiol groups to form a yellow-colored complex 2-nitro-5-thiobenzoic acid (TNB), which can be read spectrophotometrically at 412 nm. DTNB solution was prepared freshly (4 mg/ml) in 10 mM Tris-HCl, pH 7.5 buffer, containing 1 mM EDTA. 1 μM of protein was incubated with DTNB for 15 min at room temperature, and the yellow-colored product formation was monitored spectrophotometrically at 412 nm. The extent of color produced was directly proportional to the free sulphydryl groups present in the protein.

2.3.11 Analysis of protein structural models

Protein structural coordinate of TDH was obtained from the Protein Data Bank (PDB) [PDB code: 3A57]. Protein structural co-ordinates of the eukaryotic pore-forming toxins from the actinoporin family (that are structurally similar to TDH), Equinatoxin II (PDB code: 1IAZ), Sticholysin II (PDB code: 1GWY), and Fragaceatoxin C (PDB code: 3VWI) were also obtained from the PDB. The extent of structural similarity was visualized from the structural superimposition of TDH with the different actinoporins, Equinatoxin II, Sticholysin II and Fragaceatoxin C using the program WinCoot [230]. All the protein structural models were visualized -using the program PyMOL [DeLano, W. L. (2002) The PyMOL Molecular Graphics System, found online (www.pymol.org)].

2.4 Results

2.4.1 Analysis of crystal structure of TDH and its comparison with those of the actinoporin family of PFTs:

The crystal structure of TDH (PDB: 3A57) consists of a β-sandwich core which is flanked by two short α-helices. The mature TDH consists of 165 amino acids, and a single conserved disulphide bond present at the C-terminal region (between Cys151 and Cys161) [199]. TDH shares high structural similarity with eukaryotic pore-forming toxins (PFTs), actinoporins, e.g.

:

Equinatoxin II (PDB code: 1IAZ) secreted by *Actinia equina*, Fragaceatoxin C (PDB code: 3VWI) secreted by *Actinia fragacea*, Sticholysin II (PDB code: 1GWY) secreted by *Stichodactyla helianthus*. The structural comparison of TDH monomer with actinoporins suggests that the central β-sandwich core domain of TDH is similar to those of the actinoporins. However, the extended C-terminal region (CTR) of TDH that adopts extra short 3_{10}-helix configuration is unique, and is absent in the actinoporins. This CTR is tethered against the main β-sandwich domain via a single disulphide bond present between Cys151 and Cys161 residues (Fig. 2.1).

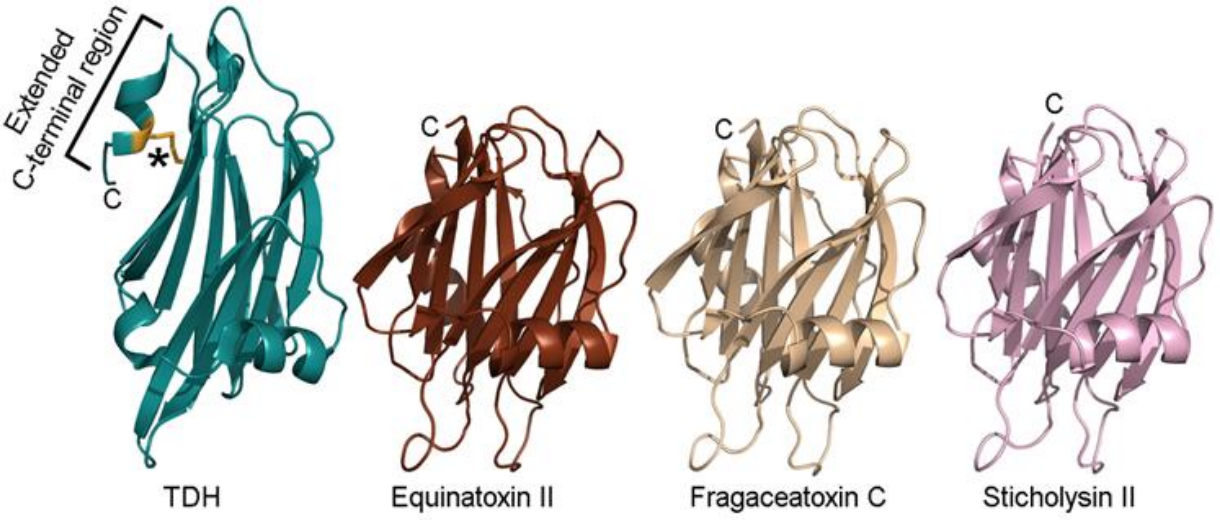

Fig. 2.1: Structural comparison of TDH with the members of actinoporin family like Equinatoxin II, Fragaceatoxin C and Sticholysin II. TDH structure highlights an extended C-terminal region, which is disulphide bonded to the main β-sandwich core. Such unique structural features like extended C-terminal tail and disulphide bond are absent in actinoporins.

The amino acid sequence alignment of TDH secreted by various bacteria in the Vibrio species like *Vibrio parahaemolyticus*, *Vibrio alginolyticus*, *Vibrio mimicus*, *Grimontia hollisae* and *Vibrio cholerae* suggests that the position of cysteine residues (C151 and C161) which form the disulphide bond is conserved across the species. (Fig. 2.2) Such unique structural features like an extended C-terminal tail and the intra-protomer disulphide bond are not present in the actinoporins which indicate that these features are unique in TDH.

:

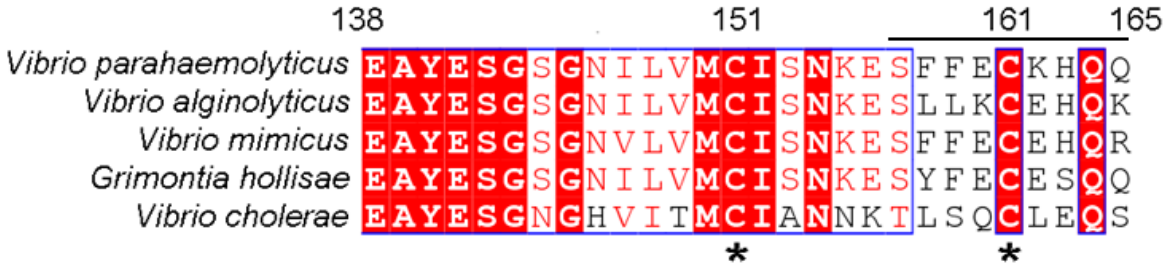

Fig. 2.2: The amino acid sequence alignment of *V. parahaemolyticus* TDH with the TDH secreted by different bacteria. The black line above the sequence is of CTR from V. parahaemolyticus and the conserved cysteine residues (C151 and C161) are marked with *.

2.4.2 Analysis of the structural model of TDH tetramer and identification of possible interactions at the oligomeric interfaces.

The crystal structure of TDH (PDB code: 3A57) shows that the protein adopts a tetrameric assembly [199]. The crystal structure also highlights some of the important amino acid residues involved in the interactions between the two neighboring protomers (Arg46 from one protomer interacting with Tyr140 from the neighboring protomer. Mutations of these residues have been found to disrupt the oligomer formation by TDH in solution [199]. Crystal structure of TDH, however, highlights several additional features that might play roles in the oligomerization mechanism of TDH. Analysis of the crystal structure shows that the C-terminal region (CTR; 157SFFECKHQQ165) of TDH is not an integral part of the core β-sandwich domain of the toxin, and it protrudes out from the main body of the toxin. Part of this CTR adopts a 3_{10}-helix configuration. Also, the CTR is positioned at the oligomeric interface where one protomer is interacting with the neighboring protomer. An intra-molecular disulphide bond between C151 and C161 residues appears to lock the CTR to the β-sandwich core domain (Fig. 2.3A).

Further analysis of the CTR at the inter-protomer interface of TDH tetramer shows that a number of polar and aromatic/hydrophobic residues within the CTR are engaged in interactions with the residues from the neighboring protomer (Fig. 2.3B).

:

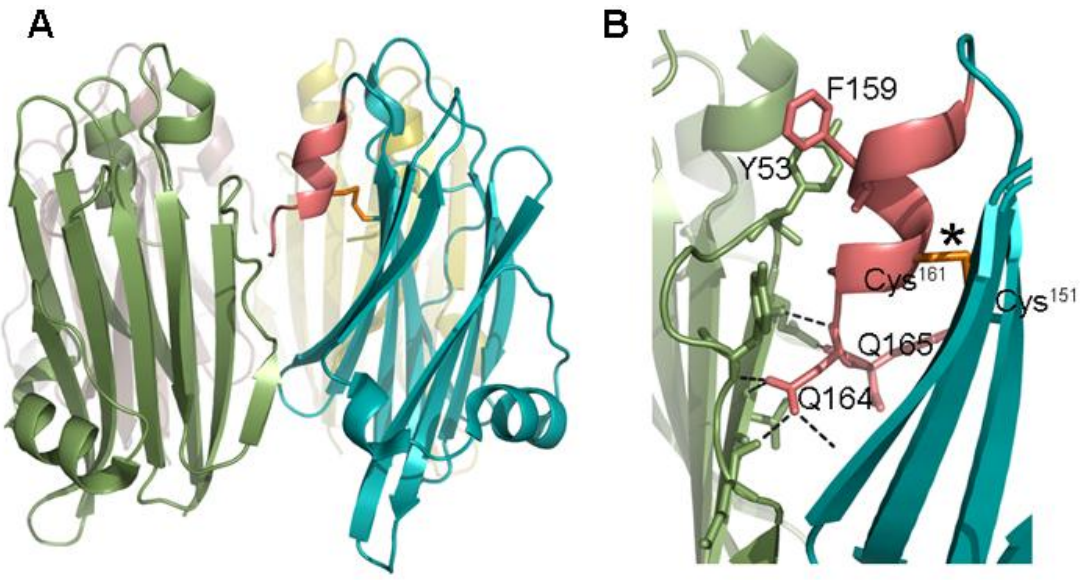

Fig 2.3: (A) The tetrameric assembly of TDH highlighting the positioning of CTR (red) at the inter-protomer interface. The disulphide bond (pale orange) which locks the CTR to the β-sandwich domain is also shown. (B) Zoomed view of the possible interactions mediated by the CTR with the neighboring protomer. The disulphide bond between C151 and C161 is highlighted with *.

The amino acid residues of CTR that are found to make possible interactions with the neighboring protomer are F159, Q164 and Q165. F159 present in CTR seems to be interacting with Y53 present in the neighboring protomer via hydrophobic interaction. Q164 and Q165 are seemed to be involved in hydrogen bond interactions with the peptide bond and side chain of the amino acid residues present in the adjacent protomer. All these interactions at the oligomeric interface via CTR highlight a strong possibility of CTR playing a significant role in oligomerization of the toxin. As mentioned earlier, such unique structural features (CTR and disulphide bond), and the above-mentioned interactions are absent in the actinoporins which remain monomer in solution. Altogether, the information obtained from the literature and the crystal structure of TDH prompted us to investigate the structure-function mechanism of CTR in the mode of action of TDH.

2.4.3 Purification and structural characterization of TDH-ΔCTR$^{157–165}$

In order to explore the function of CTR in the structure-mechanism of TDH, we constructed a truncated variant of TDH (TDH-ΔCTR$^{157–165}$) lacking the CTR (Fig. 2.4A). The construct

:

corresponding to the wild type TDH (WT-TDH) shown in the figure below depicts a short helix (red colored) at the C-terminal end representing the CTR. The TDH-ΔCTR$^{157–165}$ construct lacks the motif corresponding to the CTR (157SFFECKHQQ165). The TDH-ΔCTR$^{157–165}$ was expressed in *E. coli* origami cells, and was purified from the soluble fraction of the cell lysate. The mutant was purified to homogeneity and the size of the protein was confirmed on SDS-PAGE/Coomassie staining (Fig. 2.4B).

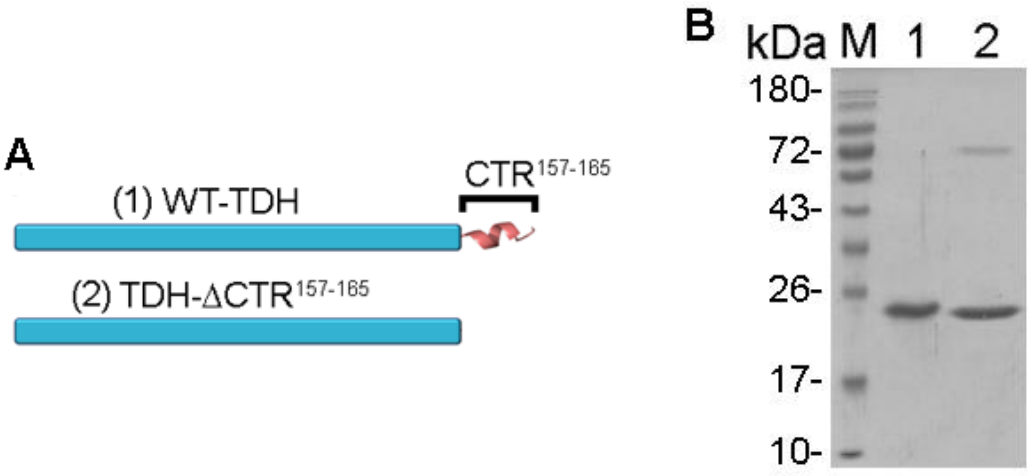

Fig. 2.4: (A) The cartoon representation of the constructs WT-TDH consists of a short helix (red) at the C-terminal end. The construct of mutant lacks this short helix consisting of residues from 157-165. (B) SDS-PAGE coomassie staining profile of WT-TDH (lane 1) and TDH-ΔCTR$^{157–165}$ (lane 2). Marker is represented in lane M

2.4.4 Comparison of functional pore-forming activity of WT-TDH and TDH-ΔCTR$^{157–165}$

In order to investigate the role of CTR (residues 157-165) in the membrane-damaging pore-forming activity of TDH, we incubated human erythrocytes with the WT-TDH and TDH-ΔCTR$^{157–165}$. The tendency of the TDH and its variant to make pores in the target erythrocyte membranes was observed by treating the human erythrocytes with different concentrations of the proteins for 1 h at 37°C. The extent of hemoglobin release from the cells (hemolytic activity) due to the membrane-damaging pore-forming activity of the toxin variants was assessed spectrophotometrically, and was correlated to the functionality of the proteins (Fig. 2.5).

:

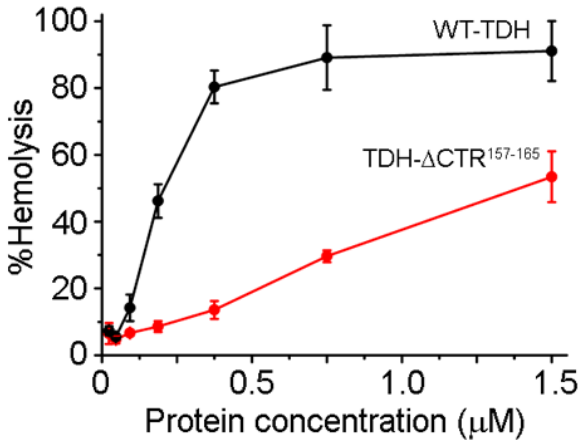

Fig. 2.5: Membrane-damaging hemolytic activity profile of WT-TDH and TDH-ΔCTR$^{157–165}$ against human erythrocytes.

When compared with the hemolytic activity profile of the wild-type toxin (WT-TDH), TDH-ΔCTR$^{157–165}$ displayed significantly reduced hemolytic activity against human erythrocytes. At a concentration of 0.375 μM, TDH-ΔCTR$^{157–165}$ exhibited 13.5% hemolytic activity, as compared to the 80% hemolytic activity displayed by WT-TDH. At 0.75 μM concentration, TDH-ΔCTR$^{157–165}$ showed <30% activity, while WT-TDH showed ~90% hemolytic activity. Altogether this data suggested that the truncation of CTR abrogated the functional pore-formation activity of the toxin to a drastic extent.

2.4.5 Characterization of secondary and tertiary structural organization of TDH-ΔCTR$^{157–165}$

Deletion of the CTR affected the membrane-damaging pore-forming activity of TDH. Therefore, we wanted to examine whether the deletion of the CTR affected the secondary and/or tertiary structural organization of the truncated protein. For this, we examined the far-UV CD (as the signature of secondary structural organization) and intrinsic tryptophan fluorescence emission profile (as the signature of overall tertiary structural organization) of the truncated protein, and compared them with those of the wild type protein. In the far-UV CD experiments, both WT-TDH and TDH-ΔCTR$^{157–165}$ showed nearly overlapping ellipticity profile (Fig. 2.6A). This data suggested that the truncation of CTR did not affect the overall

:

secondary structural organization of the toxin. Next, we monitored the intrinsic tryptophan fluorescence emission profile of TDH-ΔCTR$^{157–165}$ to examine any possible change in the environment of the tryptophan residues present in the truncated mutant (as the signature of any change in the overall tertiary structural organization of the protein). In this experiment, both WT-TDH and TDH-ΔCTR$^{157–165}$ showed nearly similar and overlapping tryptophan fluorescence emission profile suggesting that the truncation of CTR from TDH did not affect the overall folding and tertiary structural organization of the protein (Fig. 2.6B). Altogether these data confirmed that the truncation of CTR from TDH did not trigger any noticeable change in the overall secondary and tertiary structural organization of the protein.

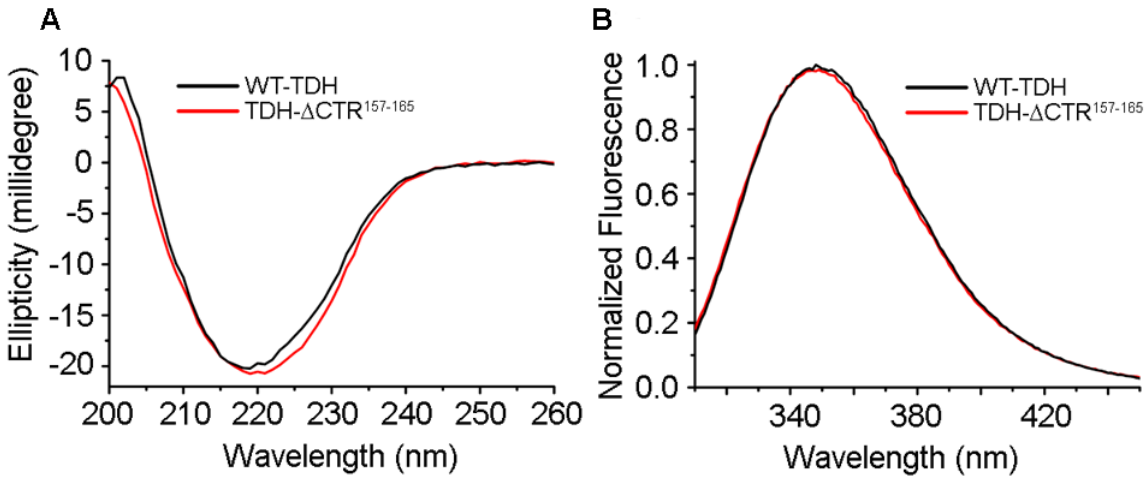

Fig. 2.6: (A) Far-UV CD spectra profile of WT-TDH and TDH-ΔCTR$^{157–165}$. (B) Normalized intrinsic tryptophan emission spectra of WT-TDH and TDH-ΔCTR$^{157–165}$.

2.4.6 Determination of the quaternary structural organization of the truncated form of TDH lacking the CTR

In the crystal structure of TDH tetrameric assembly, the C-terminal region (CTR) of the protein is found to be positioned at the inter-protomer interface, and is also found to make prominent interactions with the neighboring protomer, using a number of aromatic/hydrophobic and/or polar interactions. Based on such observations, we wanted to investigate whether the CTR played any crucial role in the oligomerization of the toxin. For this, we monitored the solution oligomerization tendency of the truncated form of TDH (TDH-ΔCTR$^{157–165}$) by sedimentation velocity analytical ultracentrifugation (AUC) experiment. The AUC profile showed that the major population of TDH-ΔCTR$^{157–165}$ existed

:

as monomer in solution, whereas, consistent with the earlier reports, WT-TDH existed as tetramer in solution (Fig. 2.7).

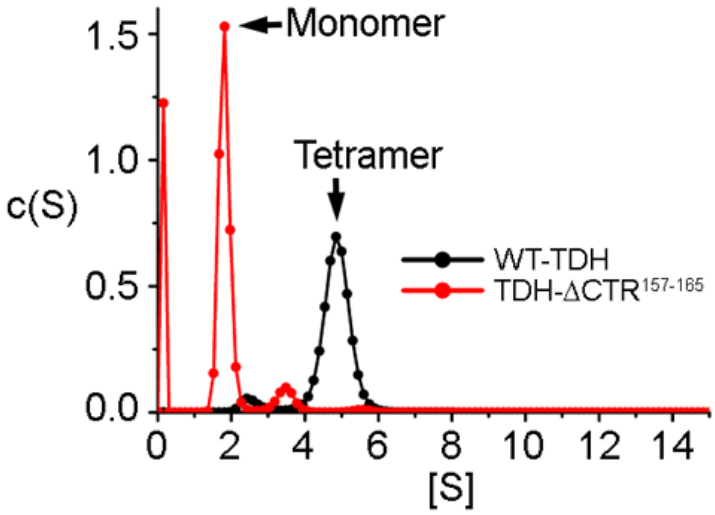

Fig. 2.7: Sedimentation velocity AUC profile of WT-TDH and TDH-ΔCTR$^{157–165}$

For WT-TDH, the plot of sedimentation coefficient distribution, c(S), gave the major peak at around a sedimentation coefficient value ([S]) of 4.8, corresponding to a tetrameric state of the protein. For TDH-ΔCTR$^{157–165}$, c(S) plot showed the major peak at around a sedimentation coefficient value of 1.8, corresponding to a monomeric state, along with a very small peak corresponding to the tetrameric state of the truncated protein. Altogether, this data suggests that the truncation of CTR from TDH abrogated the solution tetrameric assembly of the TDH.

In order to further confirm the solution monomeric state of TDH-ΔCTR$^{157–165}$, we performed size-exclusion chromatography. The WT-TDH, being in its oligomeric state (high molecular weight), came into early fraction, at around 46.3 ml. On the other hand, TDH-ΔCTR$^{157–165}$ eluted in latter fraction, at around 52.6 ml, indicating the truncated mutant to be of lower molecular weight species (corresponding to the size of the monomeric protein) (Fig. 2.8). Size-exclusion chromatography column of Sephacryl S-200 was calibrated with the molecular weight markers. The void volume (V_o) of the column was estimated by passing Blue Dextran 2000 (corresponding to the molecular weight 2000 kDa). Elution volume of Aprotinin (Molecular mass of 6.5 kDa) is also indicated in the chromatogram.

:

In sum, the sedimentation velocity AUC and size-exclusion chromatography data confirmed that the truncation of the CTR abolished the ability of TDH to form the tetrameric assembly in solution.

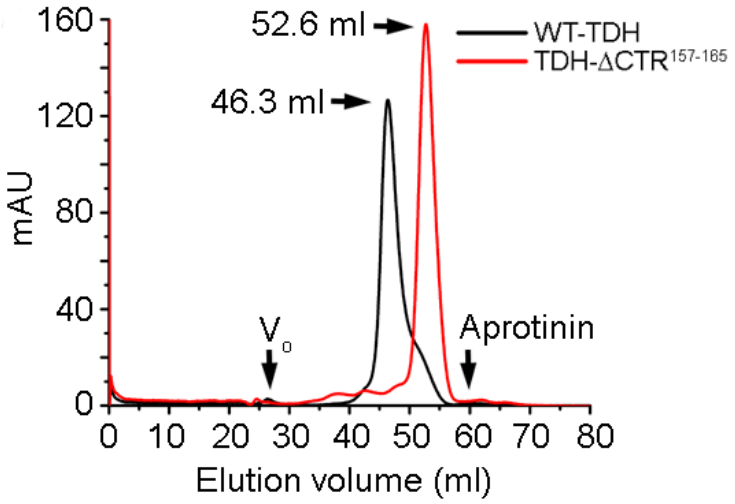

Fig. 2.8: Size-exclusion chromatography profile of WT-TDH and TDH-ΔCTR$^{157–165}$.

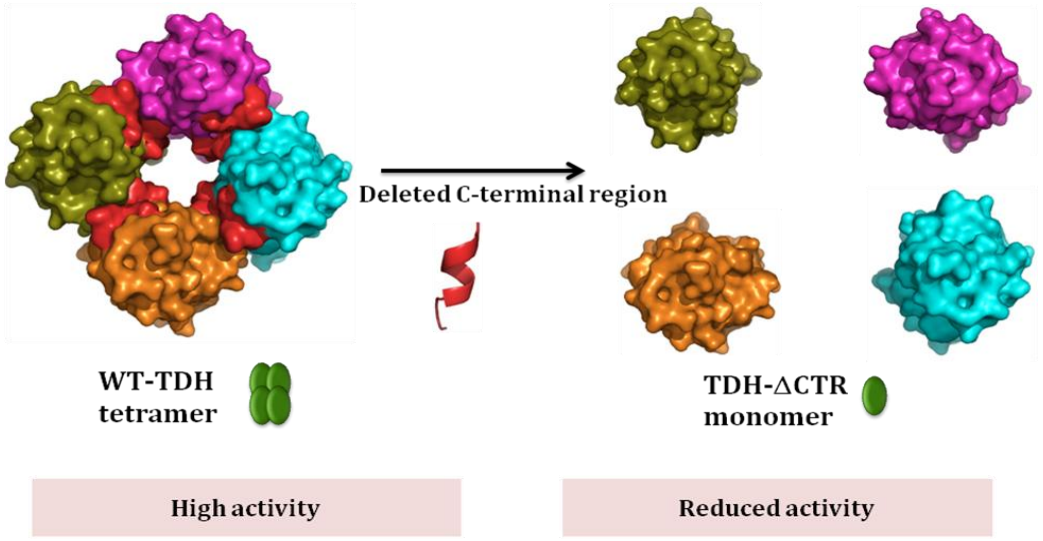

Fig. 2.9: Major effect of CTR: Cartoon representation of TDH tetramer highlighting CTR (red). Removal of CTR abrogates oligomerization and protein exists as monomer with reduced activity.

:

2.4.7 Truncation of CTR compromises the membrane-binding ability of TDH against human erythrocytes

We found that the truncation of CTR from TDH disrupted the solution oligomerization of the toxin, and the truncated protein existed as monomer in solution. The tendency to make pores on the target cells was significantly reduced for this truncated mutant of TDH. We next wanted to know if this loss in functionality was due to the reduced membrane-binding ability of TDH-ΔCTR$^{157–165}$. For this we tested the binding ability of TDH-ΔCTR$^{157–165}$ with the human erythrocytes by using flow cytometry-based assay. The flow cytometry data suggested that the binding ability of TDH-ΔCTR$^{157–165}$ was significantly reduced, as compared to WT-TDH (Fig. 2.10).

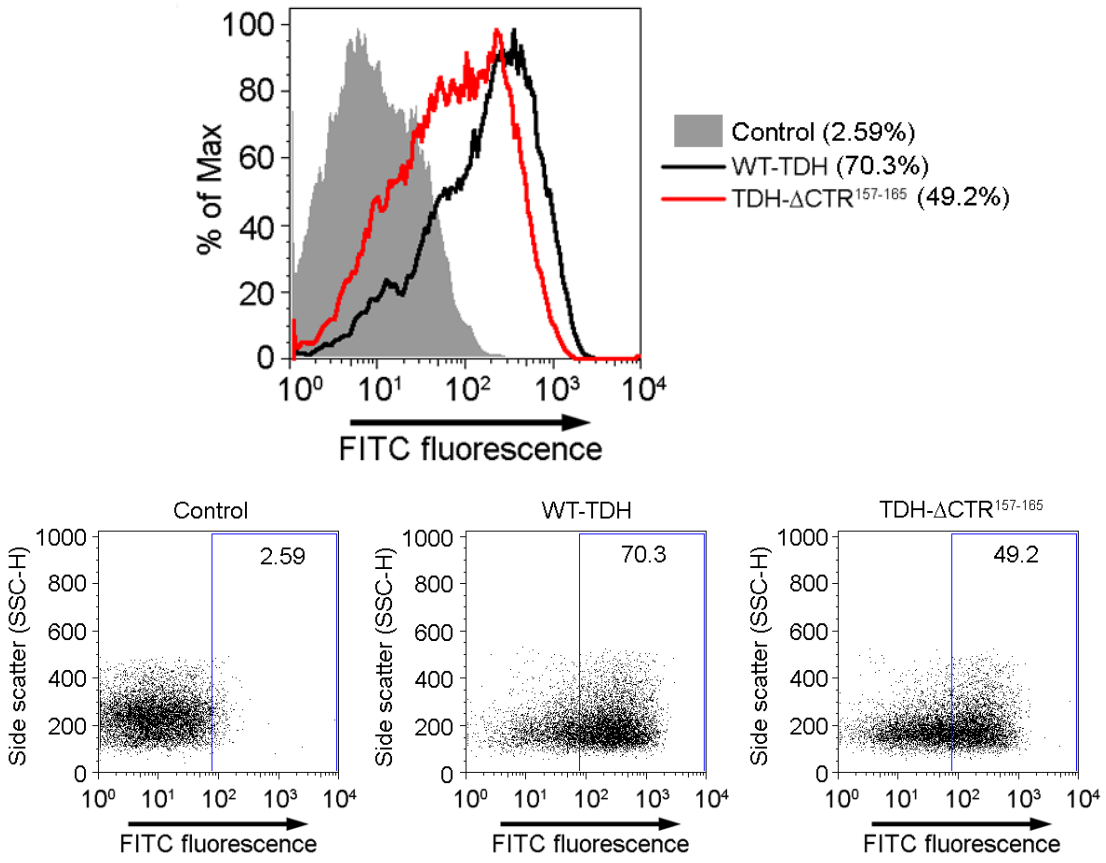

Fig. 2.10: Binding of WT-TDH (black line) and TDH-ΔCTR$^{157–165}$ (red line) with human erythrocytes determined by the flow cytometry-based assay.

This data clearly suggested that being monomer, there was a significant loss in the membrane-binding ability of TDH-ΔCTR$^{157–165}$, and this observation explained the loss in the

:

hemolytic activity of TDH-ΔCTR$^{157–165}$. In other words, deletion of the CTR not only affected the oligomerization ability of TDH, but it also affected the membrane-binding efficacy of the protein, and thus leading to the compromised functionality of the truncated toxin.

2.4.8 Mutation of the aromatic amino acid residue within the CTR does not affect the functional pore-forming activity and solution oligomerization of TDH

Analysis of the crystal structure of TDH suggests that the side chain of Phe159 present within the CTR makes hydrophobic stacking interaction with Tyr53 from the neighboring protomer (at the oligomeric interface). To investigate if this interaction plays any significant role in the oligomerization of the toxin via CTR, we introduced single point mutation of Phe159Ala and Tyr53Ala in TDH. We wanted to examine if these mutations disrupt the functional membrane-damaging pore-forming activity of the toxin. To assess any change in the functional pore-forming ability of the mutants, we performed hemolytic activity assay with human erythrocytes at 37 °C for 1 h by using different toxin concentration (Fig. 2.11).

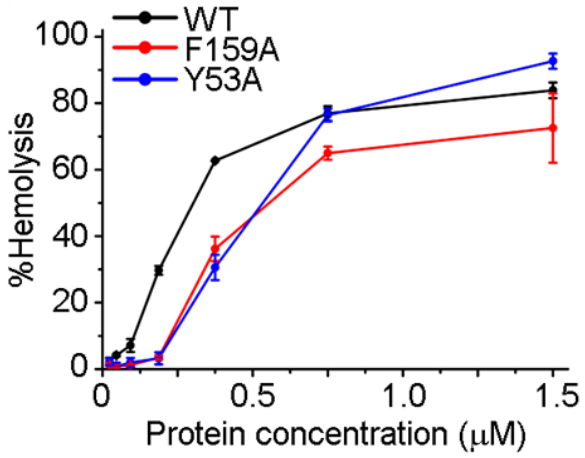

Fig. 2.11: Membrane-damaging hemolytic activity profile of WT-TDH, Phe159Ala and Tyr53Ala against human erythrocytes

Both the mutants (Phe159Ala-TDH and Tyr53Ala-TDH) showed almost similar hemolytic activity profile as compared to WT-TDH. At 1.5 μM protein concentration, Phe159Ala showed 70% of activity while Tyr53Ala showed close to 80% of the activity, which is almost similar to

:

80% of WT-TDH activity. This data suggested that the interactions between Phe159 and Tyr53 do not play any significant role in the functional pore-formation by TDH.

Next, we wanted to examine if the interaction between Phe159 and Tyr53 play any significant role in the oligomerization mechanism of the toxin. For this, we performed sedimentation velocity AUC and size-exclusion chromatography to monitor their solution oligomeric state. The AUC profile showed that the major population of both the mutants existed as tetramer in solution, with a very small population being present in the monomeric state (Fig. 2.12). This data suggested that the interaction between Phe159 and Tyr53 do not play any crucial role in the solution oligomerization of the toxin.

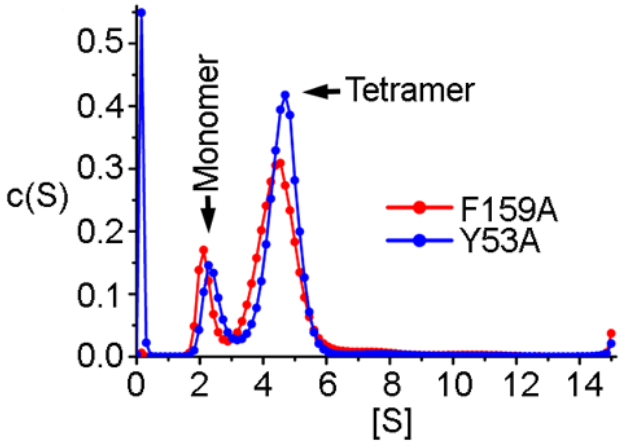

Fig. 2.12: Sedimentation velocity analytical ultracentrifugation profile of WT-TDH, Phe159Ala and Tyr53Ala

In order to further confirm the solution tetrameric state of Phe159Ala-TDH and Tyr53Ala-TDH, we performed size-exclusion chromatography. The WT-TDH, being in its tetrameric state, eluted at around 46.3 ml. Phe159Ala-TDH and Tyr53Ala-TDH showed nearly similar elution profile as compared to that of WT-TDH; Phe159Ala-TDH and Tyr53Ala-TDH eluted around 50 ml and 48.2 ml, respectively (Fig. 2.13). Such elution profile confirmed the tetrameric states of Phe159Ala-TDH and Tyr53Ala-TDH, similar to that of WT-TDH.

:

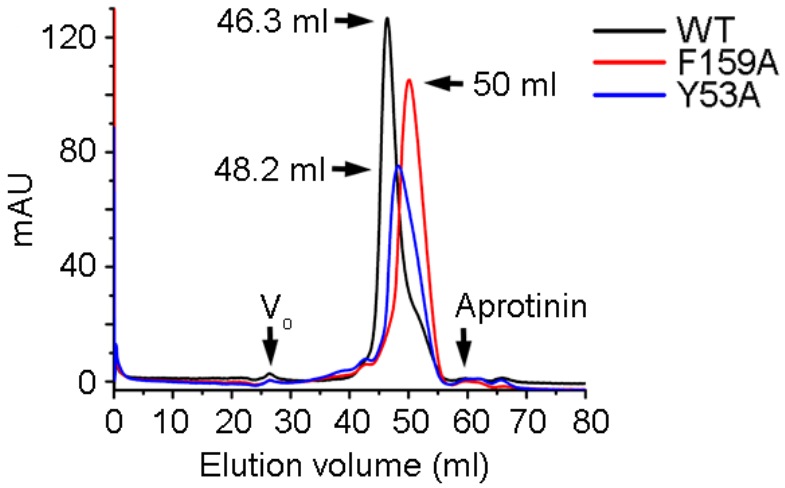

Fig. 2.13: Size-exclusion chromatography profile of F159A and Y53A mutants as compared to that of wild-type TDH (WT). Elution volumes of Blue Dextran 2000 (Vo, void volume) and aprotinin (6.5 kDa) are also indicated.

Altogether, these data suggested that the hydrophobic interaction between Phe159, located within the CTR from one protomer, and Tyr53 from the neighboring protomer at the oligomeric interface are not critical for maintaining the solution oligomers.

2.4.9 Mutation of Gln164Ala within the CTR disrupts solution oligomerization and membrane-damaging pore-forming activity of TDH.

Analysis of the crystal structure showed that the CTR interacts with the neighboring protomer via another important residue, Gln164. From the crystal structure, it appears that Gln164 (within the CTR) is involved in multiple interactions with the adjacent protomer at the oligomeric interface. Therefore, we wanted to explore whether Gln164 plays any role in the oligomerization mechanism of TDH. To test this hypothesis, we generated a mutant variant of TDH harboring mutation of Gln164Ala, and tested its membrane-damaging activity and solution oligomerization ability. When tested for its membrane-damaging activity against the human erythrocytes, Gln164Ala-TDH showed significant compromised hemolytic activity (Fig. 2.14).

:

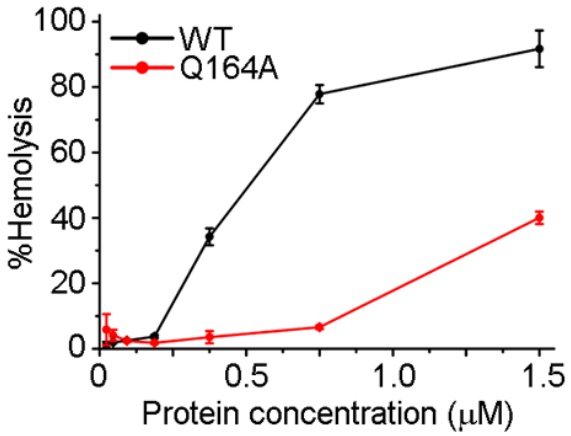

Fig. 2.14: Membrane-damaging hemolytic activity of Gln164Ala-TDH and WT-TDH against human erythrocytes.

At a concentration of 0.375 μM, WT-TDH showed 40% of hemolytic activity whereas Gln164Ala shows around 5% of the activity. When the toxin concentration was increased to 0.75 μM, WT-TDH showed 80% hemolysis, while Gln164Ala-TDH showed 10% activity. Altogether, this data suggests that a single point mutation of Gln164Ala within the CTR abrogated the functional pore-forming activity of the toxin to a significant extent.

Next, we examined whether this drop in functionality was due to disruption of the oligomeric assembly of the mutant. To test this possibility, we assessed the sedimentation velocity AUC and size-exclusion chromatography profile of Gln164Ala-TDH. The AUC profile of Gln164Ala-TDH showed that the mutant existed exclusively as monomer in solution (Fig. 2.15). The profile showed a single peak corresponding to the sedimentation coefficient value of ~2, corresponding to that of a monomeric species.

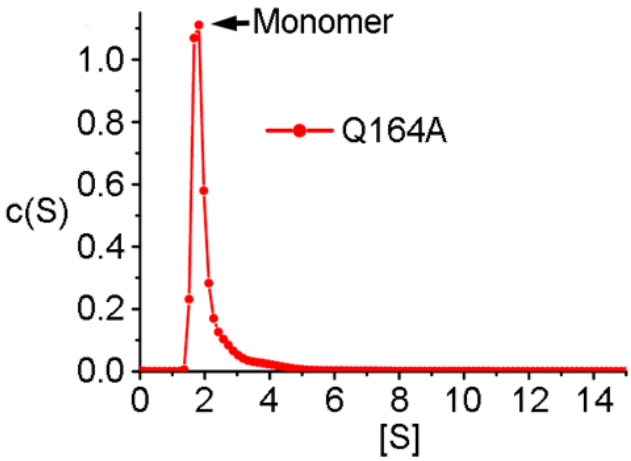

Fig. 2.15: Sedimentation velocity AUC profile of Gln164Ala mutant of TDH (Q164A)

:

We also performed the size-exclusion chromatography to confirm the monomeric state of Gln164Ala (Fig. 2.16).

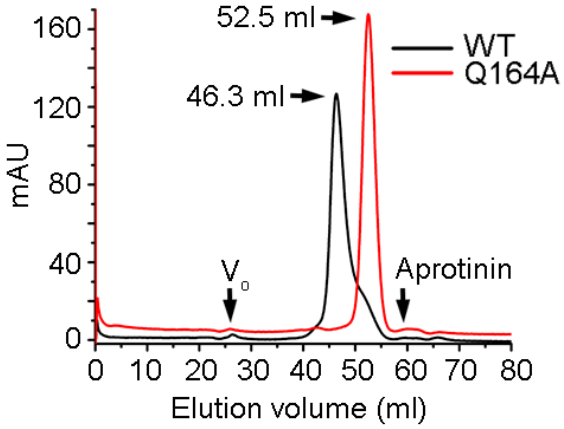

Fig. 2.16: Size-exclusion chromatography profile of Gln164Ala mutant (Q164A)

Gln164Ala-TDH eluted at around 52.5 ml from the size-exclusion chromatography column, while the tetrameric form of WT-TDH eluted at 46.3 ml. This elution profile of Gln164Ala-TDH suggested reduced molecular assembly of the mutant protein in solution. Altogether, these results confirmed a critical role of Gln164 residue, present within the CTR, in the solution oligomerization mechanism of the toxin. We wanted to examine if the loss in membrane-damaging activity and solution oligomerization ability of the toxin was due to any change in the secondary and tertiary structural features of the toxin. For this we examined far-UV CD and intrinsic tryptophan fluorescence emission profile of the mutant (Fig 2.17A).

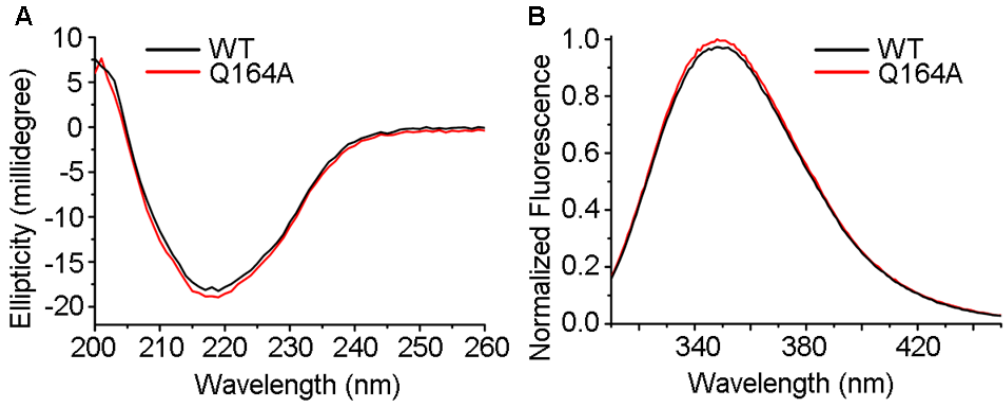

Fig. 2.17: (A) Far-UV CD spectra of WT and Q164A. (B) Normalized intrinsic tryptophan fluorescence emission spectra of WT and Q164A.

:

Gln164Ala-TDH showed nearly similar and overlapping far-UV CD and intrinsic tryptophan fluorescence emission profile as observed with the wild type TDH protein, suggesting that the single point mutation in CTR of Gln164Ala did not affect the overall secondary and tertiary structural organization of the protein (Fig. 2.17B).

2.4.10 Mutation of Gln164Ala within the CTR compromises membrane-binding ability of the toxin.

The mutation of Gln164Ala critically abrogated the functional pore-forming activity and solution oligomerization ability of TDH. We next wanted to know if this drop in functionality was due to reduced membrane-binding ability of Gln164Ala-TDH. For this we tested the binding ability of Gln164Ala with the human erythrocytes by using flow cytometry-based assay. The flow cytometry data suggested that the binding ability of Gln164Ala-TDH was critically compromised as compared to WT-TDH (Fig. 2.18).

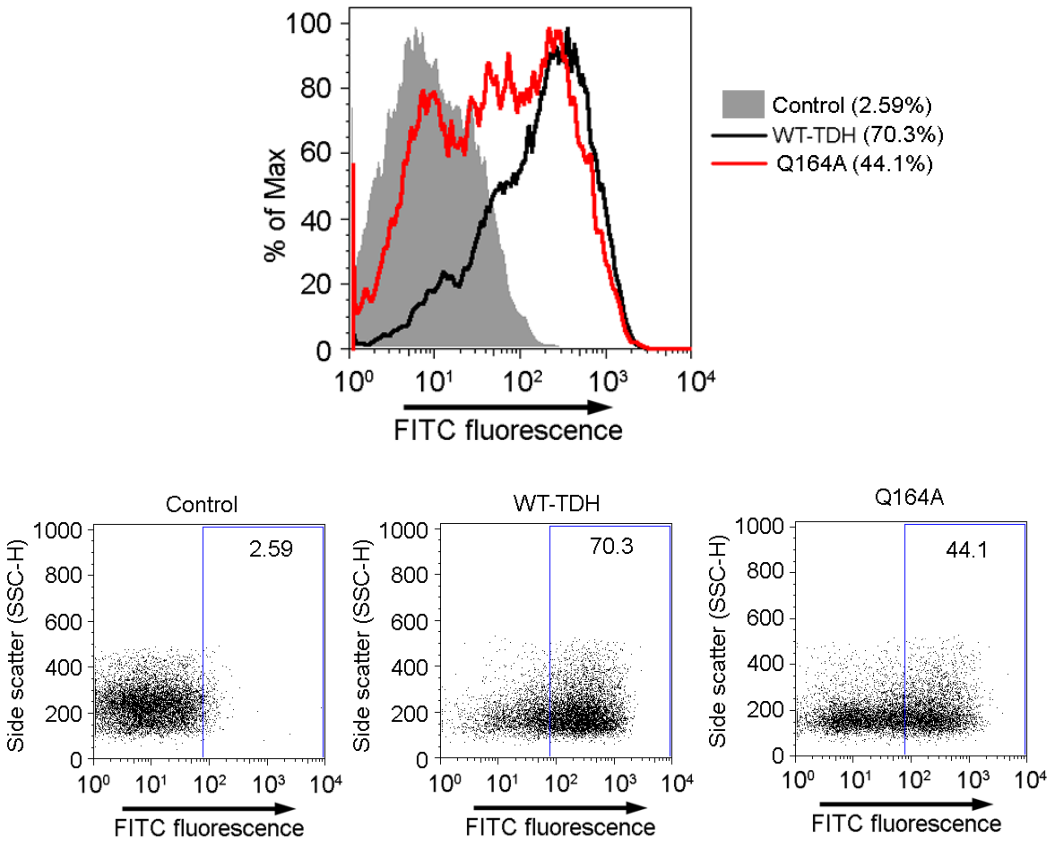

Fig. 2.18: Binding of WT-TDH (black line) and Gln164Ala (red line) with human erythrocytes as determined by the flow cytometry-based assay.

:

When compared with the percentage of target cells bound with the toxin, we observed that 70.3% of cells were bound with the WT-TDH as compared to 44.1% of cells were bound with Gln164Ala-TDH. This data clearly suggested that Gln164Ala-TDH, being monomer, showed compromised membrane-binding ability, which further explained reduced hemolytic activity of Gln164Ala-TDH.

2.4.11 Mutation of Gln165Ala within the CTR does not affect the functional pore-forming activity and solution oligomerization of the toxin

The primary amino acid sequence and the crystal structure of the TDH shows that there are two consecutive Gln residues at positions 164 and 165 within the CTR, at the C-terminal end of TDH. As described above, Gln164 acts as a critical amino acid residue which plays significant role in the membrane-damaging pore-forming activity and solution oligomerization of the toxin. As they are similar amino acid, just one after another, we questioned whether Gln165 can also play similar roles. To investigate the role of Gln165 in structure-function mechanism of TDH, we generated a mutant (Gln165Ala) of TDH. When examined for its membrane-damaging activity, we found that there is no change in the hemolytic activity profile of Gln165Ala, as compared to WT-TDH. This data suggested that Gln165 does not play any functional role in the mechanism of action of TDH (Fig. 2.19).

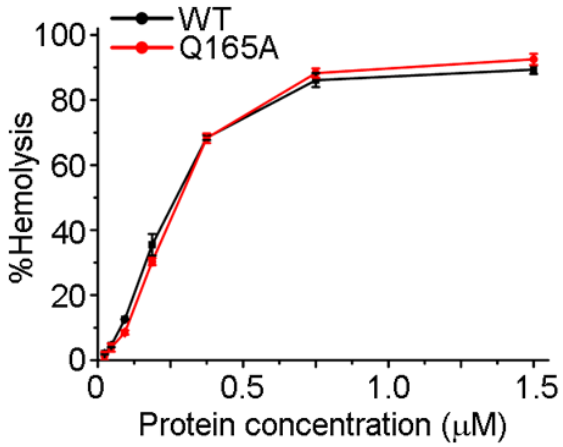

Fig. 2.19: Membrane-damaging hemolytic activity of wild-type TDH (WT) and the Q165A mutant against human erythrocytes.

:

Next, we wanted to test whether Gln165Ala shows any defect in the solution oligomerization ability of the toxin. For this, we performed sedimentation velocity AUC and size-exclusion chromatography. The AUC profile showed that the major peak of Gln165Ala corresponded to the sedimentation coefficient value of 5, suggesting it to be a tetramer in solution (Fig. 2.20).

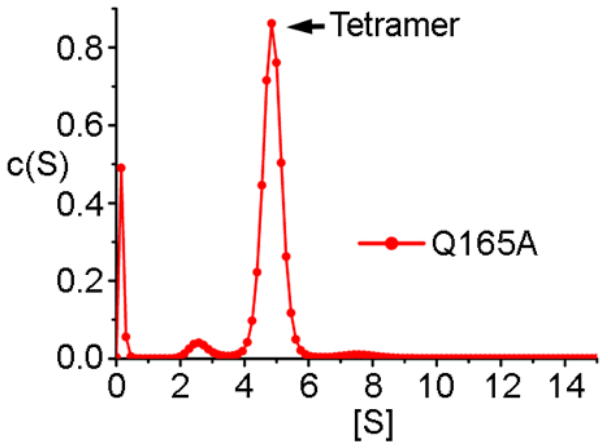

Fig. 2.20: Sedimentation velocity AUC profile of Gln165Ala (Q165A)

We confirmed the tetrameric state of Gln165Ala-TDH by size-exclusion chromatography. The elution profile of Gln165Ala-TDH overlapped with that of WT-TDH, and eluted at around 46.3 ml. (Fig 2.21). This data confirmed that Gln165Ala-TDH existed exclusively as tetramer. Altogether, these results showed that Gln165 residue does not play any critical role in the oligomerization mechanism of TDH, and also in the membrane-damaging pore-forming activity of the toxin.

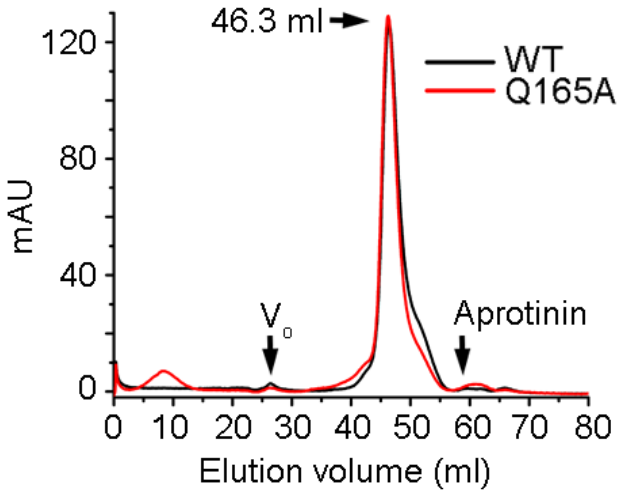

Fig. 2.21: Size-exclusion chromatography profile of Gln165Ala-TDH (Q165A)

:

2.4.12 Intra-protomer disulphide bond between Cys151 and Cys161 restrains the CTR to facilitate oligomerization of TDH and membrane-damaging activity

Analysis of the TDH crystal structure reveals that an intra-protomer disulphide bond (between Cys151-C161) appears to tether the CTR to the core β-sandwich domain of the toxin. The locking of CTR via a disulphide bond positions the CTR at the inter-protomer interface which might facilitate the interaction between Gln164 within the CTR and the residues from the neighboring protomer, thus maintaining the tetrameric assembly of TDH in solution. Based on this notion, we wanted to test if the disulphide bond present between C151 and C161 plays any critical role in the structure-function mechanism of TDH.

Two strategies used to break the disulphide bond:

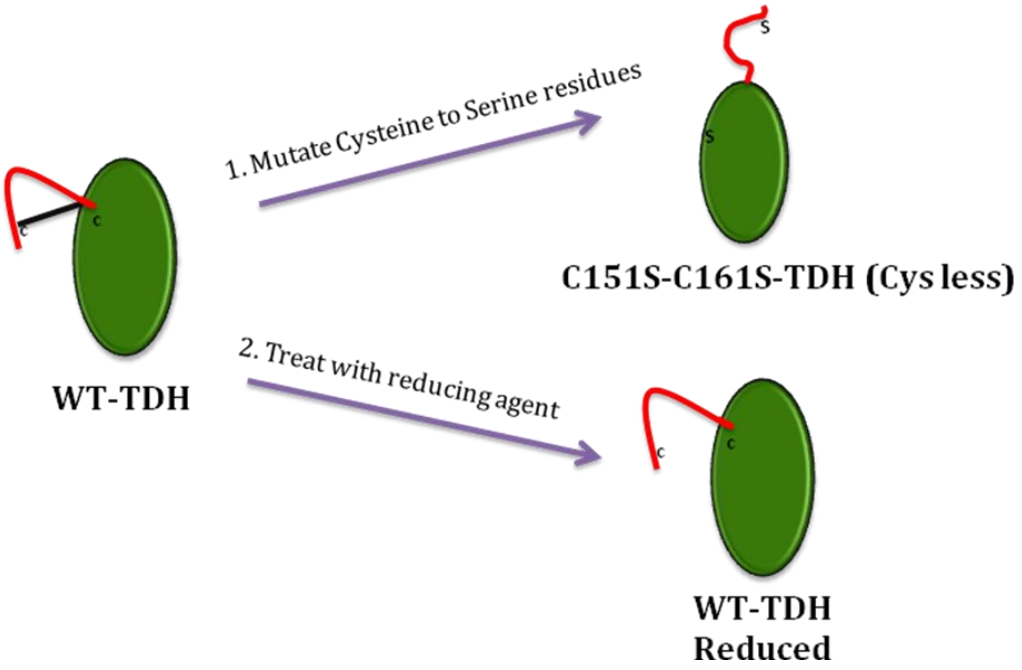

Fig. 2.22: Two strategies to break the disulphide bond: (1) Cysteine residues were mutated to serine (Cys151Ser-Cys161Ser). In this case the disulphide bond is not formed in the protein. (2) Treat the WT-TDH protein with a reducing agent to break the pre-formed disulphide bond.

:

Strategy (1): Disruption of the disulphide bond via mutation of the cysteine residues to serine (Cys151Ser-Cys161Ser) breaks the tetrameric assembly of TDH and compromises the membrane-damaging activity of the toxin:

We wanted to investigate whether the the intra-protomer disulphide bond play any crucial role in positioning of CTR at the intra-protomer interface, thereby facilitating the solution oligomerization of TDH. For this we disrupted the disulphide bond by generating a construct, Cys151Ser-Cys161Ser-TDH. In this mutant, the disulphide bond would never form. Therefore, we wanted to investigate how the absence of disulphide bond formation affected the solution oligomerization ability and membrane pore-formation activity of the toxin. When tested for the functional pore-forming activity against human erythrocytes, we found a significant drop in the hemolytic activity as compared to the WT-TDH (Fig. 2.23).

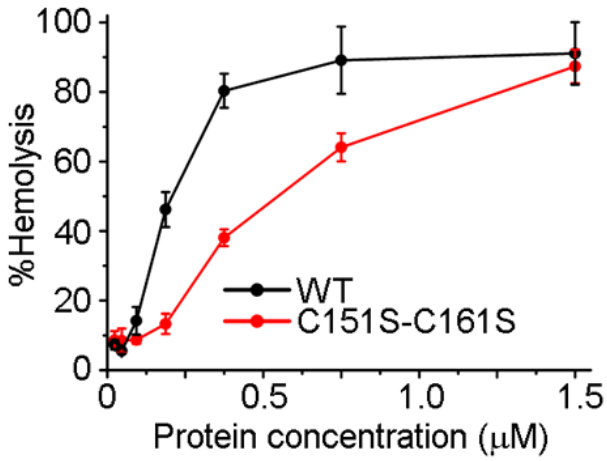

Fig. 2.23: Membrane-damaging hemolytic activity of wild type TDH (WT) and the TDH variant harboring the mutations of Cys151Ser and Cys161Ser (C151S-C161S) against human erythrocytes.

At a concentration of 0.5 μM, Cys151Ser-Cys161Ser showed nearly 40% of the activity whereas WT-TDH showed 80% of the hemolytic activity. The hemolytic profile suggests that disruption of disulphide bond formation affects the functionality of the toxin.

We next wanted to determine if this loss in activity was due to changes in the secondary and tertiary structural integrity of the toxin. For this we performed far-UV CD spectroscopy and intrinsic tryptophan fluorescence studies (Fig. 2.24A).

:

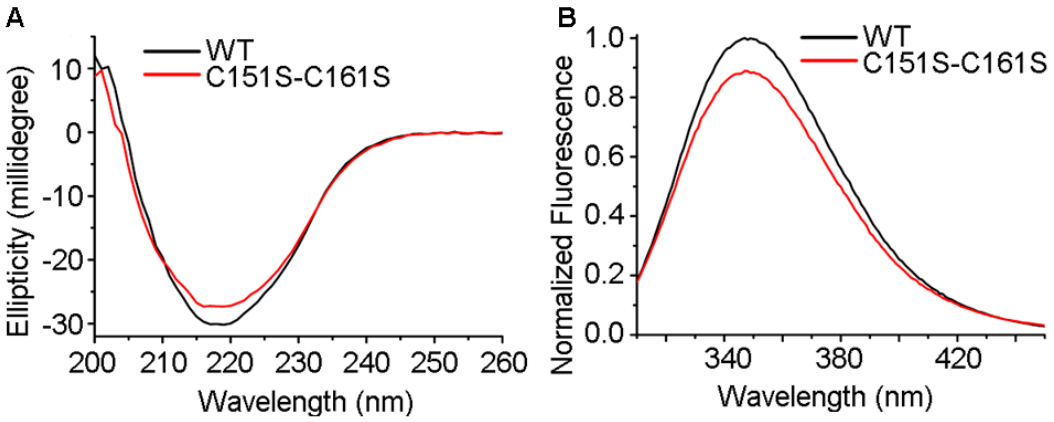

Fig. 2.24: (A) Far-UV CD spectra of WT and Q164A. (B) Normalized intrinsic tryptophan fluorescence emission spectra of WT-TDH and Cys151Ser-Cys161Ser.

Far-UV CD data revealed that both the wild type and the mutant proteins showed overlapping profile. This data suggested that the disruption of disulphide bond did not affect the overall secondary structural integrity of the toxin. The change in tertiary structural organization of the protein was monitored by assessing the intrinsic tryptophan fluorescence emission studies (Fig. 2.24 B). In this experiment, both, WT-TDH Cys151Ser-Cys161Ser showed overlapping spectrum suggesting that the absence of disulphide formation in TDH did not affect the overall folding and tertiary structure of the protein. Altogether these data suggested that the Cys151Ser-Cys161Ser mutation in TDH did not change the overall secondary and tertiary structural organization of the protein.

2.4.13 Disruption of disulphide bond compromises solution oligomerization:

Analysis of the crystal structure of TDH suggests that disulphide bond between Cys151 and Cys161 residues act to tether the CTR at the inter-protomer interface. The restraining of CTR via disulphide bond therefore may act facilitates oligomerization of TDH via CTR-mediated interactions. To test this, we performed the sedimentation velocity AUC experiments with Cys151Ser-Cys161Ser-TDH. The AUC profile of the Cys151Ser-Cys161Ser-TDH suggested that the major population of the mutant peaked at the sedimentation coefficient value of 2, suggesting the major population of the mutant existed as monomer in solution. There is also a small peak at the sedimentation coefficient value of 4.2, corresponding to the tetramer population (Fig. 2.25).

:

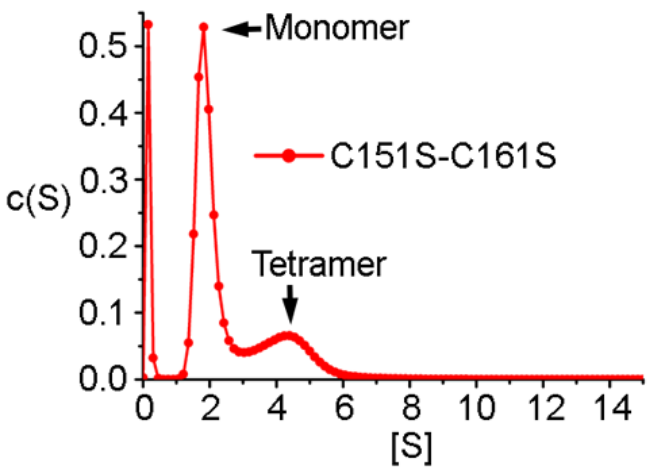

Fig. 2.25: Sedimentation velocity AUC profile of Cys151Ser-Cys161Ser (C151S-C161S).

To confirm the monomeric state of Cys151Ser-Cys161Ser mutant, we performed size-exclusion chromatography. Analysis of the size-exclusion chromatography profile showed that the mutant lacking the disulphide bond (Cys151Ser-Cys161Ser-TDH) eluted at around 52.3 ml, which corresponded to the monomeric state of the protein. Elution profile of Blue Dextran 2000 (Vo) and Aprotinin were also monitored as the standards (Fig. 2.26).

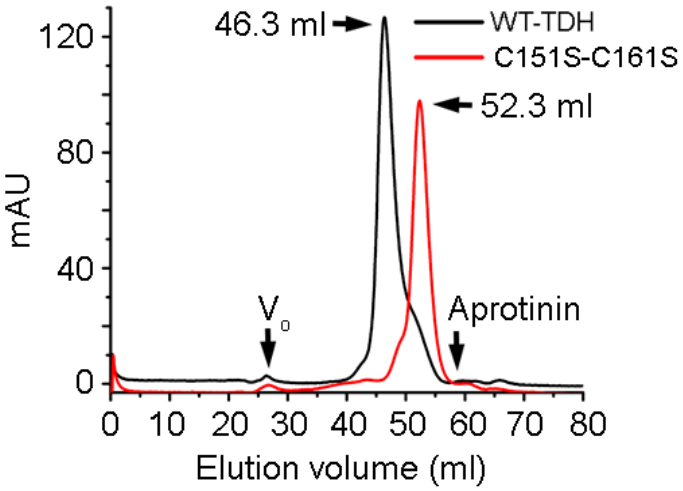

Fig. 2.26: Size-exclusion chromatography profile of WT-TDH and Cys151Ser-Cys161Ser (C151S-C161S).

:

The sedimentation velocity AUC profile and size-exclusion chromatography data confirmed that the Cys151Ser-Cys161Ser mutant of TDH existed as monomer in solution. In other words, disruption of the disulphide bond formation in the mutant (C151S-C161S) abrogated solution oligomerization of the toxin. This data proved our hypothesis and speculation that formation of the disulphide bond indeed locks the CTR at the oligomeric interface, and this restraining of CTR allows Q164 to make interaction with the neighboring protomer, thus facilitating the oligomerization. In the absence of disulphide bond, the CTR possibly becomes too flexible that in turn prohibits the positioning of CTR at the oligomeric interface. As a result, Q164 cannot establish interactions with the residues from the neighboring protomer. As a result, the mutant remains as monomer in solution.

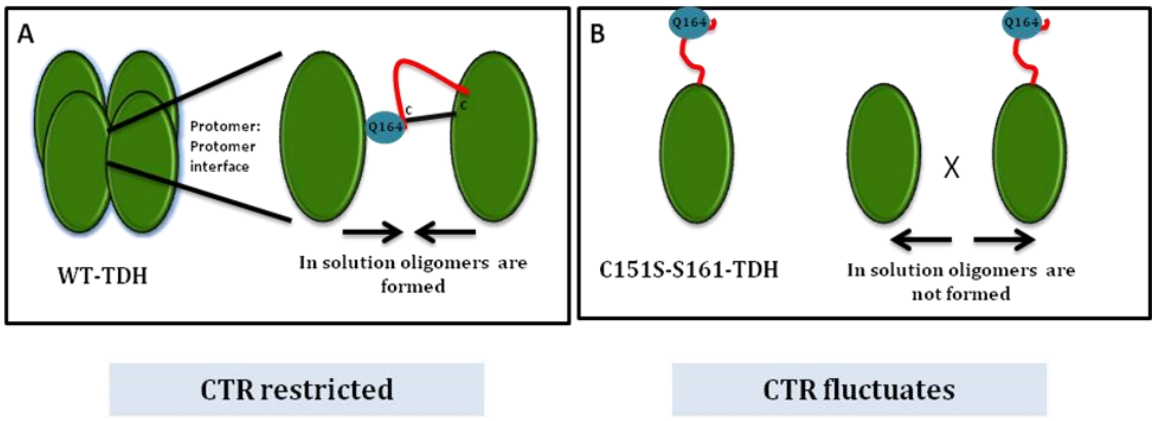

Fig. 2.27 Mechanism of disulphide bond mediated oligomerization: (A) Formation of disulphide bond positions CTR at oligomeric interface which facilitates interaction of Gln164 with neighboring protomer thereby forming oligomers in solution. (B) Absence of disulphide bond formation makes CTR flexible thereby preventing Gln164 interaction, generating monomers in solution.

Similar observations were obtained by the computational based MD simulation studies carried out by our collaborators, Dr. Shashi Bhushan Pandit and Mr. Swapnil Tichkule. To explore the role of disulphide bond in restraining the possible structural/conformational fluctuation of the CTR, MD simulation of TDH monomer was performed for 30 ns in the presence of explicit water, with or without the disulphide bond (Fig. 2.28). The atomic fluctuations of residues were averaged for 30 ns and the results suggested that in the absence of the disulphide bond the CTR exhibited greater

:

flexibility, when compared with the disulphide bond. Altogether these results confirmed that the Cys151-Cys161 disulphide bond restricted the motion of the CTR.

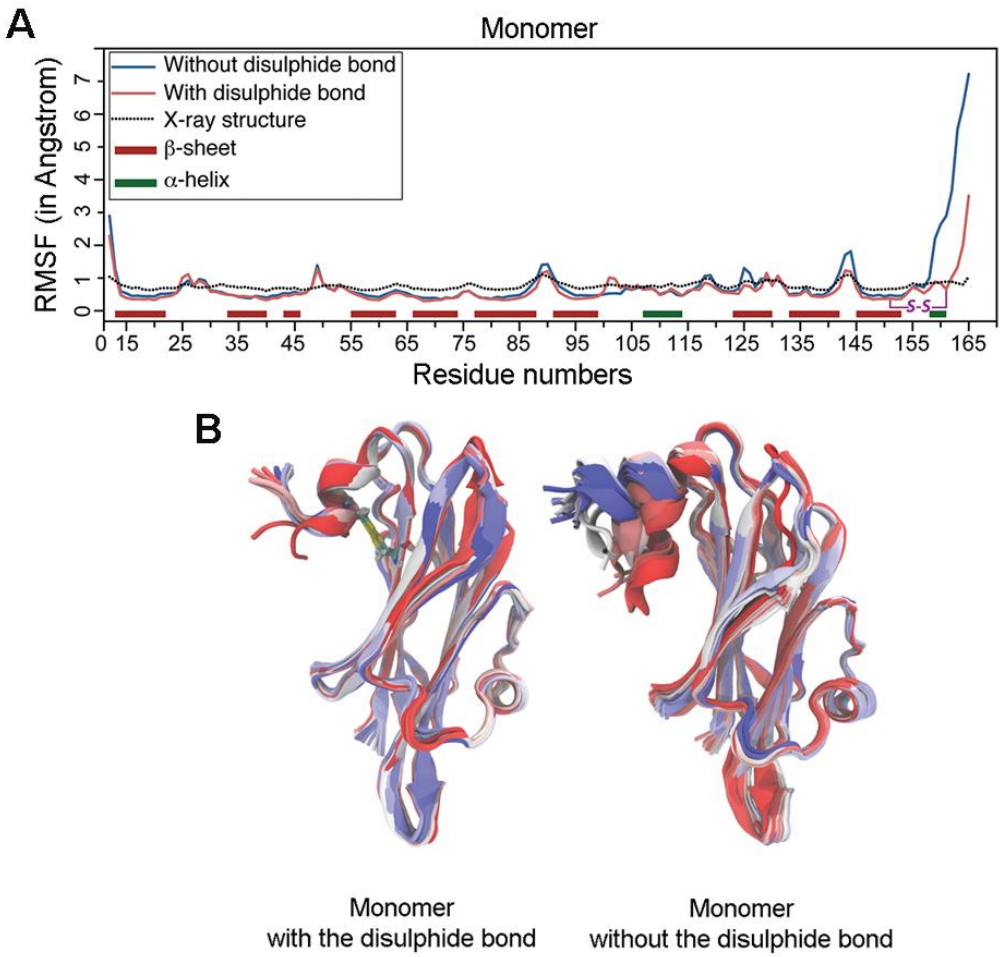

Fig. 2.28: MD simulation of TDH monomeric structure in the presence and absence of disulphide bond between Cys151 and Cys 161 residues: (A) RMSF comparison is shown for the TDH monomers with and without the disulphide bond. The RMSF computed from B-factor obtained from the X-ray crystal structure is shown as a dotted line. (B) Conformations of the TDH monomer structures with or without the disulphide bond during the simulations were aligned to illustrate the relative motion of the CTR with respect to the rest of the domain. TDH monomer with the disulphide bond was simulated against TDH monomer without disulphide bond. Color indicates time, with red being the early stages of the simulations and blue indicating the later stages of the simulations (Figure taken from Kundu *et.al*., Biochemical Journal, 2017).

2.4.14 Disruption of the disulphide bond in Cys151Ser-Cys161Ser mutant compromises membrane-binding ability of the toxin

The disruption of disulphide bond formation in the mutant Cys151Ser-Cys161Ser compromises the solution oligomerization and functional pore-forming activity of the toxin. We wanted to

:

investigate if the loss in the functionality was due to compromised membrane-binding ability of the toxin. For this we tested the membrane binding efficacy of Cys151Ser-Cys161Ser with the human erythrocytes by using flow-cytometry based assay (Fig. 2.29).

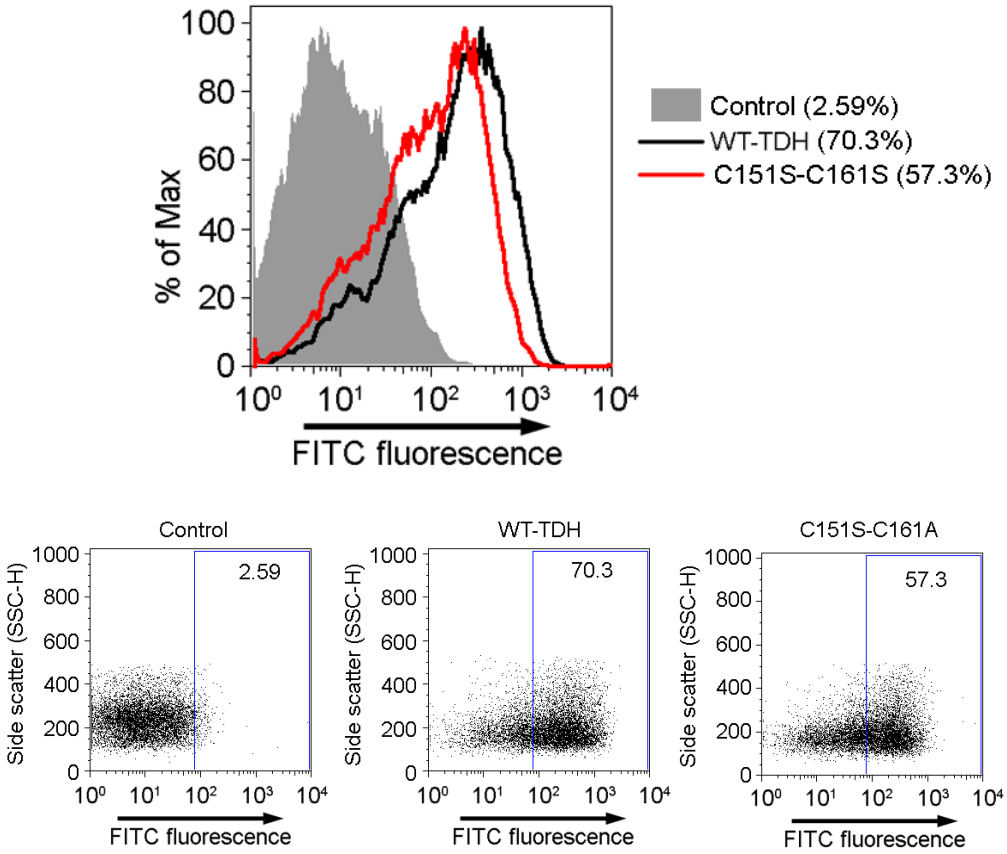

Fig. 2.29: Binding of WT-TDH (black line) and Cys151Ser-Cys161Ser (C151S-C161S) (red line) with human erythrocytes determined by the flow cytometry-based assay.

The flow cytometry data suggested that the binding ability Cys151Ser-Cys161Ser is significantly compromised as compared to WT-TDH. When we compared the percentage of cell population with bound TDH variants, we found that ~70% cell population were having bound WT-TDH. In contrast, only 57.3% of the cells were having bound Cys151Ser-Cys161Ser-TDH. This data clearly suggested Cys151Ser-Cys161Ser-TDH showed compromised membrane-binding ability.

:

2.4.15 Disruption of the intra-protomer disulphide bond during the folding/assembly process compromises oligomerization, while reduction in the disulphide bond after completion of the folding/assembly process does not affect the oligomerization of TDH

<u>Strategy (2): Disruption of the disulphide bond by treating WT-TDH with a reducing agent does not affect solution oligomerization and membrane-damaging activity of the toxin</u>:

As discussed above, disruption of the disulphide formation (strategy 1) in the TDH (Cys151Ser-Cys161Ser) compromises the solution oligomerization and pore-forming activity of the toxin. Next, we wanted to test the second strategy (strategy 2) of breaking the disulphide bond, i.e. treating the WT-TDH with a reducing agent (DTT/TCEP), and then to study its solution oligomerization ability and membrane-damaging activity. The WT-TDH (reduced with 1 mM DTT) was treated with human erythrocytes, and the cell-killing ability of the WT-TDH (reduced) was monitored. Surprisingly, we found that there was no change in the hemolytic activity profile of WT-TDH under the reducing condition, as compared to that under the non-reducing condition. Thus, disruption of the pre-formed disulphide bond in WT-TDH, with a reducing agent, did not show any change in the functionality of the toxin (Fig. 2.30).

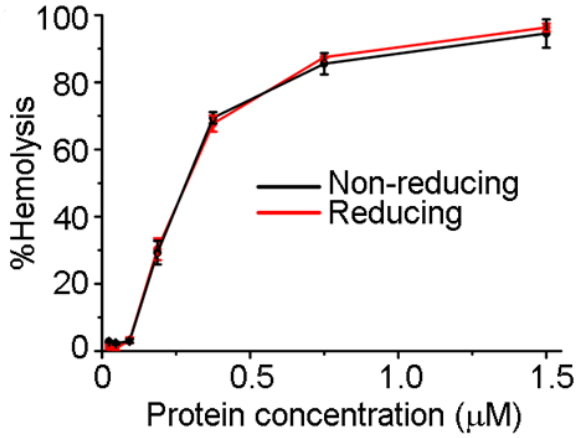

Fig. 2.30: Hemolytic activity of wild-type TDH against human erythrocytes, in the presence of the reducing agent DTT (reducing) and without DTT treatment (non-reducing).

:

Next, we wanted to investigate if the disruption of the disulphide bond in WT-TDH with a reducing agent (strategy 2) affected the solution oligomerization ability of the toxin. For this we performed sedimentation velocity AUC experiment of the reduced WT-TDH (treated with 0.1 mM TCEP). The reducing conditions were maintained during the AUC experiment as well. The AUC profile of reduced WT-TDH showed that the major population of the protein existed as tetramer in solution (Sedimentation coefficient value 5) (Fig. 2.31).

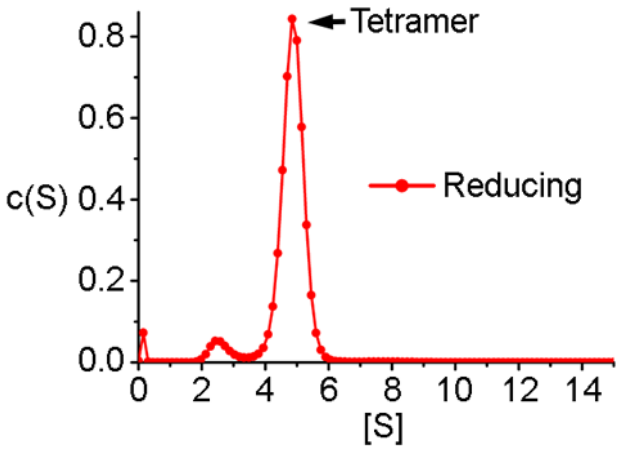

Fig. 2.31: Sedimentation velocity AUC profile of wild-type TDH, under reducing conditions in the presence of 0.1 mM TCEP.

So, the two strategies of breaking the disulphide bond showed opposite results. Strategy 1, where there was no possibility of disulphide bond formation in the protein (via usage of Cys151Ser-Cys161Ser mutation), showed that the toxin existed as monomer. The strategy 2, in which we reduced the pre-formed disulphide bond by treating the WT-TDH protein with a reducing agent, showed that the toxin existed as tetramer.

In order to resolve this, we hypothesized that it is possible that the preformed tetrameric assembly of wild-type TDH, once generated via interactions involving Gln164 and the other critical residues important for oligomerization, cannot be disassembled via disruption of the disulphide bond. In other words, once the Gln164 interacts with its neighboring protomer, disruption of the disulphide bond does not affect oligomerization because Gln164 has already interacted, and this interaction now plays a major role in oligomerization of the toxin.

:

Denaturation and renaturation of WT-TDH from inclusion bodies, in the presence and absence of the reducing agent (Fig. 2.32)

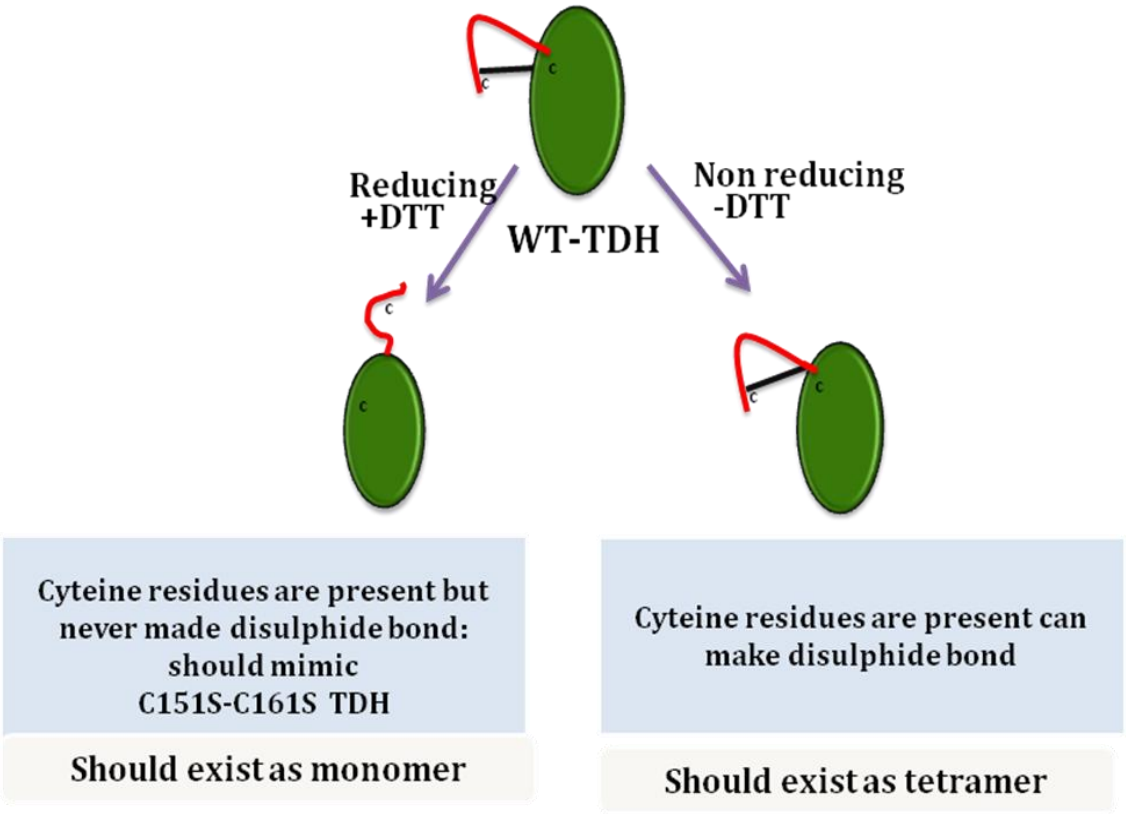

Fig. 2.32: Scheme for denaturation and renaturation of WT-TDH from inclusion bodies. Renaturation of protein in the presence of DTT was expected to exist as monomer and renaturation in the absence of DTT was expected to exist as tetramer.

To understand further the role of the disulphide bond in mediating the oligomerization mechanism of the toxin, we attempted to refold the WT-TDH protein from the denatured form, in the presence and absence of a reducing agent. WT-TDH from the insoluble inclusion body was solubilized under denaturing conditions of 8 M urea, refolded and purified, in the presence of DTT throughout the process to ensure the blockade of disulphide bond formation. We also refolded the protein in the absence of DTT, to allow formation of disulphide bond formation. We expected that the protein refolded under the reducing agent would display compromised activity and would exist in solution

:

as monomers, because in this case disulphide won't be formed and CTR would be fluctuating, thus possibly inhibiting proper positioning of Gln164 and its interaction to the neighboring protomer. On contrary, we expected that protein refolded under non-reducing conditions would generate tetramers because here disulphide bond would be allowed to formed, and thus CTR would be positioned at the oligomeric interface, and Gln164 would be able to interact with the neighboring protomer.

After refolding of the proteins in respective conditions (reducing/non-reducing), we tested the membrane-damaging functional pore-forming activity of the proteins with human erythrocytes. The hemolytic activity profile suggested that WT-TDH refolded under reducing conditions showed reduced hemolytic activity as compared to WT-TDH, refolded under the non reducing conditions (Fig. 2.33).

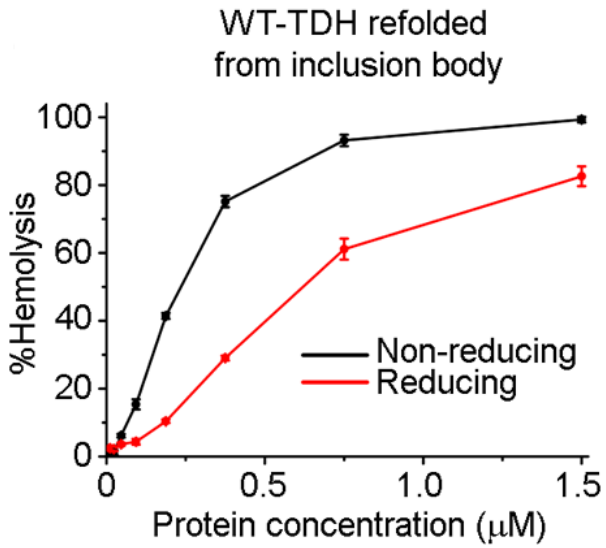

Fig. 2.33: Membrane-damaging hemolytic activity of TDH, refolded under non-reducing (in the absence of DTT) and reducing conditions (in the presence of DTT), against human erythrocytes.

We wanted to investigate if this decrease in hemolytic activity profile was due to loss in secondary and tertiary structural integrity of WT-TDH protein (reducing/non reducing) during refolding. Proteins refolded under both the reducing and non-reducing conditions displayed similar secondary and tertiary structural organizations, as observed from the far-UV CD and tryptophan fluorescence spectra (Fig. 2.34 A and B respectively).

:

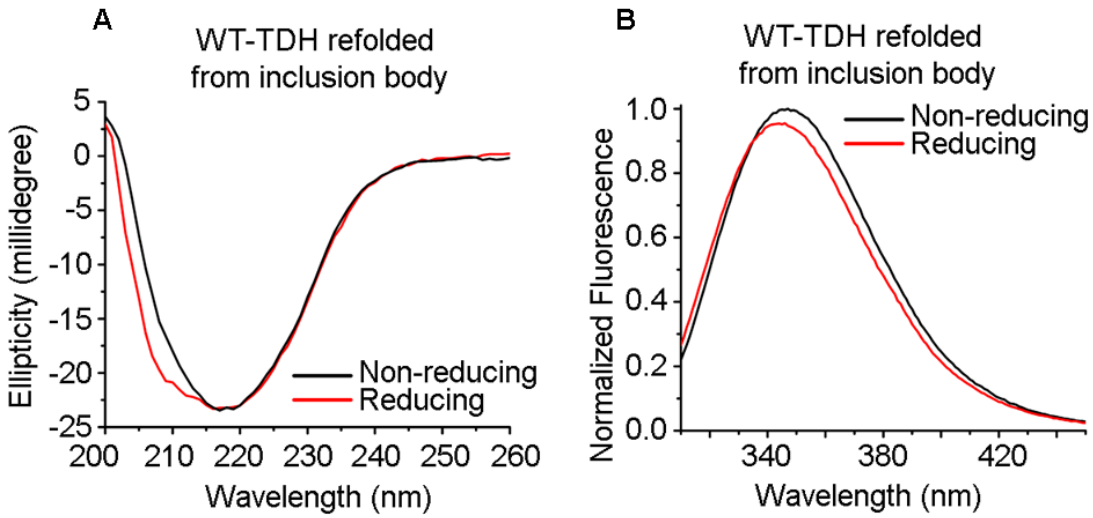

Fig. 2.34: (A) Far-UV CD spectrum of TDH, refolded under reducing conditions (in the presence of DTT), was collected in the presence of 0.1 mM TCEP to maintain the reducing conditions. Far-UV CD spectrum of the protein refolded under non-reducing conditions (in the absence of DTT) was monitored in the absence of TCEP, as the control. (B) Normalized intrinsic tryptophan fluorescence in the presence and absence of 0.1 mM TCEP

The far-UV CD and intrinsic tryptophan fluorescence emission spectra of protein refolded from inclusion bodies were similar to those proteins isolated from the soluble fraction of bacterial cell lysates. Small differences were observed in the profile of the protein refolded under reducing conditions, probably due to the presence of small amount of misfolded proteins generated during refolding process.

Next, we wanted to determine the solution oligomerization state of the WT-TDH proteins refolded under reducing and non-reducing conditions. For this, we performed sedimentation velocity AUC experiments, and the AUC profile suggested that the major population of proteins refolded under reducing conditions existed as monomer (Fig. 2.35).

:

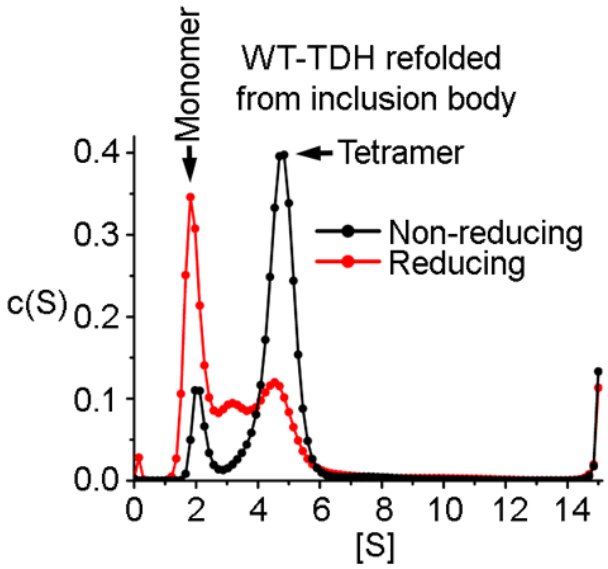

Fig. 2.35: Sedimentation velocity AUC profile of TDH, refolded under reducing conditions (in the presence of DTT), was monitored in the presence of 0.1 mM TCEP. The sedimentation velocity AUC profile of the protein refolded under non-reducing conditions was monitored in the absence of TCEP, as the control.

On the other hand, the WT-TDH protein refolded under non-reducing conditions showed a major peak belonging to the population of tetrameric assembly in solution. This data confirmed that the disruption of disulphide bond formation during the process of protein folding/assembly (under reducing conditions) did not allow the restraining of CTR at the oligomeric interface, and as a result CTR becomes too flexible, because of which Gln164 was unable to come to its proper position (protomer:protomer interface). As a result, the major population of the protein remained in solution as monomers. Altogether, these data suggested that the blockade of Cys151-Cys161 disulphide bond formation prior to the folding/assembly of TDH could compromise the tetramerization of the protein in solution, but not after the completion of the folding and assembly process. The present results also highlight that the formation of disulphide bond from the process of folding and assembly itself regulates the solution oligomerization process in TDH.

:

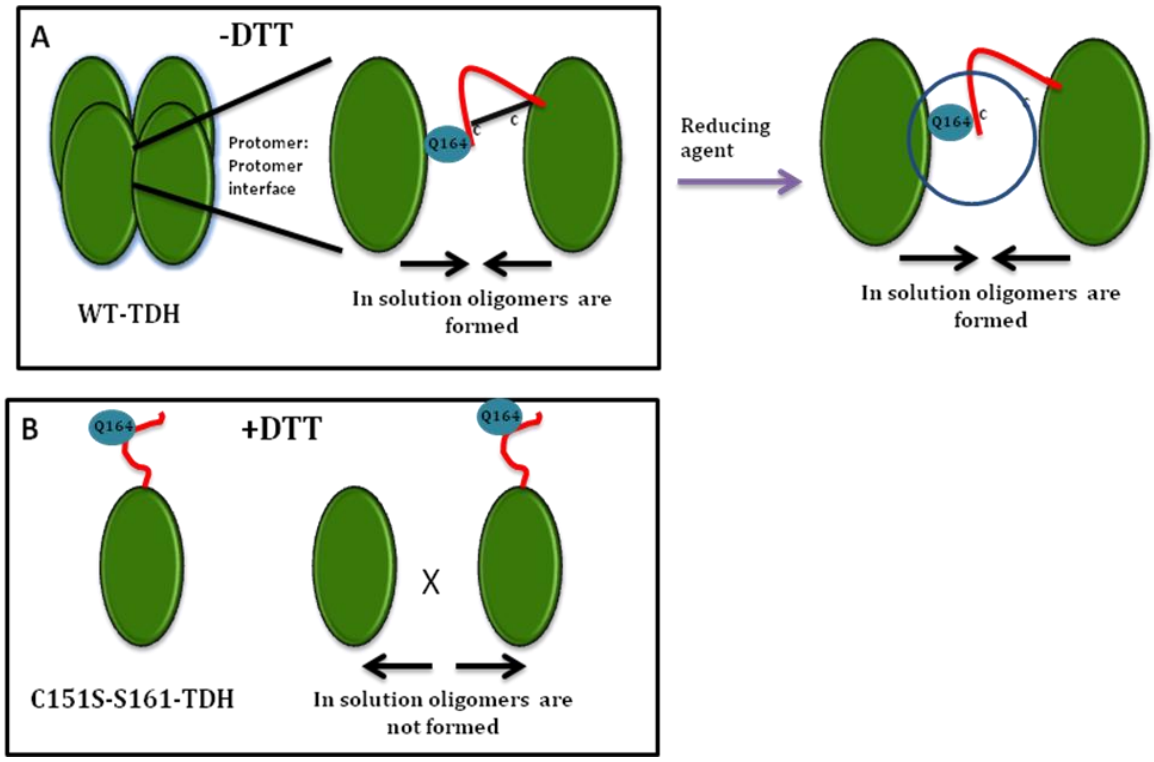

Fig. 2.36: Disulphide bond formation regulates the process of solution oligomeriazation: (A) The refolded protein in the absence of DTT (-DTT) allowed the formation of disulphide bond, and positioned the CTR at the oligomeric interface thereby facilitating the interaction of Gln164 to its neighboring protomer, hence maintaining the tetramers. Now reduction of preformed disulphide bond by a reducing agent reduces the disulphide bond, but still tetramers are maintained because of the interaction of Gln164. The Gln164 interaction remains unaffected by reduction of the preformed disulphide bond. (B) The refolded protein in the presence of DTT (+DTT) does not allow disulphide bond formation. As a result CTR fluctuates, and Gln164-mediated interactions get inhibited, thereby generating monomers in solution.

:

2.5 Discussion and conclusion

Bacterial PFTs are, in general, secreted as water-soluble monomers, which upon associating with target cell membranes converts into oligomeric pores [127, 231]. The mode of action of *V. parahaemolyticus* TDH shows an atypical mechanism in that it exists as a tetramer in solution. Tetramer formation in solution appears to be important for the membrane-damaging activity of TDH. A previous study has identified two of the key residues (Arg46 and Tyr140), within the core β-sandwich domain of TDH, that are implicated in oligomerization of the toxin. Our present study shows that the C-terminal segment of TDH, which does not appear to be an integral part of the core β-sandwich domain, plays a critical regulatory role in the oligomerization process of the toxin8. Restrained configuration of the C-terminal segment, mediated by the disulphide bridge that tethers this region to the β-sandwich domain, appears to be critical for creating the inter-protomer contact toward oligomerization of TDH. Such a mechanism for regulating the oligomerization process has not been documented for any other bacterial PFT. Even for the structural homologues of TDH in the eukaryotic actinoporin family, such a regulatory mechanism does not appear to be operational. Equinatoxin II, Fragaceatoxin C, and Sticholysin II represent the 'structurally most well-characterized' members in the eukaryotic actinoporin family. TDH shares similar structural organization for the core β-sandwich domain as displayed by those of Equinatoxin II, Fragaceatoxin C, and Sticholysin II. However, none of these actinoporins possesses any C-terminal extension beyond the β-sandwich domain. In addition, all three actinoporins lack any Cys residue in their primary structures. Consistent with such a notion, oligomerization of the actinoporins appears to be triggered only upon interaction with target membranes [171, 231]. The presence of the CTR motif, therefore, appears to provide a unique advantage for TDH in terms of allowing its prior oligomerization in solution. The functional implication of such CTR-mediated oligomerization is also manifested in the observation that prior oligomerization in solution is critical in the optimal mode of action of TDH. Future studies would be required to explore in detail how the structure-function mechanisms have evolved, in TDH and its structurally related homologues in the eukaryotic actinoporin family of PFTs, toward employing differential regulation of their oligomerization process.

Based on our study, it is possible to hypothesize that the C-terminal segment of TDH acts as a mediator to allow tetramerization of the protein in solution prior to membrane interaction. In the

:

absence of C-terminal segment-mediated oligomerization, the membrane-binding and subsequent pore-formation event are compromised to a marked extent. It is important to emphasize, however, that even in the absence of the C-terminal segment-mediated tetramer formation in solution, TDH can display a prominent ability to bind to target cells. This observation clearly suggests that even in the absence of oligomerization in solution, the monomeric form of TDH mutants can bind to target cells. TDH may harbor potential structural motif(s) for binding to target membranes; however, the identity of such structural motif(s) remains unknown at present. In the absence of CTR-mediated oligomerization, TDH variants may bind to target cells by employing such structural motif(s) present within the monomeric unit of the toxin. In the presence of the CTR-mediated oligomerization of TDH in solution, binding is possibly augmented due to the increased avidity of the tetrameric form of the toxin molecules. It is also important to note that even in the absence of CTR-mediated oligomerization in solution, TDH variants show noticeable membrane-damaging activity. This observation indicates that the monomeric TDH mutants are capable of forming oligomeric pores upon binding to target cells. This can be explained by the fact that TDH contains additional key residues (Arg46 and Tyr140) within the core β-sandwich domain that are implicated in oligomerization of the toxin; such residues possibly facilitate the oligomerization of the protein upon membrane association, in the absence of prior tetramer formation in solution. In sum, the present study provides critical insights regarding the structure-function mechanism of *V. parahaemolyticus* TDH. The study also extends our current understanding regarding the structural mechanisms employed by PFT family members.

:

Chapter 3

Implications of the N-terminal region (NTR) of TDH in the membrane-damaging activity of the toxin*

*** This part of the study is in communication as: Kundu, N**., Verma, P., Dhar, V., & Chattopadhyay, K. (2018). Intrinsically disordered N-terminal region of *Vibrio parahaemolyticus* thermostable direct hemolysin regulates the membrane-damaging action of the pore-forming toxin.

:

Chapter 3

Implications of the N-terminal region (NTR) of TDH in the membrane-damaging activity of the toxin

3.1 Abstract

Thermostable direct hemolysin (TDH) is a major virulence factor secreted by the gram-negative bacterial pathogen *Vibrio parahaemolyticus*. TDH has been characterized as a membrane-damaging pore-forming toxin (PFT) with potent cytolytic/cytotoxic activity. Mature form of the TDH polypeptide chain adopts a core β-sandwich domain that exists as a tetramer in solution. The 11-amino acid long N-terminal region (NTR) of the mature TDH is predicted to be intrinsically disordered, and could not be modelled in the crystal structure presumably due to its high degree of structural/conformations fluctuations. In the present study, we have explored the role of the NTR in the structure-function mechanism of TDH. Our data show that the presence of the NTR modulates the physicochemical properties of TDH, in terms of augmenting the amyloidogenicity of the protein. Presence of the NTR acts to generate surface-exposed hydrophobic patch(s) on TDH, and favors partitioning of the toxin to the amphipathic phase of the membrane lipid bilayer of liposomes. Deletion of the NTR compromises binding of TDH toward the target cell membranes, and drastically affects the membrane-damaging cytolytic/cytotoxic activity of the toxin. Mutations of the aromatic/hydrophobic residues within the NTR also confer compromised cell-killing activity. Interestingly, restraining of the NTR against the core β-sandwich domain, via engineered disulphide bond, also abrogates the cytolytic/cytotoxic activities of TDH, suggesting that the flexible configuration of the disordered NTR is crucial for the functionality of the toxin. Based on our study, we propose a model explaining the role of the NTR in the membrane-damaging functions of TDH.

:

3.2 Introduction

The mature form of the TDH primary structure consists of 165 amino acid residues, and it adopts a core β-sandwich domain structure (Fig. 3.1A). The primary structure of the mature TDH highlights an N-terminal 11-amino acid long sequence (^{1}FELPSVPFPAP^{11}; NTR) (Fig. 3.1B), which does not appear to be a part of the core β-sandwich domain. This NTR could not be modelled in the crystal structure of TDH, presumably due to high conformation fluctuation of the motif [232]. The NTR is found to be enriched in aromatic/hydrophobic residues, and it also contains number of proline residues. Moreover, theoretical/computational analysis predicts NTR to be intrinsically disordered (Fig. 3.1C). However, there is no information available till date whether the NTR plays any role in the mechanism of action of TDH.

The present chapter discusses the implications of the NTR in the structure-function mechanism of TDH. The results obtained from the study showed that the presence of the NTR contributes toward some of the unique physicochemical properties of TDH. Deletion of the NTR critically affected the membrane-damaging activity of the toxin. Mutations of the key aromatic/hydrophobic residues within the NTR affected the TDH functionalities. Covalent trapping of the NTR against the β-sandwich domain, via engineered disulphide bond, also compromised the cytolytic/cytotoxic activity of TDH against the target cells, suggesting that the predicted conformational fluctuation of the N-terminal arm is presumably required for the optimal functionalities of the toxin. These results provided new critical insights regarding the implications of the NTR present in TDH for the membrane-damaging cytolytic/cytotoxic activity of the toxin.

:

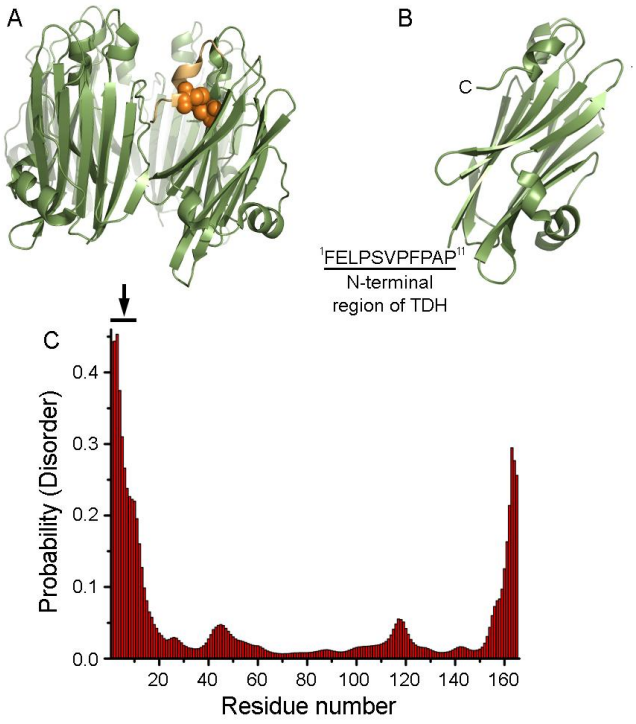

Fig. 3.1: Intrinsically disordered N-terminal region (NTR) of TDH. A) Tetrameric assembly of TDH. The extended C-terminal region (CTR) is highlighted in orange color. B) Monomeric unit of TDH is shown with the amino acid sequence of the NTR. C) Analysis of the TDH primary structure predicted the NTR to be highly disordered. Predicted disordered region(s) in the TDH primary structure was calculated using PASTA 2.0 available online (http://protein.bio.unipd.it/pasta2/index.html) [233]. Segment corresponding to the NTR is indicated with an arrow.

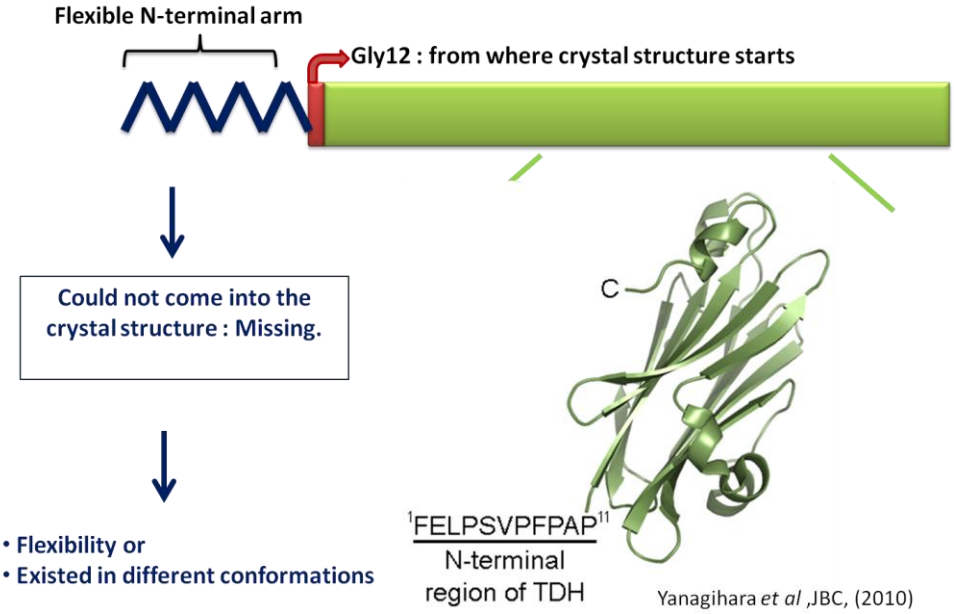

Fig. 3.2: N-terminal region: what is known so far?

The cartoon representation of WT-TDH highlighting flexible NTR (blue zigzag line). The crystal structure lacks first 11 residues (NTR) and structure starts from residue Gly12 (represented by red arrow). Rest of the amino acids forms a compact β-sandwich structure surrounded by 2 short helices (represented in green).

:

3.3 Materials and Methods

3.3.1 PCR amplification and cloning of the nucleotide constructs of the TDH variants into the pET-14b vector

Nucleotide sequences encoding the TDH variants (wild type, NTD, F1A-F8A-TDH, L3A-V6A-TDH, and S5C-S13C-TDH) were amplified by polymerase chain reaction (PCR)-based approach using the wild-type construct as the template (as described in the previous chapter).

S.No.	Primer	Sequence (5'-3')
1	TDH FW 5'	ATATTGCTCGAGATGTTTGAGCTTCCATCTGTCCC
2	TDH RC 3'	AACATTGGATCTTATTGTTGATGTTTACATTCAAAAAACGAT
3	NTD FW 5'	ATTGAACTCGAGATGGGTTCTGATGAGATATTGTTTGTTGTTCGA
4	S5C-S13C FW 5'	CTCGAGATGTTTGAGCTTCCATGTGTCCCTTTTCCTGCCCCCGG TTGTGATGAGATATTG
5	F1A-F8A FW 5'	CTCGAGATGGCCGAGCTTCCATCTGTCCCTGCCCCTGCCC
6	L3A-V6A FW 5'	CTCGAGATGTTTGAGGCCCCATCTGCCCCTTTTCCTGCCC

3.3.2 Protein expression and purification from soluble fraction

The nucleotide sequence coding for the wild type TDH and its variants were cloned into the pET-14b expression vector (Novagen) between the Xho1 and BamH1 sites. The proteins were expressed and purified as described in the previous chapter.

3.3.3 Far-UV circular dichroism (CD) measurements

Far-UV CD spectra of the TDH variants were recorded on a Chirascan spectropolarimeter (Applied Photophysics, Leatherhead, Surrey, UK) equipped with a peltier-based temperature-controlled sample chamber, using a quartz cuvette of 5 mm pathlength. The spectra of each protein were taken, and were buffer corrected (as described in the previous chapter).

:

3.3.4 Intrinsic tryptophan fluorescence emission measurements

Intrinsic tryptophan fluorescence spectra of the TDH variants (in 1 mM Tris-HCl buffer, pH 7.5) were recorded on a Fluoromax-4 spectrofluorimeter (Horiba Scientific, Edison, NJ). The spectra were collected and buffer corrected (as described in the previous chapter).

3.3.5 Hemolytic activity assay to monitor pore-forming activity of the TDH variants

The pore-forming activity of the TDH variants were determined against the human erythrocytes (suspended in PBS (pH 7.5); corresponding to OD_{600} ~0.9) by measuring the release of hemoglobin (hemolytic activity assay), spectrophotometrically at 415 nm, over a period of 1 h at 37 °C (as described in the previous chapter).

3.3.6 Sedimentation velocity analytical ultracentrifugation

Oligomerization states of wild type TDH and NTD in solution were examined by sedimentation velocity analytical ultracentrifugation (AUC) on a Beckman Coulter ProteomeLab XL-I analytical ultracentrifuge equipped with an An-50 Ti 8-hole rotor (as described in the previous chapter).

3.3.7 ANS (1-anilinonaphthalene-8-sulfonic acid) fluorescence measurement

ANS is an environment sensitive dye. When present in the aqueous solution, it shows nominal fluorescence emission, but when bound to the hydrophobic surface on proteins it shows increased fluorescence emission, along with a blue shift in the emission wavelength maximum [234]. The presence of any exposed hydrophobic patch on the surface of the TDH variants was examined by recording the ANS fluorescence on a Fluoromax-4 (Horiba Scientific, Edison, NJ) spectrofluorimeter equipped with a Peltier-based temperature controller. ANS fluorescence was recorded in 10 mM Tris-HCl buffer (pH 7.5), in the presence of 5 μM of protein, using a final ANS concentration of 10 μM in the solution. Steady-state ANS fluorescence was recorded upon excitation at 350 nm, using excitation and emission slit widths of 2 nm and 5 nm, respectively.

:

3.3.8 ThT fluorescence measurement to monitor amyloid formation

Ability of the TDH variants to form amyloid-like aggregates was examined by monitoring the Thioflavin T (ThT) fluorescence in the presence of the protein at 60 ^{o}C [197]. ThT shows strong fluorescence emission when bound to β-sheet rich, amyloid like structures [234, 235]. The ThT fluorescence was monitored in 10 mM Tris-HCl buffer (pH 7.5). The kinetics of amyloid formation was monitored at 60 ^{o}C. Initially, the buffer was preincubated at 60 ^{o}C for 5 minutes, and then the protein (1 μM) along with ThT was added to get a final ThT concentration of 10 μM in the reaction volume. The kinetics of amyloid formation was monitored by exciting at 450 nm, and using emission wavelength of 485 nm, with excitation slit width of 1 nm and emission slit width of 2.5 nm. The spectra were corrected with the blank containing the ThT without protein.

3.3.9 Mammalian cell culture

T84 human intestinal epithelial cells were maintained and propagated in DMEM [supplemented with 10% fetal bovine serum (FBS), 100 units ml^{-1} penicillin and 100 μg ml^{-1} streptomycin (Invitrogen Life Technologies)], at 37°C in a humidified atmosphere of 5% CO_2. THP-1 human monocytic cells was maintained in RPMI 1640 (Invitrogen Life Technologies, Carlsbad, CA, USA) supplemented with 10 % fetal bovine serum (FBS; Invitrogen), 100 units ml^{-1} penicillin and 100 μg/ml streptomycin (Invitrogen) [129].

3.3.10 Cytotoxicity measurements using LDH release assay

T84 human intestinal epithelial cells and THP-1 human monocytic cells (10^5 cells) were incubated with the TDH variants (using the protein concentration of 1 μM) for 24 h at 37 °C in a 96 well plate. After 24 hours of treatment, cells were pelleted and supernatant for each of the treated samples was collected and subjected to LDH-release assay. LDH release assay was performed using the CytoTox 96® NonRadioactive Cytotoxicity Assay kit (Promega Corporation, Madison, WI), as per the manufacturer's instructions. It is based on the principle that upon permeabilization of the plasma membranes due to the membrane-damaging activity of the TDH variants, cytosolic enzyme lactate dehydrogenase (LDH) would be released into the culture supernatant. After addition of the substrates like tetrazolium salts, LDH released in the

:

culture supernatant, converts the salt into a colored product (formazen) that can be monitored spectrophotometrically at 490 nm. Cells treated with Triton X-100 served as the positive control, and cells without any treatment served as the negative control to calculate the %cytotoxicity. Data shown are the average ± standard deviation from the three independent treatments.

3.3.11 Surface Plasmon Resonance to determine binding to the liposome membranes

Binding of TDH and NTD to the membrane lipid bilayer of the Asolectin-cholesterol liposomes and the PC (phosphatidylcholine)-cholesterol liposomes was examined by using surface plasmon resonance on a Biacore 3000 instrument (GE Healthcare Life Sciences) [128, 129]. Briefly, the L1 chip was preconditioned with HEPES Buffer Saline [20 mM HEPES, 150 mM NaCl, pH 7.5 (HBS)]. The liposomes (0.150 mg/ml) were coated on an L1 chip with a flow rate of 2 μl/min for 5 min. Loosely bound liposomes were removed by giving one injection of 20 mM NaOH for 12 seconds with a flow rate of 100 μl/min, thereby stabilizing the baseline. Non-specific binding of the protein to the L1 chip surface was blocked by passing 0.1 mg/ml of BSA for 3 min with a flow rate of 10 μl/min. Binding of the TDH variants to the membrane lipid bilayer of the liposomes was examined by flowing the protein, with a flow rate of 5 μl/ min for 10 min, followed by additional wash with HBS without protein to achieve final end point response signals corresponding to the irreversibly bound fraction of the protein. The whole surface was regenerated by injecting 40 mM octyl β-D-glucopyranoside for 2 min at a flow rate of 10 μl/min followed by another round of injection with higher protein concentration was given. The sensogram plots were generated with the BIAevaluation 4.1.1. software (GE Healthcare Life Sciences).

3.3.12 Flow cytometry-based assay to monitor binding of the TDH variants with the target cells

Binding of the TDH variants to the human erythrocytes, T84 and THP-1 cells were determined by the flow-cytometry-based assay, as described in the previous chapter. Briefly, cells (10^6 cells) were incubated with the TDH variants (0.25 μM protein for the human erythrocytes; 1 μM protein for T84 and THP-1 cells) for 1 hour at 37 ^oC in a reaction volume of 100 μl. For human erythrocytes and THP-1 cells, incubation was in PBS

:

containing dextran (10 mM; the average molecular weight of the dextran was 9000–11000) (Sigma-Aldrich), while for the T84 cells incubation was in PBS. After the protein treatment, cells were washed, and treated with the rabbit anti-TDH antiserum for 1 hour at 37 ^{o}C. After washing, cells were treated with FITC (fluorescein isothiocyanate)-conjugated goat anti-rabbit secondary antibody for 1 hour at 37 ^{o}C. Cells were analyzed for the FITC fluorescence on a FACSCalibur (BD Biosciences) flow cytometer. The FITC fluorescence signal was directly proportional to the binding of the TDH variants to the target cells. The cells treated with anti-TDH and FITC-conjugated anti-rabbit antibodies without the protein treatment, were taken as the negative control.

3.4 Results

3.4.1 Purification and characterization of the secondary, tertiary and quaternary structural features of the truncated form of TDH lacking the N-terminal region (NTR)

TDH primary structure consists of an 11-amino acid long sequence at the N-terminal end of the mature toxin (^{1}FELPSVPFPAP^{11}; NTR). This NTR, however, is not modelled in the crystal structure of TDH (PDB id: 3A57), presumably due to high conformational flexibility of this region [199].

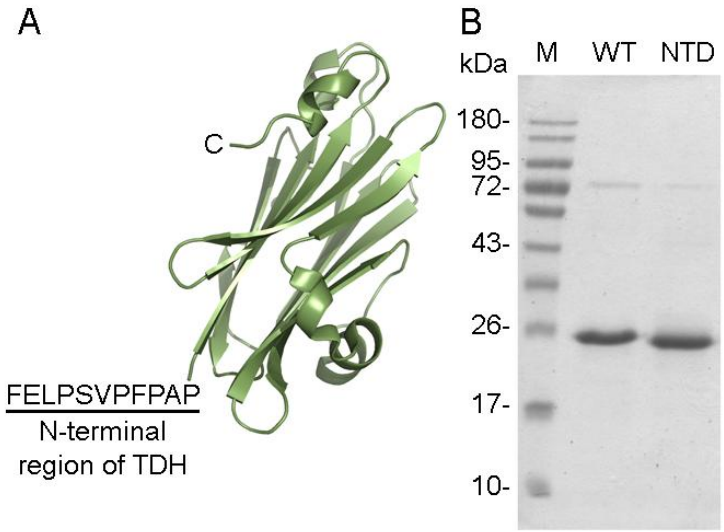

Fig. 3.3: (A) Structural model of TDH crystal structure highlighting the N-terminal region of TDH with the sequence of NTR. The structure represents the core β-sandwich domain with two short helices (green). (B) SDS-PAGE/Coomassie staining of purified protein WT-TDH and NTD. NTD shows marginal shift in size when compared to WT-TDH. Lane M represents the marker of known molecular weight.

:

To explore the functional implication of the NTR in the mode of action of TDH, we constructed a truncated variant of the toxin deleting the NTR (NTR-deleted; NTD) (Fig. 3.3A). Consistent with the absence of the NTR in the truncated protein, NTD, when analyzed by SDS-PAGE/Coomassie staining, showed marginal shift in its band position as compared to the wild type protein (Fig. 3.3B).

Also, Far-UV CD spectra and the intrinsic tryptophan fluorescence emission profile of NTD were found to be nearly overlapping to those of the wild type TDH, suggesting that the truncation of the NTR did not affect the overall secondary and tertiary structural organization of the protein to any noticeable extent (Fig. 3.4A-B). Another unique and notable structural feature of TDH is that it exists as a tetramer in solution. Such tetrameric assembly in solution has been shown to be important for membrane damaging activity of TDH. Therefore, we wanted to examine whether NTD, in the absence of the NTR, retained the ability to form the tetrameric assembly in solution. Sedimentation velocity AUC profile of NTD showed a major peak corresponding to the sedimentation coefficient value of 4.2, suggesting that the majority of NTD existed as tetramer in solution, with only a small population being present as monomer (Fig. 3.5).

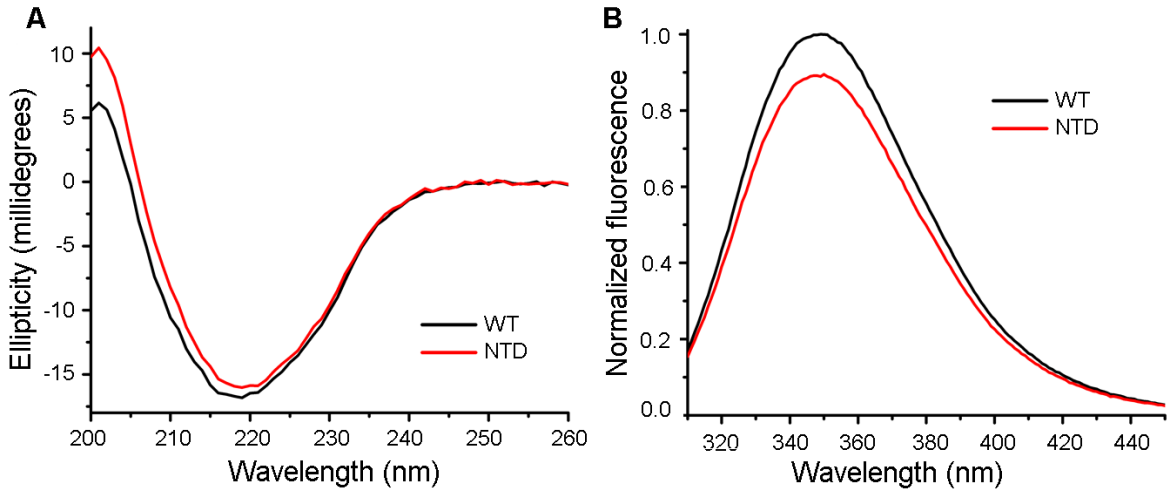

Fig. 3.4: (A) Far-UV CD spectroscopy profile of WT-TDH and NTD, (B) Intrinsic tryptophan fluorescence emission profile of WT-TDH and NTD mutant.

:

Altogether these data suggested that the deletion of the NTR did not affect the overall secondary, tertiary and quaternary structural arrangement of the protein to any noticeable extent.

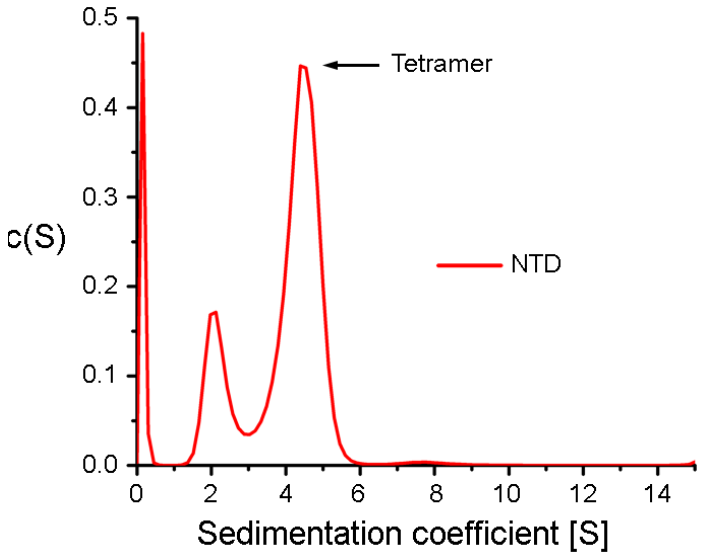

Fig. 3.5: Sedimentation velocity AUC profile of NTD (N-terminal deleted mutant) showing that the majority population of NTD exists as tetramer.

3.4.2 Deletion of the NTR compromises the amyloidogenicity of TDH

TDH is known to display prominent amyloidogenic property in terms of transforming into β-sheet rich, amyloid aggregates, when incubated at higher temperature of 60 ^{o}C [236]. The tendency to form the amyloid-like aggregates is commonly attributed to the presence of intrinsically disordered region(s) within the primary structure of a protein. Based on the analysis of the TDH primary structure, NTR is predicted to be intrinsically disordered (Fig. 3.1C). Therefore, we wanted to test whether the presence of the NTR contributes toward the amyloidogenicity of TDH. For this, we examined ThT fluorescence in the presence of the TDH variants (wild type and NTD), upon incubating the proteins at higher temperature of 60 ^{o}C. As reported in the earlier study [236], incubation of the wild type TDH at 60 ^{o}C displayed significant increase in the ThT fluorescence (Fig. 3.6), thereby confirming the formation of the amyloid fibrils. In contrast, deletion of the NTR resulted in the significant reduction in the amyloidogenic property of TDH, as suggested by the reduced ThT fluorescence emission observed in the presence of NTD under the similar experimental

:

setup (Fig. 3.6). Overall, these data suggested that the deletion of the intrinsically disordered NTR compromised the amyloidogenic propensity of TDH, to a prominent extent.

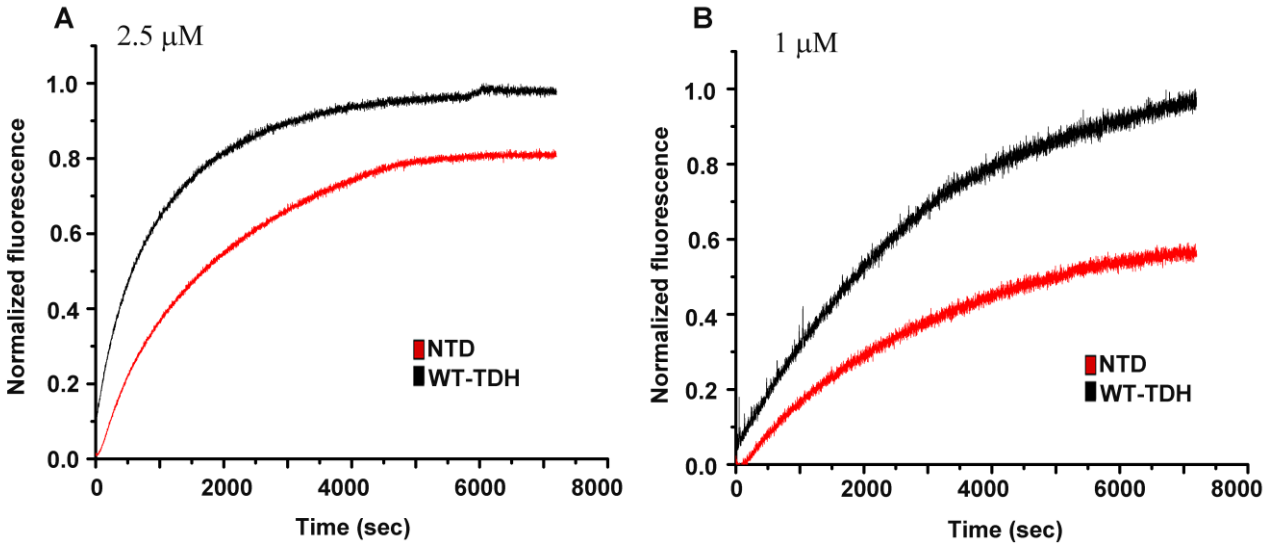

Fig. 3.6: Amyloidogenecity of TDH: Kinetics of amyloid-like fibril formation at 2.5 μM (A), and 1 μM (B) protein concentration.

3.4.3 NTR contributes toward generation of the surface-exposed hydrophobic patch(s) on TDH

Analysis of the primary amino acid sequence of TDH suggests that the NTR consists of a number of aromatic/hydrophobic residues (^{1}FELPSVPFPAP^{11}). Therefore, we wanted to examine whether the presence of the NTR contributes toward constituting any hydrophobic patch/pocket on the TDH surface. For this, we compared and analysed the ability of the TDH variants (wild type and NTD) to bind to ANS (1-anilinonaphthalene-8-sulfonic acid), an environment-sensitive hydrophobic fluorophore. ANS shows nominal fluorescence when present in the polar environment. Upon binding to the surface-exposed hydrophobic patches/pockets on the proteins, it shows significant increase in the fluorescence emission profile, along with the prominent blue shift in the fluorescence emission wavelength maximum [234, 237, 238]. However, when incubated in the presence of the wild type TDH, ANS fluorescence was found to be increased to a prominent extent, along with a blue shift in the fluorescence emission wavelength maximum, thus suggesting binding of ANS to the surface-exposed hydrophobic patch(s) on TDH (Fig. 3.7). However, in the presence of NTD, ANS fluorescence was found to be almost negligible, and nearly similar to that

:

observed with the buffer control (Fig. 3.7). Altogether, these data suggested that TDH indeed consists of a hydrophobic patch(s) on its surface, and the presence of the NTR presumably plays a critical role toward constituting such hydrophobic patch(s).

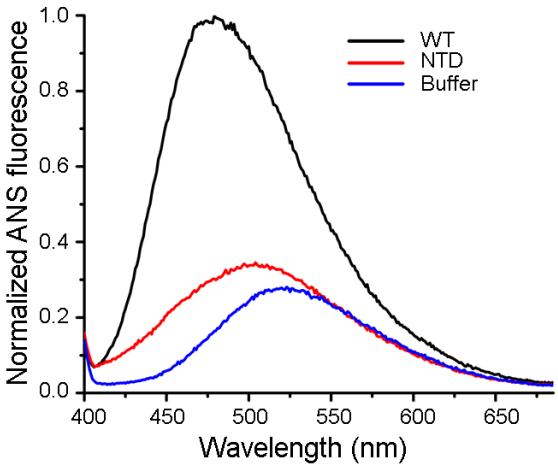

Fig. 3.7: ANS fluorescence emission profile of WT-TDH and NTD-TDH. ANS spectrum in the buffer containing no protein is shown in blue.

3.4.4 Deletion of the NTR compromises the binding ability of TDH toward the membrane lipid bilayer of the liposomes

As mentioned above, NTR is enriched with a number of aromatic/hydrophobic residues, and the presence of the NTR appears to facilitate formation of 'surface-exposed hydrophobic patch' on TDH. Presence of the NTR contributes toward the binding of TDH to the hydrophobic fluorophore, ANS. Based on such observation, we tested whether the presence of the NTR could play any role in the binding ability of TDH toward the amphipathic phase of the membrane lipid bilayer of the synthetic lipid vesicles or liposomes. For this, we examined binding of the TDH variants (wild type and NTD) with the Asolectin-cholesterol (Fig. 3.8) and PC-cholesterol (Fig. 3.9) liposome membranes, by using an SPR-based assay. Results obtained from the SPR-based assay suggested that NTD displayed prominent reduction in binding to the membrane lipid bilayer of the Asolectin-cholesterol and PC-cholesterol liposomes, as compared to those observed with the wild type protein.

:

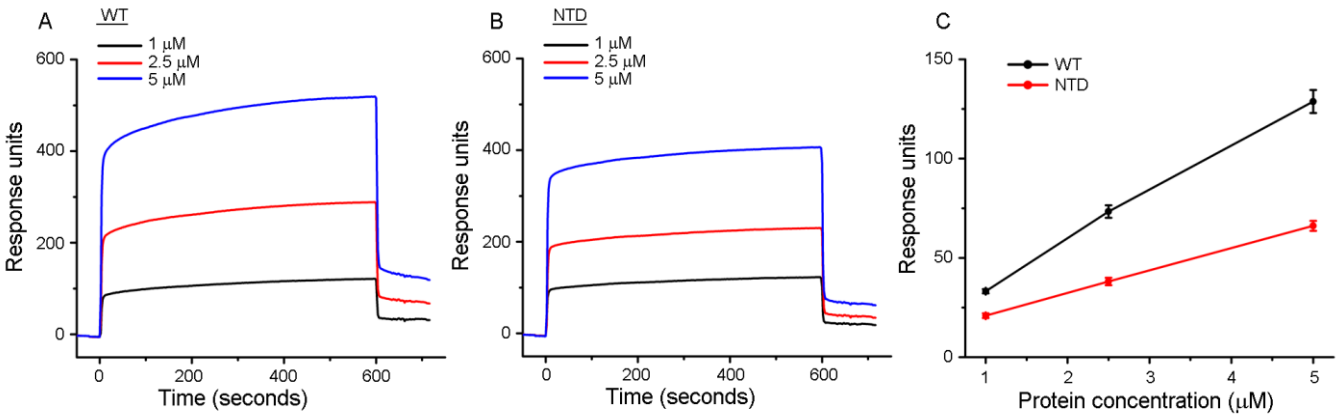

Fig. 3.8: Truncation of the NTR from TDH compromises the binding efficiency toward the membrane lipid bilayer of the Asolectin-cholesterol liposomes: Binding of the TDH variants (NTD and WT) to the membrane lipid bilayer of the Asolectin-cholesterol (A-C) was examined by the SPR-based assay. A-B, Real time binding sensograms of the TDH variants with the Asolectin-cholesterol liposomes. C, End point binding profile of the TDH variants with the Asolectin-cholesterol liposomes.

This observation suggests that the presence of the NTR indeed contributes toward partitioning of TDH into the membrane lipid bilayer of the liposomes. Our data suggest that the deletion of the NTR from TDH affected the binding efficacy of the toxin with the membranes of the liposomes.

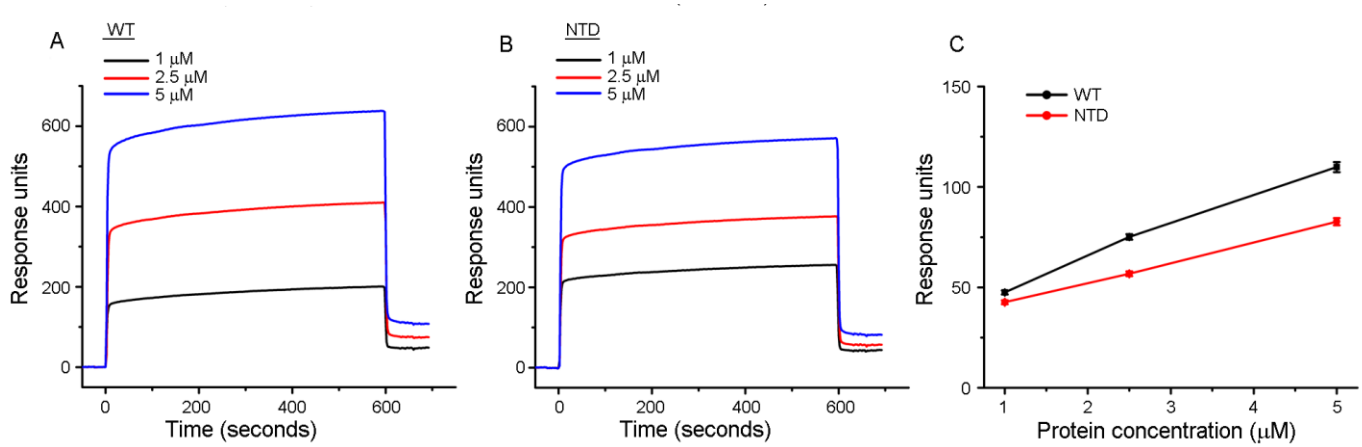

Fig. 3.9: Truncation of the NTR from TDH compromises the binding efficiency toward the membrane lipid bilayer of the PC-cholesterol liposomes: Binding of the TDH variants (NTD and WT) to the membrane lipid bilayer of the PC-cholesterol (A-C) was examined by the SPR-based assay. A-B, Real time binding sensograms of the TDH variants with the PC-cholesterol liposomes. C, End point binding profile of the TDH variants with the PC-cholesterol liposomes.

:

3.4.5 Presence of the NTR plays a critical role in the membrane-damaging cytolytic activity of TDH

In order to explore the functional implication of the NTR in the mode of action of TDH, we examined whether the deletion of the NTR affected the cytolytic/cytotoxic activity of the toxin. For this we performed the hemolytic activity assay. In this assay, NTD displayed drastically reduced ability to cause the lysis of human erythrocytes, when compared to the wild type TDH (Fig. 3.10). Consistent with the earlier studies, wild type TDH protein exhibited potent hemolytic activity against the human erythrocytes under the similar experimental conditions. For example, WT-TDH showed nearly 90% hemolytic activity at a concentration of 0.75 μM. In contrast, 0.75 μM of NTD displayed less than 5% hemolytic activity under the similar experimental conditions.

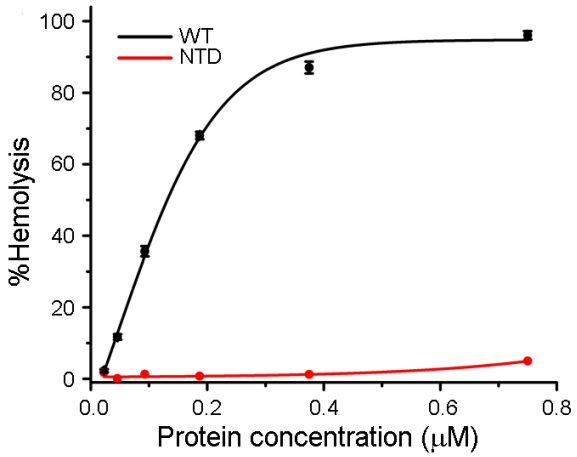

Fig. 3.10: Hemolytic activity profile of WT-TDH and NTD incubated with human erythrocytes with different toxin concentration.

Next, we wanted to determine whether the reduced cytolytic activity of NTD was due to the deficient binding ability toward the target cells. For this, we performed flow cytometry-based assay of binding with the human erythrocytes. Our result suggested that the binding of NTD with human erythrocytes was severely compromised, as compared to those observed with the wild type protein (Fig. 3.11). Fractions of the cell population having bound TDH variants were found to be considerably less in the case of NTD treatment, as compared to that observed upon treatment with the wild type protein.

:

Therefore, this data suggested that the presence of the NTR plays an important role in the optimal binding process of TDH toward the target human erythrocytes cell membranes, and promotes efficient membrane-damaging cytolytic activity of the toxin.

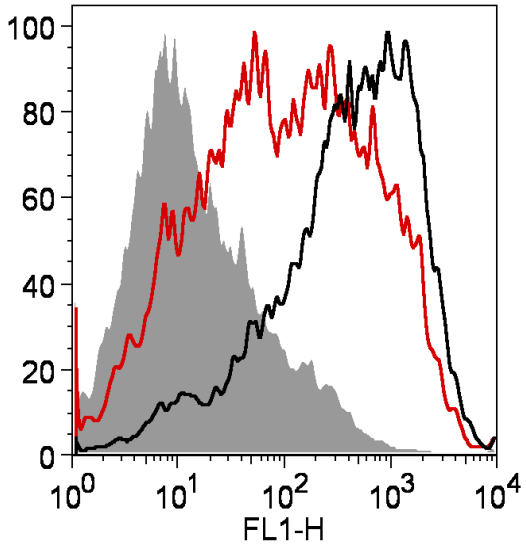

Fig. 3.11: Binding profile of NTD and WT-TDH to the membrane human erythrocytes by flow cytometry-based assay

3.4.6 Deletion of the N-terminal region (NTR) compromises the membrane-damaging cytotoxic activity of TDH

Deletion of the NTR showed a drastic reduction in the functional pore-forming activity against human erythrocytes. We also examined the cytotoxic activity of TDH against the T84 intestinal epithelial cells, and THP-1 monocytic cells by employing the LDH-release assay of cytotoxicity. In this assay we observed that no prominent cytotoxicity was induced by NTD (at a concentration of 1 μM) against both the cell types studied. In contrast, wild type TDH (at a concentration of 1 μM) induced potent cytotoxicity (~75-80%) in both the cell types, under the similar experimental conditions (Fig. 3.12). This data suggested that the removal of the NTR from TDH critically affected the cytotoxic activity of the toxin.

:

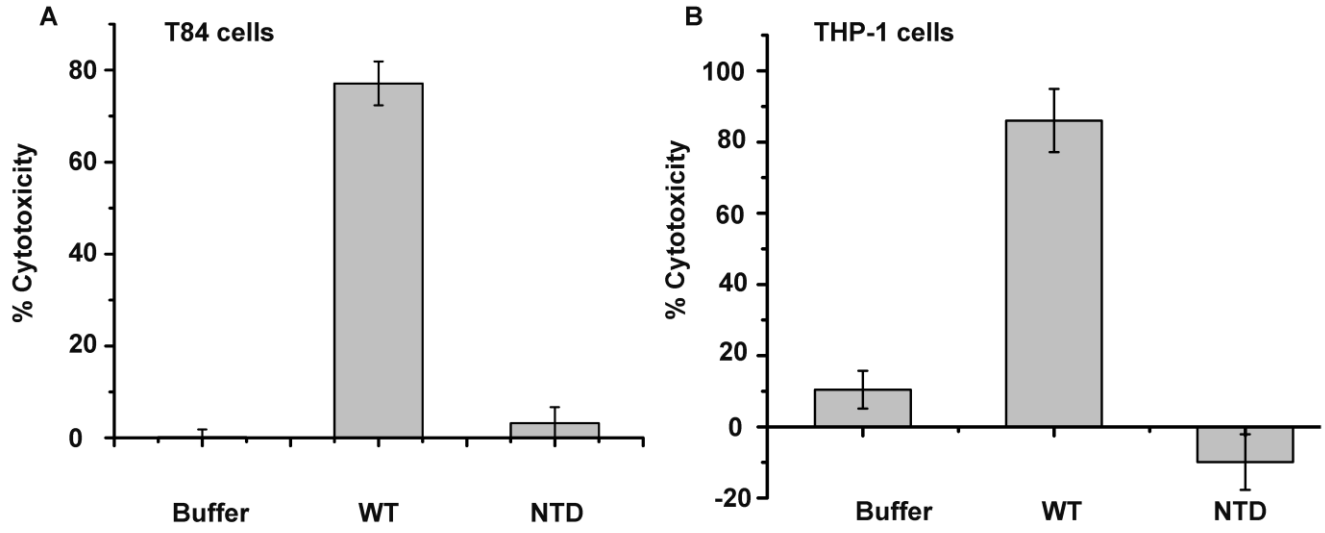

Fig. 3.12: (A) Cytotoxic activity profile of WT-TDH and NTD in human intestinal cells T84, (B) Cytotoxic activity profile of WT-TDH and NTD in human monocytic cell line THP-1

Next, we wanted to determine whether the reduced cytotoxic activity of NTD was due to the deficient binding ability of the truncated protein toward the target cells. For this, we performed the flow cytometry-based assay of binding with the T84 and THP-1 cells. Our results showed that the binding of NTD with the T84 and THP-1 cells were severely compromised, as compared to those observed with the wild type protein (Fig. 3.13). Fractions of the cell population having bound TDH variants were found to be considerably less in the case of NTD treatment, as compared to that observed upon treatment with the wild type protein.

Therefore, this data suggested that the presence of the NTR plays an important role in the optimal binding process of TDH toward the target cell membranes, and promotes efficient membrane-damaging cytotoxic activity of the toxin.

:

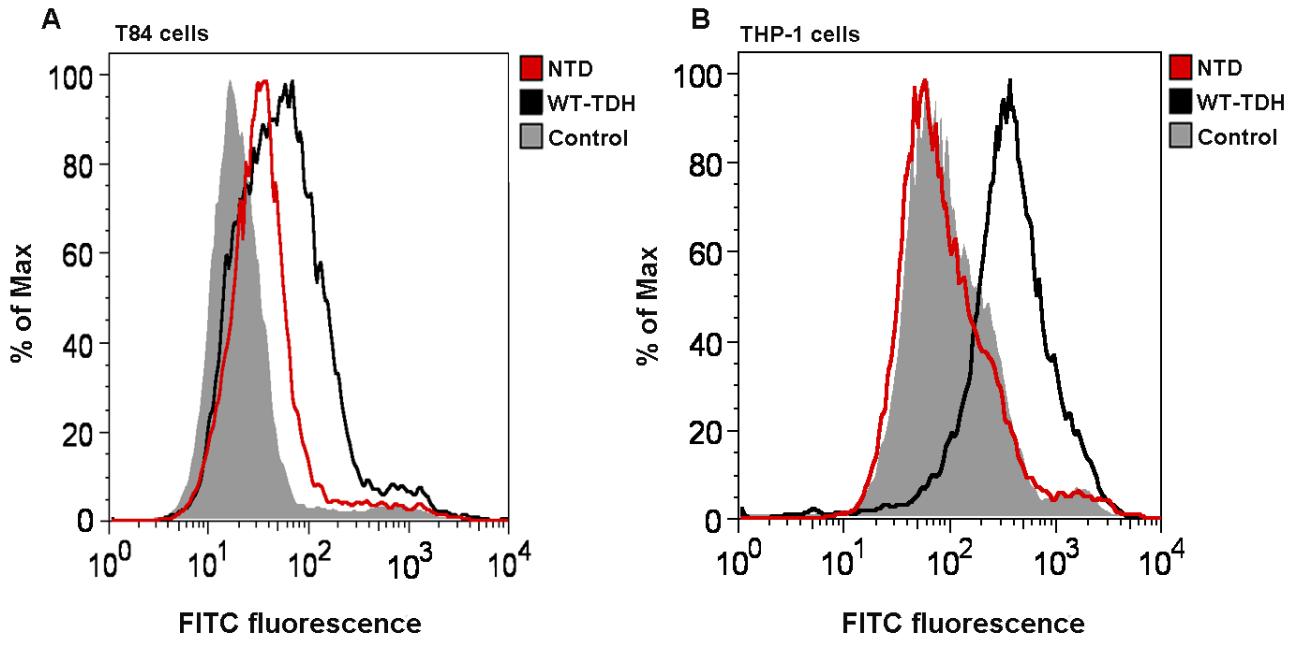

Fig. 3.13: (A) Flow cytometry-based binding profile of WT-TDH and NTD in human intestinal cells T84 (B) Flow cytometry-based binding profile of WT-TDH and NTD in human monocytic cell line THP-1

3.4.7 Aromatic and hydrophobic residues within the NTR play critical roles in binding and cytolytic/cytotoxic activity of TDH

The NTR of TDH harbors a number of aromatic/hydrophobic residues. We explored whether the aromatic/hydrophobic residues within the NTR play any role in the cytolytic/cytotoxic activity of TDH. For this, we generated two mutant variants of TDH: in one mutant both the phenylalanine residues at position 1 and 8 were mutated to alanine (F1A-F8A-TDH), and in the other case the leucine residue at position 3 and valine residues at position 6 were mutated to alanine (L3A-V6A-TDH). Both the mutants displayed nearly similar far-UV CD (Fig. 3.14) and intrinsic tryptophan fluorescence emission profile (Fig. 3.15), as compared to those of the wild type TDH, suggesting wild type like secondary and tertiary structural organization of the mutated variants Both the mutated variants, F1A-F8A-TDH and L3A-V6A-TDH, displayed marked reduction in the hemolytic activity against the human erythrocytes, as compared to the wild type protein (Fig. 3.16). At a concentration of 0.75 μM, F1A-F8A-TDH and L3A-V6A-TDH displayed ~50% and ~30% hemolytic activity,

:

respectively, while the wild type TDH showed ~90% activity under the similar experimental conditions.

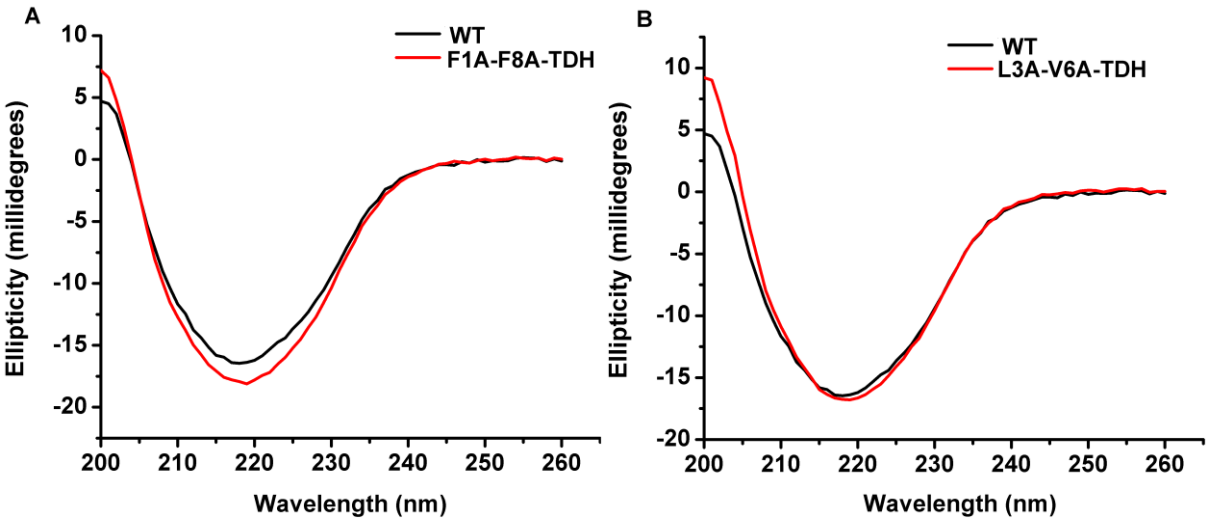

Fig. 3.14: (A) Far-UV CD spectroscopy profile of WT-TDH and F1A-F8A-TDH, (B) Far-UV CD spectroscopy profile of WT-TDH and L3A-V6A-TDH mutants.

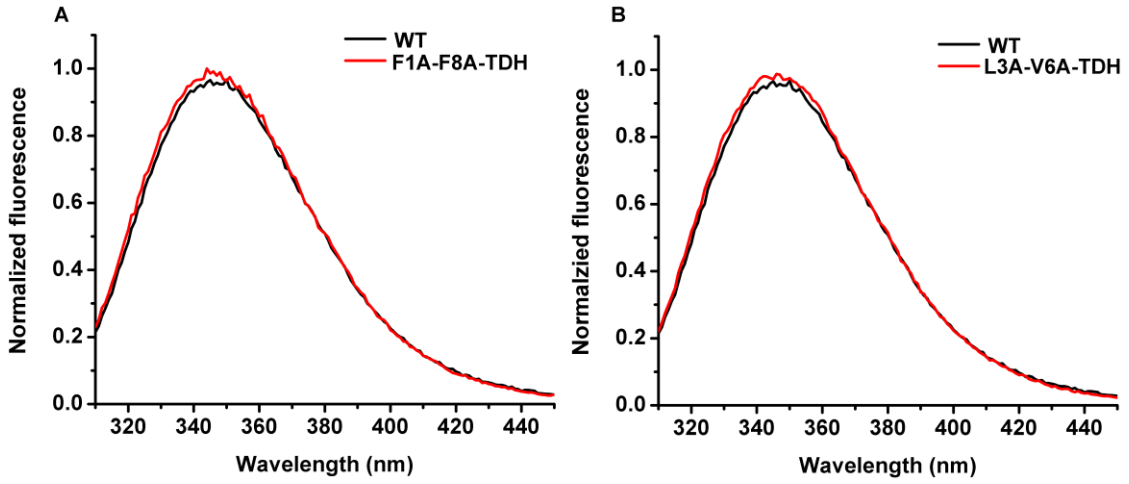

Fig. 3.15: (A) Intrinsic tryptophan fluorescence emission profile of WT-TDH and F1A-F8A-TDH, (B) Intrinsic tryptophan fluorescence emission profile of WT-TDH and L3A-V6A-TDH mutants.

:

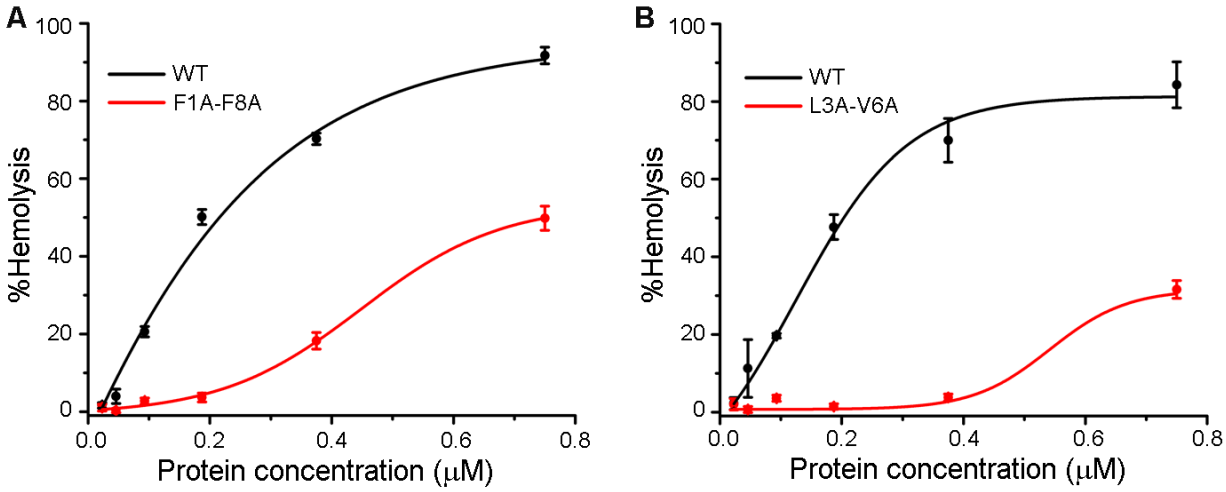

Fig. 3.16: (A) Hemolytic activity profile of WT-TDH and F1A-F8A-TDH (B) Hemolytic activity profile of WT-TDH and L3A-V6A-TDH

Next, we wanted to determine if the reduced cytolytic activity was due to the compromised membrane-binding ability of the mutated variants of the toxin. Flow cytometry-based assay of binding showed that the binding efficiencies of both the mutants toward the human erythrocytes were significantly reduced as compared to that of the wild type TDH (Fig.3.17).

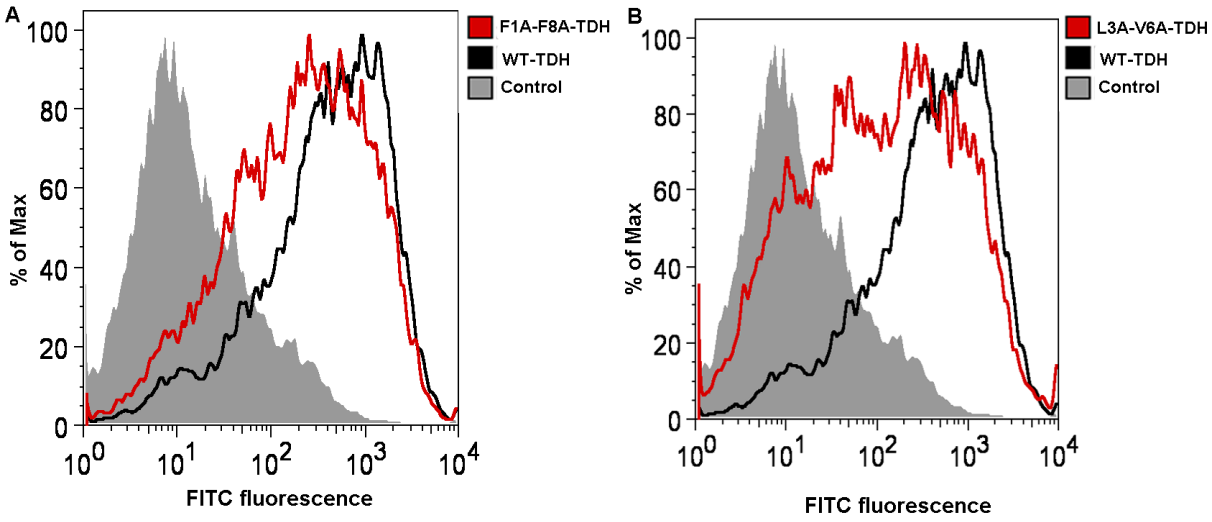

Fig. 3.17: (A) Flow cytometry based binding profile of WT-TDH and F1A-F8A-TDH (B) Flow cytometry based binding profile of WT-TDH and L3A-V6A-TDH

:

Consistent with the reduced membrane-damaging hemolytic activity, F1A-F8A-TDH and L3A-V6A-TDH (at a protein concentration of 1 μM) also displayed significant reduction in their cytotoxic activity against the T84 intestinal epithelial cells and THP-1 monocytic cells, as compared to those observed with the wild type protein (Fig. 3.18A-B). Mutations of F1A-F8A were found to cause more deleterious effect on the cytotoxicity, as compared to the mutations of L3A-V6A. F1A-F8A-TDH could not display any noticeable cytotoxicity (<5% cytotoxicity) in both the T84 and THP-1 cells, while L3A-V6A-TDH showed moderate to low-level cytotoxicity in the range of ~20-40% (Fig. 3.18A-B). As mentioned above, wild type TDH displayed ~75-80% cytotoxicity in these cell types, under the similar experimental condition.

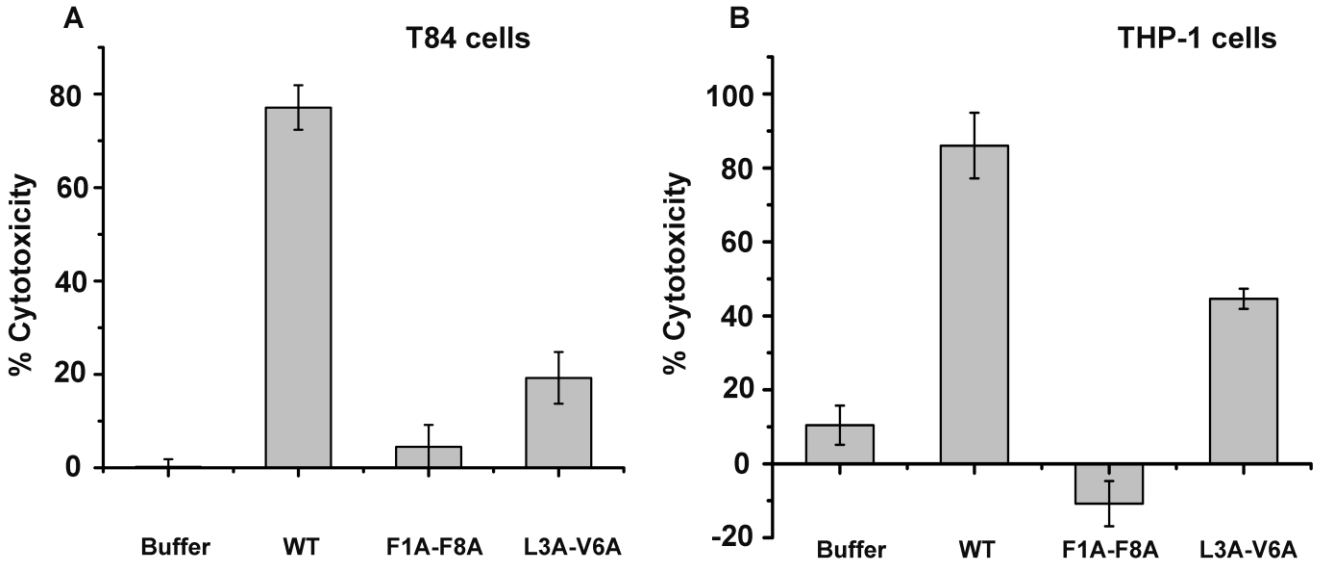

Fig. 3.18: (A) Cytotoxic activity profile of WT-TDH, F1A-F8A-TDH and L3A-V6A-TDH in human intestinal cells T84 (B) Cytotoxic activity profile of WT-TDH, F1A-F8A-TDH and L3A-V6A-TDH in human monocytic cell line THP-1

When examined for their binding ability to the membranes of T84 and THP-1 cells, both the mutants were found to display noticeably reduced binding as compared to the wild type protein (Fig. 3.19A-D). Altogether, these results suggested that the aromatic/hydrophobic residues within the NTR of TDH play crucial roles in the membrane-damaging cytotoxic activity of the toxin.

:

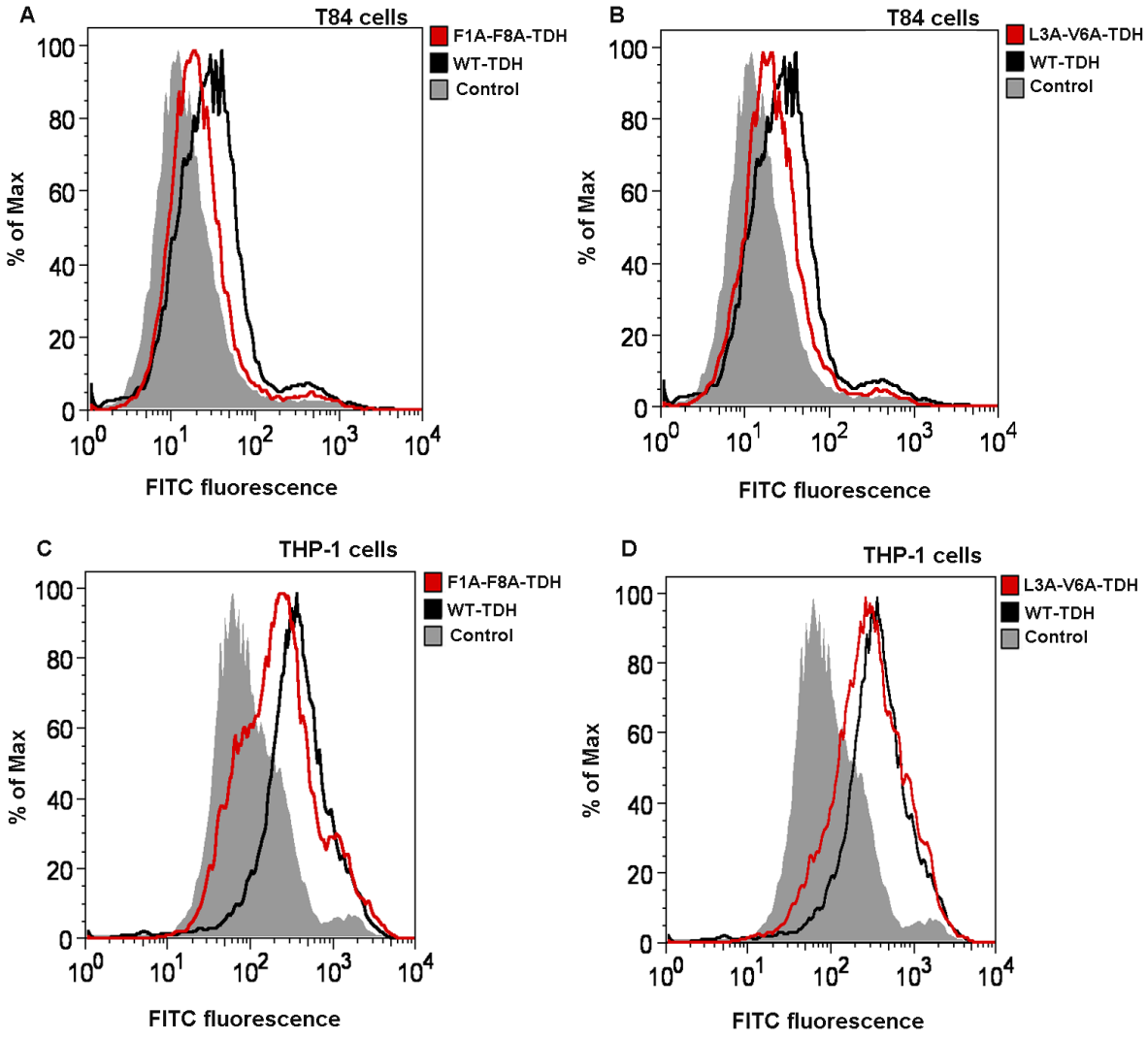

Fig. 3.19: (A) Flow cytometry based-binding profile of WT-TDH, F1A-F8A-TDH with T84 cells, (B) L3A-V6A-TDH in T84 cells, (C) F1A-F8A-TDH with THP-1 cells, (D) L3A-V6A-TDH with THP-1 cells

3.4.8 Trapping of N-terminal region (NTR) via engineered disulphide bond abrogates the membrane-damaging cytolytic/cytotoxic activity of TDH

Analysis of the crystal structure of TDH predicts the NTR as an intrinsically disordered region (Fig. 3.1C). Also, the NTR could not be modelled in the TDH crystal structure, presumably due to high degree of structural/conformational fluctuation of this region [199]. We wanted to explore the functional implication, if any, of such predicted flexibility of the NTR in the mode of action of TDH. For this, we attempted to restrain the predicted

:

structural/conformational fluctuation of the NTR. We constructed a variant by introducing two cysteine residues (Ser5Cys and Ser13Cys) in TDH (S5C-S13C-TDH) (Fig. 3.20A). Presence of these two engineered cysteine residues would allow formation of a disulphide bond that, in turn, would restrain the NTR against the core β-sandwich domain of TDH.

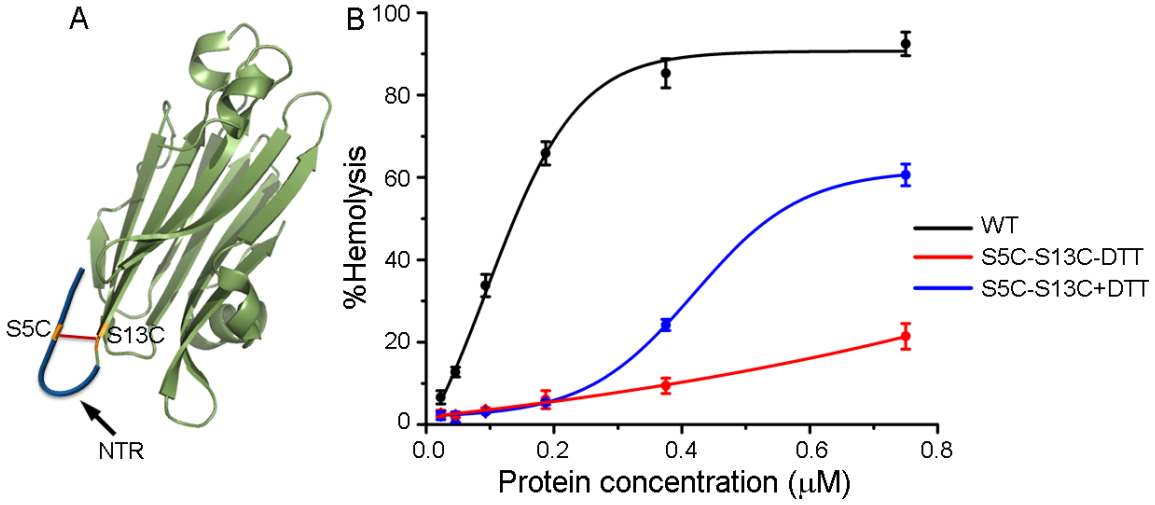

Fig. 3.20: Introduction of two cysteine residues via double mutations of Ser5Cys and Ser13Cys in TDH (S5C-S13C) allowing the formation of an disulphide bond that, in turn, would lock the NTR. B. Hemolytic activity (against the human erythrocytes) of S5C-S13C in the absence or presence of the reducing agent DTT. Presence of the reducing agent would break the disulphide bond involving the engineered Cys residues in S5C-S13C mutant, thereby opening the locking of NTR.

Far-UV CD and intrinsic tryptophan emission fluorescence profile of S5C-S13C-TDH were found to be nearly similar to those observed with the wild type TDH, suggesting that there was no overall change in the secondary and tertiary structural organization of the protein upon incorporation of the two additional cysteine residues (Fig. 3.21A-B)

:

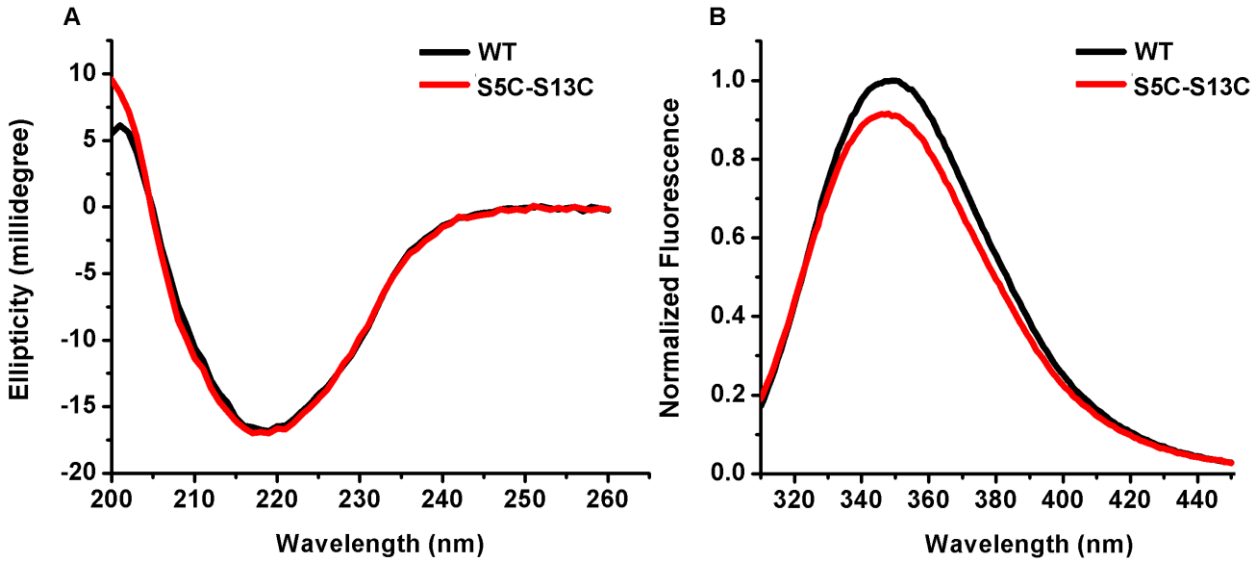

Fig. 3.21: (A) Far-UV CD spectra of WT-TDH and S5C-S13C-TDH highlighting the secondary structural information (B) Intrinsic tryptophan fluorescence emission profile of S5C-S13C-TDH suggesting that the tertiary structure of the mutant remains intact.

When tested for the functional pore-forming activity of the S5C-S13C-TDH, the variant showed marked reduction in the hemolytic activity. At a protein concentration of 0.75 μM, it induced nominal ~20% hemolytic activity against the human erythrocytes, as compared to ~90% hemolytic activity of the wild type TDH (Fig. 3.20B). Interestingly, when monitored in the presence of the reducing agent DTT (1 mM), hemolytic activity of S5C-S13C-TDH was found to be rescued, although not fully, but at least to a prominent level (~60% hemolytic activity, at a protein concentration of 0.75 μM) (Fig. 3.20B). S5C-S13C-TDH also displayed reduced cytotoxic activity (<10% cytotoxicity) against the T84 and THP-1 cells, and such compromised cytotoxic activity was reversed, at least to a noticeable extent, when the experiments were conducted in the presence of the reducing agent DTT (Fig. 3.22). These data suggested that restraining of the NTR via engineered disulphide bond formation abrogated the membrane-damaging cytolytic/cytotoxic activity of the toxin. Also, the release of the restrained configuration of the NTR via reduction of the disulphide bond, by treating with DTT, restored the cytolytic/cytotoxic activity of TDH. These results, in turn, allowed us to conclude that, not only the presence of the NTR, but also the

:

structural/conformational flexibility of this motif is critical for the efficient execution of the membrane-damaging cell-killing activity of TDH.

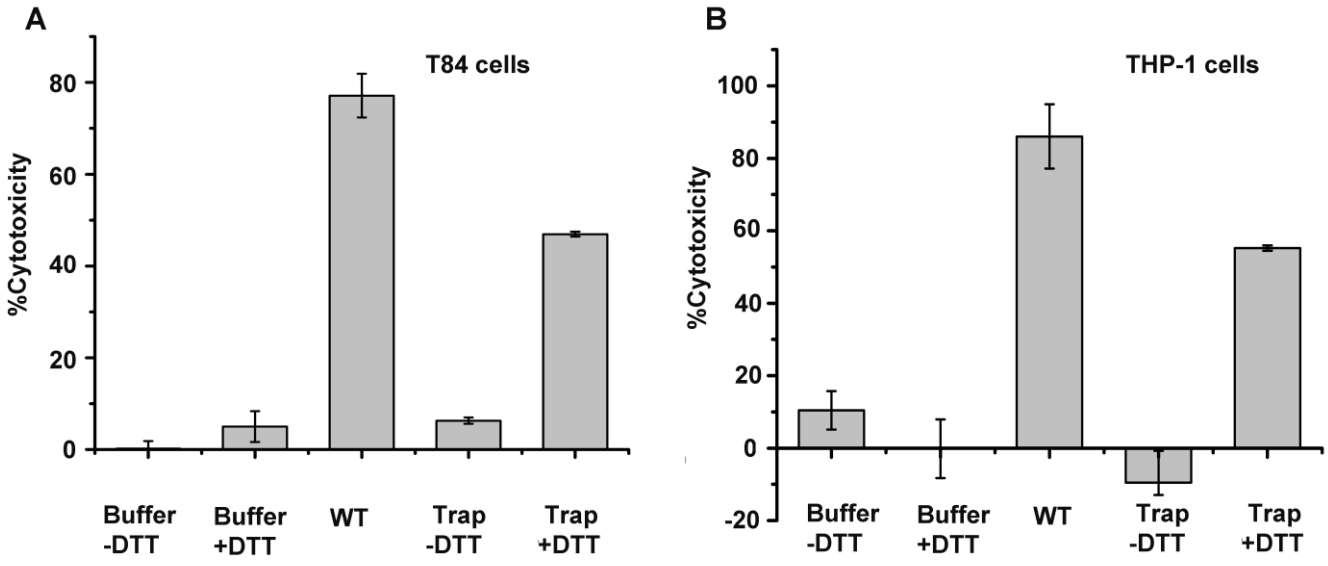

Fig. 3.22: (A) Cytotoxic activity profile of WT-TDH and S5C-S13C-TDH (in the absence and presence of 1 mM DTT) against the T84 human intestinal epithelial cells (A), and THP-1 human monocytic cells (B).

3.5 Discussion and conclusion

The available crystal structure of TDH lacks the first 11 residue-long N-terminal region (NTR), presumably due to its tendency to adopt multiple conformations, or possibly due to its structural/conformational fluctuations [199]. Based on the analysis of the amino acid sequence, NTR is predicted to be intrinsically disordered. Lack of any available study related to the role of the flexible NTR in the mode of action of TDH prompted us to investigate its functional implications in the cell-killing mechanism of TDH. The present chapter has discussed the results of our detail investigation on the role of the NTR in the structure-function mechanism of TDH. By using a truncated variant of TDH, deleting the first 11-residues corresponding to the flexible NTR, we showed that NTR plays a critical role in the membrane-damaging pore-forming activity of the toxin. Our data showed that the NTR also plays a significant role in the anchoring/binding of the toxin to the target cell membrane.

:

The analysis of the primary amino acid sequence of TDH has suggested that the NTR sequence is rich in hydrophobic residues (^{1}FELPSVPFPAP^{11}). Accordingly, the presence of the NTR was found to contribute toward formation of surface-exposed hydrophobic patch(s) that binds hydrophobic dye ANS. It is therefore reasonable that NTR contributes to the membrane-binding activity of TDH. When the hydrophobic amino acids present in the NTR were specifically mutated, like in the mutants F1A-F8A-TDH and L3A-V6A-TDH, we found a significant reduction in the membrane-damaging and membrane-binding activities. In particular, F1A-F8A-TDH showed significantly reduced membrane-damaging activities. These results suggested that the aromatic-hydrophobic amino acids like F1-F8 are the key residues that play critical roles in the process. When we restrained the flexibility of the by engineering a disulphide bond (that would lock the NTR against the core β-sandwich domain; in the mutant S5C-S13C-TDH), the mutant showed reduced functional membrane-damaging activity. In contrast, when the trap was opened by treating with DTT, the compromised membrane-damaging activity was rescued. This data confirmed that flexibility of the NTR is a crucial structural feature in TDH which plays important role in the cytolytic/cytotoxic responses generated by TDH. It is important to note that the deletion, mutations, and covalent trapping (restraining the structural/conformational fluctuation) of the NTR affected the cytolytic/cytotoxic activity of TDH to a greater extent, while the membrane-binding ability was found to be affected less drastically. It is possible that NTR alone may not be responsible in membrane binding, and additional structural motif(s) in TDH may be involved in mediating the membrane-binding process of the toxin. In contrast, efficient membrane-damaging ability of TDH appears to be critically dependent on the presence of the NTR, presumably with its intrinsically disordered configuration. It is possible that the NTR might play critical role during the process of structural rearrangement/readjustment upon membrane binding, for the efficient execution of the subsequent cell-killing mechanism of TDH.

TDH shows high structural similarity for its core β-sandwich domain with the eukaryotic actinoporins like Equinatoxin II, Fragaceatoxin C and Sticholysin II [170]. However, analysis of the actinoporin structures suggests distinct structural disposition of their NTR segments. Actinoporin structure shows the presence of an extended (~30 amino acid long) NTR, part of which adopts α-helical transmembrane motif. The crystal structure of the transmembrane form

of Fragaceatoxin C further suggests that the NTR undergoes structural/conformational reorganization upon membrane binding, and transforms into an elongated membrane-inserted α-helical structure that forms the transmembrane region of the pore complex [181]. Similar roles of the NTRs of other actinoporins, like Equinatoxin II have also been suggested through biochemical/biophysical studies [33, 170]. The crystal structure of the transmembrane pore state of TDH has not been elucidated yet. Also, there is no information available in the literature, at present, regarding the identity of the transmembrane motif used by TDH to form the membrane pore. Based on the critical role(s) of the NTR in the mechanism of action of TDH, as shown for the first time in the present study, it is possible to speculate that the NTR may form the membrane pore-forming motif of the toxin. However, the NTR consists of only 11 residues that would be too short to span the entire ~25 Å depth of the plasma membrane, and to form the transmembrane motif. Nevertheless, the results obtained from the present work suggest that NTR plays a critical role in the efficient membrane-binding ability, and membrane-damaging cytolytic/cytotoxic activity of TDH.

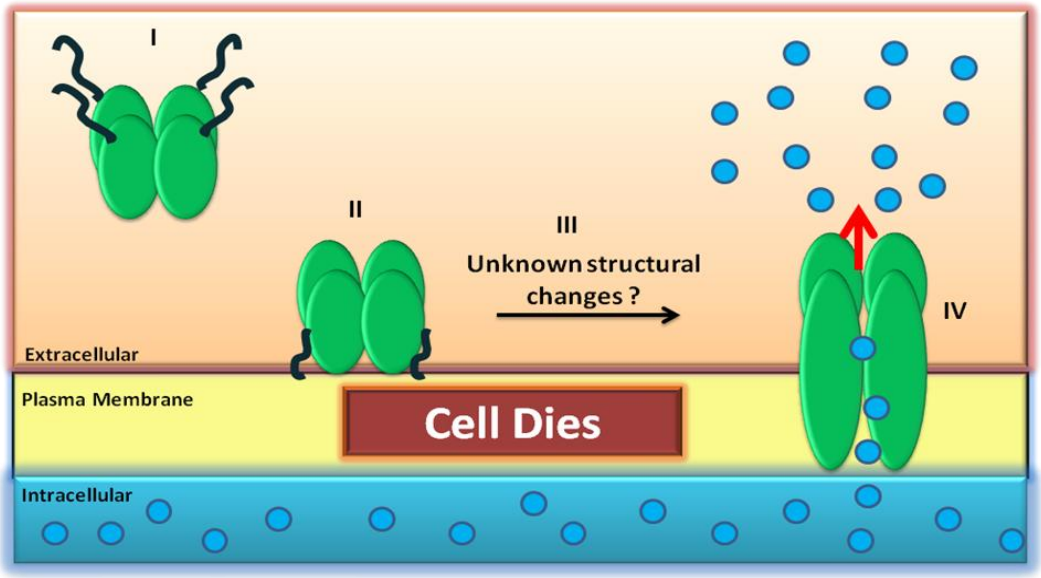

Fig. 3.23: N-terminal region-mediated binding mechanism of TDH: (I) TDH is present as a tetramer in solution with flexible N-terminal region (NTR; marked as black zigzag structure). (II) NTR mediates the association of the toxin on to the cell membrane surface. (III) Structural changes possibly take place upon binding to the target membranes. (IV) Pore-formation in the membrane resulting in the membrane permeabilization and cell death.

:

Conventional/archetypical PFTs generally generates ‘protein-only’ transmembrane pores on the target membranes, which can be classified as either α-PFT or β-PFT, depending on the type of secondary structures used in the construction of the transmembrane region [127, 231]. However, additional mechanisms of the membrane pore-formation by the PFTs have emerged in the recent years. For example, many pore-forming proteins and peptides are now shown/predicted to form the ‘so-called’ ‘toroidal pores’

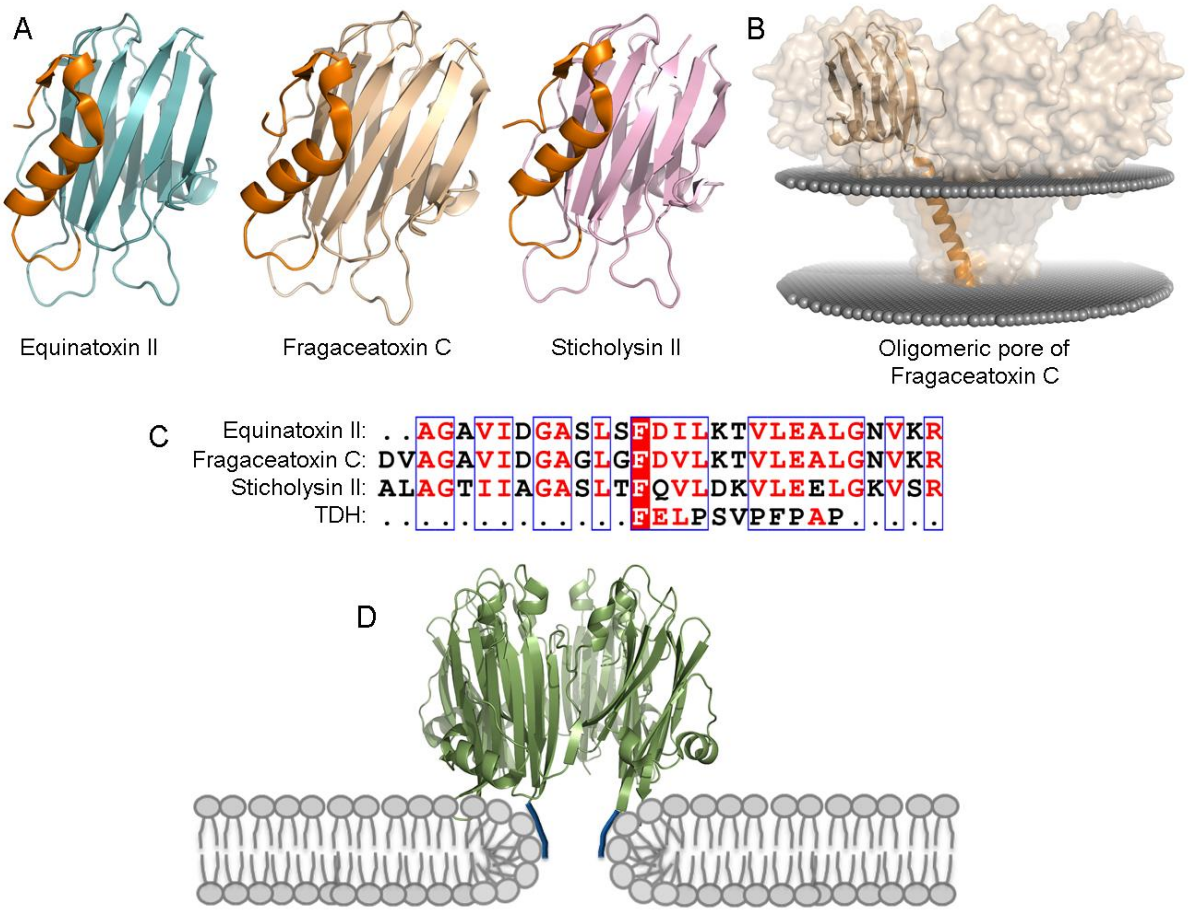

Fig. 3.24: Proposed model for the role of the NTR in the membrane-damaging cytolytic/cytotoxic activity of TDH. A. Structural models of Equinatoxin II, Fragaceatoxin C, and Sticholysin II highlighting the presence of an extended NTR (shown in orange) in the eukaryotic actinoporin family of PFTs. B. Structural model of the oligomeric pore state of Fragaceatoxin C showing involvement of the NTR (in orange color) in generating the transmembrane motif. C. Amino acid sequence alignment of the NTR of TDH with those of Equinatoxin II, Fragaceatoxin C, and Sticholysin II. D. Proposed model speculating the role of the NTR of TDH in the membrane-damaging activity of the toxin [173, 174].

:

[170, 239]. Toroidal pores are formed by the systematic distortion of the membrane phospholipid assembly, imposed by the specialized pore-forming peptides/protein segments, where pore-linings are formed partly by the polypeptide motifs, and partly by the membrane phospholipid headgroups. Therefore, for the toroidal pore formation, it may not be necessary that the protein motif(s) would have to span the entire depth of the membrane.

Toroidal pore model has been predicted for the actinoporin family of PFTs, particularly for Equinatoxin II and Sticholysin II, where the numbers of the protomers involved in the pore-formation are limited to 3-4 [170]. In such cases, α-helices from the contributing protomers (3-4 protomers) would not be able to fill the entire pore lining, unless the lipid molecules are involved in the formation of the pore wall. Based on such observations, and also based on the results obtained from the present study, it is possible to speculate that the NTR of TDH, despite its shorter length as compared to those of the actinoporins, could be acting as the structural motif toward forming the toroidal pores on the target membranes.

However, more structural studies would be required in future to conclusively prove that TDH indeed follows the toroidal model of membrane pore formation, and NTR plays a direct role in constituting the pore architecture.

In sum, the present study provides critical new insights regarding the functional implications of the intrinsically disordered N-terminal segment of TDH. This, in turn, prompts us to elucidate the mechanistic basis of the membrane-damaging action of TDH.

:

References

:

References:

1. Singer, S.J. and G.L. Nicolson, *The fluid mosaic model of the structure of cell membranes.* Science, 1972. **175**(4023): p. 720-731.
2. Israelachvili, J.N., *Refinement of the fluid-mosaic model of membrane structure.* Biochimica et Biophysica Acta (BBA)-Biomembranes, 1977. **469**(2): p. 221-225.
3. Jacobson, K., E.D. Sheets, and R. Simson, *Revisiting the fluid mosaic model of membranes.* Science, 1995. **268**(5216): p. 1441-1443.
4. Vereb, G., et al., *Dynamic, yet structured: the cell membrane three decades after the Singer–Nicolson model.* Proceedings of the National Academy of Sciences, 2003. **100**(14): p. 8053-8058.
5. Bernardino de la Serna, J., et al., *There is no simple model of the plasma membrane organization.* Frontiers in cell and developmental biology, 2016. **4**: p. 106.
6. Lelievre, S.A. and M.J. Bissell, *Communication between the cell membrane and the nucleus: role of protein compartmentalization.* Journal of cellular biochemistry, 1998. **72**(S30–31): p. 250-263.
7. Luna, E.J. and A.L. Hitt, *Cytoskeleton--plasma membrane interactions.* Science, 1992. **258**(5084): p. 955-964.
8. Wallin, E. and G.V. Heijne, *Genome‐wide analysis of integral membrane proteins from eubacterial, archaean, and eukaryotic organisms.* Protein Science, 1998. **7**(4): p. 1029-1038.
9. Pohorille, A., K. Schweighofer, and M.A. Wilson, *The origin and early evolution of membrane channels.* Astrobiology, 2005. **5**(1): p. 1-17.
10. Davidson, J., *Selective permeability and the plasmamembrane.* The Plant World, 1916. **19**(11): p. 331-349.
11. Ek-Vitorin, J.F. and J.M. Burt, *Structural basis for the selective permeability of channels made of communicating junction proteins.* Biochimica et Biophysica Acta (BBA)-Biomembranes, 2013. **1828**(1): p. 51-68.
12. Valeva, A., et al., *Evidence that clustered phosphocholine head groups serve as sites for binding and assembly of an oligomeric protein pore.* Journal of Biological

:

Chemistry, 2006. **281**(36): p. 26014-26021.

13. Arellano-Reynoso, B., et al., *Cyclic β-1, 2-glucan is a Brucella virulence factor required for intracellular survival.* Nature immunology, 2005. **6**(6): p. 618.
14. Iacovache, I., F.G. van der Goot, and L. Pernot, *Pore formation: an ancient yet complex form of attack.* Biochimica et Biophysica Acta (BBA)-Biomembranes, 2008. **1778**(7-8): p. 1611-1623.
15. Ladant, D., J.E. Alouf, and M.R. Popoff, *The comprehensive sourcebook of bacterial protein toxins*. 2005: Academic Press.
16. Sher, D., et al., *Hydralysins, a new category of β-pore-forming toxins in cnidaria.* Journal of Biological Chemistry, 2005. **280**(24): p. 22847-22855.
17. Bernheimer, A.W. and L.S. Avigad, *Properties of a toxin from the sea anemone Stoichacis helianthus, including specific binding to sphingomyelin.* Proceedings of the National Academy of Sciences, 1976. **73**(2): p. 467-471.
18. Shogomori, H. and T. Kobayashi, *Lysenin: a sphingomyelin specific pore-forming toxin.* Biochimica et Biophysica Acta (BBA)-General Subjects, 2008. **1780**(3): p. 612-618.
19. De Sousa, M. and L. Morhy, *Enterolobin, a hemolytic protein from Enterolobium contortisiliquum seeds (Leguminosae--Mimosoideae). Purification and characterization.* Anais da Academia Brasileira de Ciencias, 1989. **61**(4): p. 405-412.
20. Pipkin, M.E. and J. Lieberman, *Delivering the kiss of death: progress on understanding how perforin works.* Current opinion in immunology, 2007. **19**(3): p. 301-308.
21. Gonzalez, M., et al., *Bacterial pore-forming toxins: the (w) hole story?* Cellular and molecular life sciences, 2008. **65**(3): p. 493-507.
22. Parker, M.W. and S.C. Feil, *Pore-forming protein toxins: from structure to function.* Progress in biophysics and molecular biology, 2005. **88**(1): p. 91-142.
23. Huffman, D.L., et al., *Mitogen-activated protein kinase pathways defend against bacterial pore-forming toxins.* Proceedings of the National academy of Sciences of the United States of America, 2004. **101**(30): p. 10995-11000.

:

24. Gekara, N. and S. Weiss, *Lipid rafts clustering and signalling by listeriolysin O*. 2004, Portland Press Limited.
25. Bonfini, A. and N. Buchon, *Pore-forming toxins trigger the purge.* Cell host & microbe, 2016. **20**(6): p. 693-694.
26. Gregory, S.M., et al., *A quantitative model for the all-or-none permeabilization of phospholipid vesicles by the antimicrobial peptide cecropin A.* Biophysical journal, 2008. **94**(5): p. 1667-1680.
27. Matsuzaki, K., S. Yoneyama, and K. Miyajima, *Pore formation and translocation of melittin.* Biophysical journal, 1997. **73**(2): p. 831-838.
28. Ladokhin, A.S., M.E. Selsted, and S.H. White, *Sizing membrane pores in lipid vesicles by leakage of co-encapsulated markers: pore formation by melittin.* Biophysical journal, 1997. **72**(4): p. 1762-1766.
29. Yan, L. and M.E. Adams, *Lycotoxins, antimicrobial peptides from venom of the wolf spiderLycosa carolinensis.* Journal of Biological Chemistry, 1998. **273**(4): p. 2059-2066.
30. Corzo, G., et al., *Oxyopinins, large amphipathic peptides isolated from the venom of the wolf spider Oxyopes kitabensis with cytolytic properties and positive insecticidal cooperativity with spider neurotoxins.* Journal of Biological Chemistry, 2002. **277**(26): p. 23627-23637.
31. Orlova, E.V., et al., *Structure of α-latrotoxin oligomers reveals that divalent cation-dependent tetramers form membrane pores.* Nature Structural and Molecular Biology, 2000. **7**(1): p. 48.
32. Nomura, K., et al., *Orientation and pore-forming mechanism of a scorpion pore-forming peptide bound to magnetically oriented lipid bilayers.* Biophysical journal, 2004. **87**(4): p. 2497-2507.
33. Malovrh, P., et al., *A novel mechanism of pore formation membrane penetration by the N-terminal amphipathic region of equinatoxin.* Journal of Biological Chemistry, 2003. **278**(25): p. 22678-22685.
34. Gutiérrez-Aguirre, I., et al., *Membrane insertion of the N-terminal α-helix of equinatoxin II, a sea anemone cytolytic toxin.* Biochemical Journal, 2004. **384**(2): p.

:

421-428.

35. Kem, W.R., *Structure and membrane actions of a marine worm protein cytolysin, Cerebratulus toxin A-III.* Toxicology, 1994. **87**(1-3): p. 189-203.

36. Hallock, K.J., et al., *Membrane composition determines pardaxin's mechanism of lipid bilayer disruption.* Biophysical journal, 2002. **83**(2): p. 1004-1013.

37. Matsuzaki, K., et al., *Relationship of membrane curvature to the formation of pores by magainin 2.* Biochemistry, 1998. **37**(34): p. 11856-11863.

38. Wang, C.-H. and W.-g. Wu, *Amphiphilic β-sheet cobra cardiotoxin targets mitochondria and disrupts its network.* FEBS letters, 2005. **579**(14): p. 3169-3174.

39. Wu, P.-L., et al., *Non-cytotoxic Cobra Cardiotoxin A5 Binds to αvβ3 Integrin and Inhibits Bone Resorption IDENTIFICATION OF CARDIOTOXINS AS NON-RGD INTEGRIN-BINDING PROTEINS OF THE Ly-6 FAMILY.* Journal of Biological Chemistry, 2006. **281**(12): p. 7937-7945.

40. Yang, L., et al., *Crystallization of antimicrobial pores in membranes: magainin and protegrin.* Biophysical journal, 2000. **79**(4): p. 2002-2009.

41. Mani, R., et al., *Membrane-dependent oligomeric structure and pore formation of a β-hairpin antimicrobial peptide in lipid bilayers from solid-state NMR.* Proceedings of the National Academy of Sciences, 2006. **103**(44): p. 16242-16247.

42. Jang, H., B. Ma, and R. Nussinov, *Conformational study of the protegrin-1 (PG-1) dimer interaction with lipid bilayers and its effect.* BMC structural biology, 2007. **7**(1): p. 21.

43. Hadders, M.A., D.X. Beringer, and P. Gros, *Structure of C8α-MACPF reveals mechanism of membrane attack in complement immune defense.* Science, 2007. **317**(5844): p. 1552-1554.

44. Rosado, C.J., et al., *A common fold mediates vertebrate defense and bacterial attack.* Science, 2007. **317**(5844): p. 1548-1551.

45. Lukoyanova, N. and H.R. Saibil, *Friend or foe: the same fold for attack and defense.* Trends in immunology, 2008. **29**(2): p. 51-53.

46. Aerts, A., et al., *The mode of antifungal action of plant, insect and human defensins.* Cellular and molecular life sciences, 2008. **65**(13): p. 2069-2079.

:

47. Madison, M.N., et al., *Human defensin α-1 causes Trypanosoma cruzi membrane pore formation and induces DNA fragmentation, which leads to trypanosome destruction.* Infection and immunity, 2007. **75**(10): p. 4780-4791.

48. Hoover, D.M., et al., *The structure of human β-defensin-2 shows evidence of higher order oligomerization.* Journal of Biological Chemistry, 2000. **275**(42): p. 32911-32918.

49. Zakharov, S.D., et al., *On the role of lipid in colicin pore formation.* Biochimica et Biophysica Acta (BBA)-Biomembranes, 2004. **1666**(1): p. 239-249.

50. Sobko, A.A., et al., *Lipid dependence of the channel properties of a colicin E1-lipid toroidal pore.* Journal of Biological Chemistry, 2006. **281**(20): p. 14408-14416.

51. Kent, M., et al., *Oligomerization of membrane-bound diphtheria toxin (CRM197) facilitates a transition to the open form and deep insertion.* Biophysical journal, 2008. **94**(6): p. 2115-2127.

52. D'Silva, P.R. and A.K. Lala, *Organization of diphtheria toxin in membranes A hydrophobic photolabeling study.* Journal of Biological Chemistry, 2000. **275**(16): p. 11771-11777.

53. Czajkowsky, D.M., et al., *The vacuolating toxin from Helicobacter pylori forms hexameric pores in lipid bilayers at low pH.* Proceedings of the National Academy of Sciences, 1999. **96**(5): p. 2001-2006.

54. Menestrina, G., et al., *Pore-formation by Escherichia coli hemolysin (HlyA) and other members of the RTX toxins family.* Toxicology, 1994. **87**(1-3): p. 249-267.

55. Moayeri, M. and R.A. Welch, *Effects of temperature, time, and toxin concentration on lesion formation by the Escherichia coli hemolysin.* Infection and immunity, 1994. **62**(10): p. 4124-4134.

56. Bakás, L., et al., *Paradoxical lipid dependence of pores formed by the Escherichia coli α-hemolysin in planar phospholipid bilayer membranes.* Biophysical journal, 2006. **91**(10): p. 3748-3755.

57. SCHÖNHERR, R., et al., *Interaction of Serratia marcescens hemolysin (ShlA) with artificial and erythrocyte membranes.* The FEBS Journal, 1994. **223**(2): p. 655-663.

58. Dang, T.X., et al., *Prepore to pore transition of a cholesterol-dependent cytolysin*

:

visualized by electron microscopy. Journal of structural biology, 2005. **150**(1): p. 100-108.

59. Schuerch, D.W., E.M. Wilson-Kubalek, and R.K. Tweten, *Molecular basis of listeriolysin O pH dependence.* Proceedings of the National academy of Sciences of the United States of America, 2005. **102**(35): p. 12537-12542.
60. Tilley, S.J., et al., *Structural basis of pore formation by the bacterial toxin pneumolysin.* Cell, 2005. **121**(2): p. 247-256.
61. Rossjohn, J., et al., *Structures of perfringolysin O suggest a pathway for activation of cholesterol-dependent cytolysins.* Journal of molecular biology, 2007. **367**(5): p. 1227-1236.
62. Gouaux, J.E., et al., *Subunit stoichiometry of staphylococcal alpha-hemolysin in crystals and on membranes: a heptameric transmembrane pore.* Proceedings of the National Academy of Sciences, 1994. **91**(26): p. 12828-12831.
63. Montoya, M. and E. Gouaux, *β-Barrel membrane protein folding and structure viewed through the lens of α-hemolysin.* Biochimica et Biophysica Acta (BBA)-Biomembranes, 2003. **1609**(1): p. 19-27.
64. Andreeva, Z.I., et al., *Purification and cytotoxic properties of Bacillus cereus hemolysin II.* Protein expression and purification, 2006. **47**(1): p. 186-193.
65. Andreeva, Z.I., et al., *The properties of Bacillus cereus hemolysin II pores depend on environmental conditions.* Biochimica et Biophysica Acta (BBA)-Biomembranes, 2007. **1768**(2): p. 253-263.
66. Fivaz, M., M.-C. Velluz, and F.G. Van Der Goot, *Dimer dissociation of the pore-forming toxin aerolysin precedes receptor binding.* Journal of Biological Chemistry, 1999. **274**(53): p. 37705-37708.
67. Diep, D.B., et al., *Expression and properties of an aerolysin–Clostridium septicum alpha toxin hybrid protein.* Molecular microbiology, 1999. **31**(3): p. 785-794.
68. Kennedy, C.L., et al., *The α-toxin of Clostridium septicum is essential for virulence.* Molecular microbiology, 2005. **57**(5): p. 1357-1366.
69. Olson, R. and E. Gouaux, *Crystal structure of the Vibrio cholerae cytolysin (VCC) pro-toxin and its assembly into a heptameric transmembrane pore.* Journal of

molecular biology, 2005. **350**(5): p. 997-1016.

70. Jayasinghe, L. and H. Bayley, *The leukocidin pore: evidence for an octamer with four LukF subunits and four LukS subunits alternating around a central axis.* Protein Science, 2005. **14**(10): p. 2550-2561.

71. Miles, G., L. Jayasinghe, and H. Bayley, *Assembly of the bi-component leukocidin pore examined by truncation mutagenesis.* Journal of Biological Chemistry, 2006. **281**(4): p. 2205-2214.

72. Sugawara-Tomita, N., T. Tomita, and Y. Kamio, *Stochastic assembly of two-component staphylococcal γ-hemolysin into heteroheptameric transmembrane pores with alternate subunit arrangements in ratios of 3: 4 and 4: 3.* Journal of bacteriology, 2002. **184**(17): p. 4747-4756.

73. Nguyen, V.T., Y. Kamio, and H. Higuchi, *Single‐molecule imaging of cooperative assembly of γ‐hemolysin on erythrocyte membranes.* The EMBO journal, 2003. **22**(19): p. 4968-4979.

74. Tzokov, S.B., et al., *Structure of the hemolysin E (HlyE, ClyA, and SheA) channel in its membrane-bound form.* Journal of Biological Chemistry, 2006. **281**(32): p. 23042-23049.

75. Barth, H., et al., *Binary bacterial toxins: biochemistry, biology, and applications of common Clostridium and Bacillus proteins.* Microbiology and Molecular Biology Reviews, 2004. **68**(3): p. 373-402.

76. Mogridge, J., K. Cunningham, and R.J. Collier, *Stoichiometry of anthrax toxin complexes.* Biochemistry, 2002. **41**(3): p. 1079-1082.

77. Chatterjee, C., et al., *Biosynthesis and mode of action of lantibiotics.* Chemical reviews, 2005. **105**(2): p. 633-684.

78. Breukink, E., et al., *Lipid II is an intrinsic component of the pore induced by nisin in bacterial membranes.* Journal of Biological Chemistry, 2003. **278**(22): p. 19898-19903.

79. Pérez-Berná, A.J., et al., *Identification of the Membrane-active Regions of Hepatitis C Virus p7 Protein BIOPHYSICAL CHARACTERIZATION OF THE LOOP REGION*. Journal of Biological Chemistry, 2008. **283**(13): p. 8089-8101.

:

80. Clarke, D., et al., *Evidence for the formation of a heptameric ion channel complex by the hepatitis C virus p7 protein in vitro.* Journal of Biological Chemistry, 2006. **281**(48): p. 37057-37068.

81. Andreeva-Kovalevskaya, Z.I., et al., *Pore-forming proteins and adaptation of living organisms to environmental conditions.* Biochemistry (Moscow), 2008. **73**(13): p. 1473-1492.

82. Parker, M., et al., *Structure of the membrane-pore-forming fragment of colicin A.* Nature, 1989. **337**(6202): p. 93.

83. Roderer, D., et al., *Soluble oligomers of the pore-forming toxin Cytolysin A from Escherichia coli are off-pathway products of pore assembly.* Journal of Biological Chemistry, 2016. **291**(11): p. 5652-5663.

84. Oscarsson, J., et al., *Molecular analysis of the cytolytic protein ClyA (SheA) from Escherichia coli.* Molecular microbiology, 1999. **32**(6): p. 1226-1238.

85. Lai, X.-H., et al., *Cytocidal and apoptotic effects of the ClyA protein from Escherichia coli on primary and cultured monocytes and macrophages.* Infection and immunity, 2000. **68**(7): p. 4363-4367.

86. Jiang, S.-N., et al., *Inhibition of tumor growth and metastasis by a combination of Escherichia coli–mediated cytolytic therapy and radiotherapy.* Molecular therapy, 2010. **18**(3): p. 635-642.

87. Wallace, A.J., et al., *E. coli hemolysin E (HlyE, ClyA, SheA): X-ray crystal structure of the toxin and observation of membrane pores by electron microscopy.* Cell, 2000. **100**(2): p. 265-276.

88. Atkins, A., et al., *Structure-function relationships of a novel bacterial toxin, Hemolysin E the role of αG.* Journal of Biological Chemistry, 2000. **275**(52): p. 41150-41155.

89. Eifler, N., et al., *Cytotoxin ClyA from Escherichia coli assembles to a 13 - meric pore independent of its redox - state.* The EMBO journal, 2006. **25**(11): p. 2652-2661.

90. Mueller, M., et al., *The structure of a cytolytic α-helical toxin pore reveals its assembly mechanism.* Nature, 2009. **459**(7247): p. 726.

:

91. Cramer, W., et al., *Structure-function of the channel-forming colicins.* Annual review of biophysics and biomolecular structure, 1995. **24**(1): p. 611-641.

92. Wu, Z., et al., *Protein translocation by bacterial toxin channels: a comparison of diphtheria toxin and colicin Ia.* Biophysical journal, 2006. **91**(9): p. 3249-3256.

93. Parker, M.W., et al., *Refined structure of the pore-forming domain of colicin A at 2.4 Å resolution.* Journal of molecular biology, 1992. **224**(3): p. 639-657.

94. Elkins, P., et al., *A mechanism for toxin insertion into membranes is suggested by the crystal structure of the channel-forming domain of colicin E1.* Structure, 1997. **5**(3): p. 443-458.

95. Vetter, I.R., et al., *Crystal structure of a colicin N fragment suggests a model for toxicity.* Structure, 1998. **6**(7): p. 863-874.

96. Zakharov, S.D. and W.A. Cramer, *Colicin crystal structures: pathways and mechanisms for colicin insertion into membranes.* Biochimica et Biophysica Acta (BBA)-Biomembranes, 2002. **1565**(2): p. 333-346.

97. Greig, S.L., M. Radjainia, and A.K. Mitra, *Oligomeric structure of colicin ia channel in lipid bilayer membranes.* Journal of Biological Chemistry, 2009. **284**(24): p. 16126-16134.

98. Wiener, M., et al., *Crystal structure of colicin Ia.* Nature, 1997. **385**(6615): p. 461.

99. Stelzer, M.J., J. Neisess, and C. Thompson, *Aerial applications of a nucleopolyhedrosis virus and Bacillus thuringiensis against the Douglas fir tussock moth.* Journal of Economic Entomology, 1975. **68**(2): p. 269-272.

100. Martin, F.G. and M.G. Wolfersberger, *Bacillus thuringiensis delta-endotoxin and larval Manduca sexta midgut brush-border membrane vesicles act synergistically to cause very large increases in the conductance of planar lipid bilayers.* Journal of Experimental Biology, 1995. **198**(1): p. 91-96.

101. Wolfersberger, M., *The toxicity of twoBacillus thuringiensisδ-endotoxins to gypsy moth larvae is inversely related to the affinity of binding sites on midgut brush border membranes for the toxins.* Experientia, 1990. **46**(5): p. 475-477.

102. Pacheco, S., et al., *Domain II loop 3 of Bacillus thuringiensis Cry1Ab toxin is involved in a "ping pong" binding mechanism with Manduca sexta*

:

aminopeptidase-N and cadherin receptors. Journal of Biological Chemistry, 2009. **284**(47): p. 32750-32757.

103. Arenas, I., et al., *Role of alkaline phosphatase from Manduca sexta in the mechanism of action of Bacillus thuringiensis Cry1Ab toxin.* Journal of Biological Chemistry, 2010. **285**(17): p. 12497-12503.

104. Bravo, A., et al., *Oligomerization triggers binding of a Bacillus thuringiensis Cry1Ab pore-forming toxin to aminopeptidase N receptor leading to insertion into membrane microdomains.* Biochimica et Biophysica Acta (BBA)-Biomembranes, 2004. **1667**(1): p. 38-46.

105. Gómez, I., et al., *Cadherin‐like receptor binding facilitates proteolytic cleavage of helix α‐1 in domain I and oligomer pre‐pore formation of Bacillus thuringiensis Cry1Ab toxin.* FEBS letters, 2002. **513**(2-3): p. 242-246.

106. Vachon, V., R. Laprade, and J.-L. Schwartz, *Current models of the mode of action of Bacillus thuringiensis insecticidal crystal proteins: a critical review.* Journal of invertebrate pathology, 2012. **111**(1): p. 1-12.

107. Bravo, A., S.S. Gill, and M. Soberon, *Mode of action of Bacillus thuringiensis Cry and Cyt toxins and their potential for insect control.* Toxicon, 2007. **49**(4): p. 423-435.

108. Grochulski, P., et al., *Bacillus thuringiensisCrylA (a) Insecticidal Toxin: Crystal Structure and Channel Formation.* Journal of molecular biology, 1995. **254**(3): p. 447-464.

109. Bhakdi, S. and J. Tranum-Jensen, *Alpha-toxin of Staphylococcus aureus.* Microbiological reviews, 1991. **55**(4): p. 733-751.

110. Grimminger, F., et al., *Human endothelial cell activation and mediator release in response to the bacterial exotoxins Escherichia coli hemolysin and staphylococcal alpha-toxin.* The Journal of Immunology, 1997. **159**(4): p. 1909-1916.

111. Nygaard, T.K., et al., *Alpha-toxin induces programmed cell death of human T cells, B cells, and monocytes during USA300 infection.* PLoS ONE, 2012. **7**(5): p. e36532.

112. Manohar, M., et al., *Platelet damaging factor, a fifth activity of staphylococcal α-toxin.* Journal of bacteriology, 1967. **94**(1): p. 224-231.

:

113. Gouaux, E., *α-Hemolysin fromStaphylococcus aureus: an archetype of β-barrel, channel-forming toxins.* Journal of structural biology, 1998. **121**(2): p. 110-122.

114. Song, L., et al., *Structure of staphylococcal α-hemolysin, a heptameric transmembrane pore.* Science, 1996. **274**(5294): p. 1859-1865.

115. Berube, B.J. and J.B. Wardenburg, *Staphylococcus aureus α-toxin: nearly a century of intrigue.* Toxins, 2013. **5**(6): p. 1140-1166.

116. Janda, J.M. and S.L. Abbott, *Evolving concepts regarding the genus Aeromonas: an expanding panorama of species, disease presentations, and unanswered questions.* Clinical infectious diseases, 1998. **27**(2): p. 332-344.

117. Abrami, L., et al., *The glycan core of GPI‐anchored proteins modulates aerolysin binding but is not sufficient: the polypeptide moiety is required for the toxin–receptor interaction.* FEBS letters, 2002. **512**(1-3): p. 249-254.

118. Parker, M.W., et al., *Structure of the Aeromonas toxin proaerolysin in its water-soluble and membrane-channel states.* Nature, 1994. **367**(6460): p. 292.

119. Iacovache, I., et al., *Cryo-EM structure of aerolysin variants reveals a novel protein fold and the pore-formation process.* Nature communications, 2016. **7**: p. 12062.

120. Parker, M.W., F.G. Van Der Goot, and J.T. Buckley, *Aerolysin—the ins and outs of a model channel‐forming toxin.* Molecular microbiology, 1996. **19**(2): p. 205-212.

121. Degiacomi, M.T., et al., *Molecular assembly of the aerolysin pore reveals a swirling membrane-insertion mechanism.* Nature chemical biology, 2013. **9**(10): p. 623.

122. Zitzer, A., et al., *Potent membrane-permeabilizing and cytocidal action of Vibrio cholerae cytolysin on human intestinal cells.* Infection and immunity, 1997. **65**(4): p. 1293-1298.

123. Manning, P.A., M.H. Brown, and M.W. Heuzenroeder, *Cloning of the structural gene (hly) for the haemolysin of Vibrio cholerae El Tor strain 017.* Gene, 1984. **31**(1): p. 225-231.

124. Hall, R.H. and B. Drasar, *Vibrio cholerae HlyA hemolysin is processed by proteolysis.* Infection and immunity, 1990. **58**(10): p. 3375-3379.

125. Nagamune, K., et al., *In vitro proteolytic processing and activation of the recombinant precursor of El Tor cytolysin/hemolysin (pro-HlyA) of Vibrio cholerae*

:

by soluble hemagglutinin/protease of V. cholerae, trypsin, and other proteases. Infection and immunity, 1996. **64**(11): p. 4655-4658.

126. Rai, A.K., K. Paul, and K. Chattopadhyay, *Functional mapping of the lectin activity site on the β-prism domain of Vibrio cholerae cytolysin implications for the membrane pore-formation mechanism of the toxin.* Journal of Biological Chemistry, 2013. **288**(3): p. 1665-1673.

127. Rai, A.K. and K. Chattopadhyay, *Vibrio cholerae cytolysin: Structure–function mechanism of an atypical β-barrel pore-forming toxin*, in *Biochemical Roles of Eukaryotic Cell Surface Macromolecules*. 2015, Springer. p. 109-125.

128. Rai, A.K. and K. Chattopadhyay, *Trapping of Vibrio cholerae cytolysin in the membrane-bound monomeric state blocks membrane insertion and functional pore formation by the toxin.* Journal of Biological Chemistry, 2014. **289**(24): p. 16978-16987.

129. Rai, A.K. and K. Chattopadhyay, *Revisiting the membrane interaction mechanism of a membrane‐damaging β‐barrel pore‐forming toxin Vibrio cholerae cytolysin.* Molecular microbiology, 2015. **97**(6): p. 1051-1062.

130. Paul, K. and K. Chattopadhyay, *Single point mutation in Vibrio cholerae cytolysin compromises the membrane pore‐formation mechanism of the toxin.* The FEBS Journal, 2012. **279**(21): p. 4039-4051.

131. Chattopadhyay, K., D. Bhattacharyya, and K.K. Banerjee, *Vibrio cholerae hemolysin.* The FEBS Journal, 2002. **269**(17): p. 4351-4358.

132. Rai, A.K., N. Kundu, and K. Chattopadhyay, *Physicochemical constraints of elevated pH affect efficient membrane interaction and arrest an abortive membrane-bound oligomeric intermediate of the beta-barrel pore-forming toxin Vibrio cholerae cytolysin.* Archives of biochemistry and biophysics, 2015. **583**: p. 9-17.

133. Gilbert, R., *Pore-forming toxins.* Cellular and Molecular Life Sciences CMLS, 2002. **59**(5): p. 832-844.

134. Walev, I., et al., *Delivery of proteins into living cells by reversible membrane permeabilization with streptolysin-O.* Proceedings of the National Academy of

:

Sciences, 2001. **98**(6): p. 3185-3190.

135. Duncan, J.L. and R. Schlegel, *Effect of streptolysin O on erythrocyte membranes, liposomes, and lipid dispersions. A protein-cholesterol interaction.* The Journal of cell biology, 1975. **67**(1): p. 160-174.

136. Tweten, R.K., *Cholesterol-dependent cytolysins, a family of versatile pore-forming toxins.* Infection and immunity, 2005. **73**(10): p. 6199-6209.

137. Rossjohn, J., et al., *Structure of a cholesterol-binding, thiol-activated cytolysin and a model of its membrane form.* Cell, 1997. **89**(5): p. 685-692.

138. Czajkowsky, D.M., et al., *Vertical collapse of a cytolysin prepore moves its transmembrane β-hairpins to the membrane.* The EMBO journal, 2004. **23**(16): p. 3206-3215.

139. Ramachandran, R., R.K. Tweten, and A.E. Johnson, *The domains of a cholesterol-dependent cytolysin undergo a major FRET-detected rearrangement during pore formation.* Proceedings of the National academy of Sciences of the United States of America, 2005. **102**(20): p. 7139-7144.

140. Shepard, L.A., et al., *Identification of a membrane-spanning domain of the thiol-activated pore-forming toxin Clostridium perfringens perfringolysin O: an α-helical to β-sheet transition identified by fluorescence spectroscopy.* Biochemistry, 1998. **37**(41): p. 14563-14574.

141. Shatursky, O., et al., *The mechanism of membrane insertion for a cholesterol-dependent cytolysin: a novel paradigm for pore-forming toxins.* Cell, 1999. **99**(3): p. 293-299.

142. Ramachandran, R., R.K. Tweten, and A.E. Johnson, *Membrane-dependent conformational changes initiate cholesterol-dependent cytolysin oligomerization and intersubunit β-strand alignment.* Nature Structural and Molecular Biology, 2004. **11**(8): p. 697.

143. Heuck, A.P., et al., *Mechanism of membrane insertion of a multimeric β-barrel protein: perfringolysin O creates a pore using ordered and coupled conformational changes.* Molecular cell, 2000. **6**(5): p. 1233-1242.

144. Ramachandran, R., et al., *Structural insights into the membrane-anchoring*

:

mechanism of a cholesterol-dependent cytolysin. Nature Structural and Molecular Biology, 2002. **9**(11): p. 823.

145. Shepard, L.A., et al., *The mechanism of pore assembly for a cholesterol-dependent cytolysin: formation of a large prepore complex precedes the insertion of the transmembrane β-hairpins.* Biochemistry, 2000. **39**(33): p. 10284-10293.
146. Hotze, E.M., et al., *Arresting pore formation of a cholesterol-dependent cytolysin by disulfide trapping synchronizes the insertion of the transmembrane β-sheet from a prepore intermediate.* Journal of Biological Chemistry, 2001. **276**(11): p. 8261-8268.
147. Hotze, E.M., et al., *Monomer-monomer interactions drive the prepore to pore conversion of a β-barrel-forming cholesterol-dependent cytolysin.* Journal of Biological Chemistry, 2002. **277**(13): p. 11597-11605.
148. Heuck, A.P., R.K. Tweten, and A.E. Johnson, *β-Barrel pore-forming toxins: intriguing dimorphic proteins.* Biochemistry, 2001. **40**(31): p. 9065-9073.
149. Johnson, B.B. and A.P. Heuck, *Perfringolysin O structure and mechanism of pore formation as a paradigm for cholesterol-dependent cytolysins*, in *MACPF/CDC Proteins-Agents of Defence, Attack and Invasion*. 2014, Springer. p. 63-81.
150. Hamon, M.A., et al., *Listeriolysin O: the Swiss army knife of Listeria.* Trends in microbiology, 2012. **20**(8): p. 360-368.
151. Bavdek, A., et al., *Sterol and pH interdependence in the binding, oligomerization, and pore formation of Listeriolysin O.* Biochemistry, 2007. **46**(14): p. 4425-4437.
152. Moors, M.A., et al., *Expression of listeriolysin O and ActA by intracellular and extracellular Listeria monocytogenes.* Infection and immunity, 1999. **67**(1): p. 131-139.
153. Weiglein, I., et al., *Listeria monocytogenes infection of HeLa cells results in listeriolysinO-mediated transient activation of the Raf-MEK-MAP kinase pathway.* FEMS microbiology letters, 1997. **148**(2): p. 189-195.
154. Jones, S. and D.A. Portnoy, *Characterization of Listeria monocytogenes pathogenesis in a strain expressing perfringolysin O in place of listeriolysin O.* Infection and immunity, 1994. **62**(12): p. 5608-5613.
155. Jones, S., K. Preiter, and D.A. Portnoy, *Conversion of an extracellular cytolysin into*

:

a phagosome‐specific lysin which supports the growth of an intracellular pathogen. Molecular microbiology, 1996. **21**(6): p. 1219-1225.

156. Bavdek, A., et al., *pH dependence of listeriolysin O aggregation and pore‐forming ability.* The FEBS Journal, 2012. **279**(1): p. 126-141.

157. Nomura, T., et al., *Irreversible loss of membrane-binding activity of Listeria-derived cytolysins in non-acidic conditions: a distinct difference from allied cytolysins produced by other Gram-positive bacteria.* Microbiology, 2007. **153**(7): p. 2250-2258.

158. Portnoy, D.A., P.S. Jacks, and D.J. Hinrichs, *Role of hemolysin for the intracellular growth of Listeria monocytogenes.* Journal of Experimental Medicine, 1988. **167**(4): p. 1459-1471.

159. Birmingham, C.L., et al., *Listeriolysin O allows Listeria monocytogenes replication in macrophage vacuoles.* Nature, 2008. **451**(7176): p. 350.

160. Beauregard, K.E., et al., *pH-dependent perforation of macrophage phagosomes by listeriolysin O from Listeria monocytogenes.* Journal of Experimental Medicine, 1997. **186**(7): p. 1159-1163.

161. Kozorog, M., et al., *19 F NMR studies provide insights into lipid membrane interactions of listeriolysin O, a pore forming toxin from Listeria monocytogenes.* Scientific Reports, 2018. **8**(1): p. 6894.

162. Köster, S., et al., *Crystal structure of listeriolysin O reveals molecular details of oligomerization and pore formation.* Nature communications, 2014. **5**: p. 3690.

163. Basulto, A., et al., *Immunohistochemical targeting of sea anemone cytolysins on tentacles, mesenteric filaments and isolated nematocysts of Stichodactyla helianthus.* Journal of Experimental Zoology Part A: Ecological and Integrative Physiology, 2006. **305**(3): p. 253-258.

164. Šuput, D., *In vivo effects of cnidarian toxins and venoms.* Toxicon, 2009. **54**(8): p. 1190-1200.

165. Maček, P., *Polypeptide cytolytic toxins from sea anemones (Actiniaria).* FEMS microbiology immunology, 1992. **5**(1-3): p. 121-129.

166. Anderluh, G. and P. Maček, *Cytolytic peptide and protein toxins from sea anemones*

:

(Anthozoa: Actiniaria). Toxicon, 2002. **40**(2): p. 111-124.

167. Alegre-Cebollada, J., et al., *Sea anemone actinoporins: the transition from a folded soluble state to a functionally active membrane-bound oligomeric pore.* Current protein and peptide science, 2007. **8**(6): p. 558-572.
168. García-Ortega, L., et al., *The behavior of sea anemone actinoporins at the water–membrane interface.* Biochimica et Biophysica Acta (BBA)-Biomembranes, 2011. **1808**(9): p. 2275-2288.
169. Anderluh, G. and P. Maček, *Dissecting the actinoporin pore-forming mechanism.* Structure, 2003. **11**(11): p. 1312-1313.
170. Rojko, N., et al., *Pore formation by actinoporins, cytolysins from sea anemones.* Biochimica et Biophysica Acta (BBA)-Biomembranes, 2016. **1858**(3): p. 446-456.
171. Kristan, K.Č., et al., *Molecular mechanism of pore formation by actinoporins.* Toxicon, 2009. **54**(8): p. 1125-1134.
172. Podobnik, M. and G. Anderluh. *Pore-forming toxins in Cnidaria*. in *Seminars in cell & developmental biology*. 2017: Elsevier.
173. Athanasiadis, A., et al., *Crystal structure of the soluble form of equinatoxin II, a pore-forming toxin from the sea anemone Actinia equina.* Structure, 2001. **9**(4): p. 341-346.
174. Mancheno, J.M., et al., *Crystal and electron microscopy structures of sticholysin II actinoporin reveal insights into the mechanism of membrane pore formation.* Structure, 2003. **11**(11): p. 1319-1328.
175. Mechaly, A.E., et al., *Structural insights into the oligomerization and architecture of eukaryotic membrane pore-forming toxins.* Structure, 2011. **19**(2): p. 181-191.
176. Norton, R.S., *Structures of sea anemone toxins.* Toxicon, 2009. **54**(8): p. 1075-1088.
177. Alegre-Cebollada, J., et al., *Calorimetric scrutiny of lipid binding by sticholysin II toxin mutants.* Journal of molecular biology, 2008. **382**(4): p. 920-930.
178. Hinds, M.G., et al., *Solution structure of the eukaryotic pore-forming cytolysin equinatoxin II: implications for pore formation1.* Journal of molecular biology, 2002. **315**(5): p. 1219-1229.
179. Belmonte, G., et al., *Pore formation by the sea anemone cytolysin equinatoxin II in*

:

red blood cells and model lipid membranes. The Journal of membrane biology, 1993. **131**(1): p. 11-22.

180. de los Ríos, V., et al., *Sticholysin II, a cytolysin from the sea anemone Stichodactyla helianthus, is a monomer - tetramer associating protein.* FEBS letters, 1999. **455**(1-2): p. 27-30.
181. Tanaka, K., et al., *Structural basis for self-assembly of a cytolytic pore lined by protein and lipid.* Nature communications, 2015. **6**: p. 6337.
182. Fujino, T., et al., *On the bacteriological examination of shirasu-food poisoning.* Medical Journal of Osaka University, 1953. **4**(2/3): p. 299-304.
183. Ceccarelli, D., et al., *Distribution and dynamics of epidemic and pandemic Vibrio parahaemolyticus virulence factors.* Frontiers in cellular and infection microbiology, 2013. **3**: p. 97.
184. Nelapati, S., K. Nelapati, and B. Chinnam, *Vibrio parahaemolyticus-An emerging foodborne pathogen-A Review.* Vet. World, 2012. **5**(1): p. 48-62.
185. Nair, G.B., et al., *Global dissemination of Vibrio parahaemolyticus serotype O3: K6 and its serovariants.* Clinical microbiology reviews, 2007. **20**(1): p. 39-48.
186. Honda, T., et al., *Sixty years of Vibrio parahaemolyticus research.* Microbe, 2008. **3**: p. 462-466.
187. Yeung, P.M. and K.J. Boor, *Epidemiology, pathogenesis, and prevention of foodborne Vibrio parahaemolyticus infections.* Foodborne Pathogens & Disease, 2004. **1**(2): p. 74-88.
188. Blake, P.A., et al., *Disease caused by a marine vibrio: clinical characteristics and epidemiology.* New England Journal of Medicine, 1979. **300**(1): p. 1-5.
189. Makino, K., et al., *Genome sequence of Vibrio parahaemolyticus: a pathogenic mechanism distinct from that of V cholerae.* The Lancet, 2003. **361**(9359): p. 743-749.
190. Broberg, C.A., T.J. Calder, and K. Orth, *Vibrio parahaemolyticus cell biology and pathogenicity determinants.* Microbes and infection, 2011. **13**(12-13): p. 992-1001.
191. Zhang, L. and K. Orth, *Virulence determinants for Vibrio parahaemolyticus infection.* Current opinion in microbiology, 2013. **16**(1): p. 70-77.

:

192. Krachler, A.M. and K. Orth, *Functional characterization of the interaction between bacterial adhesin multivalent adhesion molecule 7 (MAM7) protein and its host cell ligands.* Journal of Biological Chemistry, 2011. **286**(45): p. 38939-38947.

193. Kustusch, R.J., C.J. Kuehl, and J.H. Crosa, *Power plays: iron transport and energy transduction in pathogenic vibrios.* Biometals, 2011. **24**(3): p. 559-566.

194. Tanabe, T., et al., *Identification and characterization of genes required for biosynthesis and transport of the siderophore vibrioferrin in Vibrio parahaemolyticus.* Journal of bacteriology, 2003. **185**(23): p. 6938-6949.

195. Funahashi, T., et al., *Identification and characterization of genes required for utilization of desferri-ferrichrome and aerobactin in Vibrio parahaemolyticus.* Biological and Pharmaceutical Bulletin, 2009. **32**(3): p. 359-365.

196. Nishibuchi, M. and J.B. Kaper, *Thermostable direct hemolysin gene of Vibrio parahaemolyticus: a virulence gene acquired by a marine bacterium.* Infection and immunity, 1995. **63**(6): p. 2093.

197. Fukui, T., et al., *Thermostable direct hemolysin of Vibrio parahaemolyticus is a bacterial reversible amyloid toxin.* Biochemistry, 2005. **44**(29): p. 9825-9832.

198. Matsuda, S., et al., *Association of Vibrio parahaemolyticus thermostable direct hemolysin with lipid rafts is essential for cytotoxicity but not hemolytic activity.* Infection and immunity, 2010. **78**(2): p. 603-610.

199. Yanagihara, I., et al., *Structure and functional characterization of Vibrio parahaemolyticus thermostable direct hemolysin.* Journal of Biological Chemistry, 2010. **285**(21): p. 16267-16274.

200. Galán, J.E. and H. Wolf-Watz, *Protein delivery into eukaryotic cells by type III secretion machines.* Nature, 2006. **444**(7119): p. 567.

201. Izore, T., V. Job, and A. Dessen, *Biogenesis, regulation, and targeting of the type III secretion system.* Structure, 2011. **19**(5): p. 603-612.

202. Chao, G., et al., *Distribution of genes encoding four pathogenicity islands (VPaIs), T6SS, biofilm, and type I pilus in food and clinical strains of Vibrio parahaemolyticus in China.* Foodborne pathogens and disease, 2010. **7**(6): p. 649-658.

:

203. Lynch, T., et al., *Vibrio parahaemolyticus disruption of epithelial cell tight junctions occurs independently of toxin production.* Infection and immunity, 2005. **73**(3): p. 1275-1283.

204. Meador, C.E., et al., *Virulence gene-and pandemic group-specific marker profiling of clinical Vibrio parahaemolyticus isolates.* Journal of clinical microbiology, 2007. **45**(4): p. 1133-1139.

205. Caburlotto, G., et al., *Effect on human cells of environmental Vibrio parahaemolyticus strains carrying type III secretion system 2.* Infection and immunity, 2010. **78**(7): p. 3280-3287.

206. Trosky, J.E., et al., *Inhibition of MAPK signaling pathways by VopA from Vibrio parahaemolyticus.* Journal of Biological Chemistry, 2004. **279**(50): p. 51953-51957.

207. Liverman, A.D., et al., *Arp2/3-independent assembly of actin by Vibrio type III effector VopL.* Proceedings of the National Academy of Sciences, 2007. **104**(43): p. 17117-17122.

208. Friebel, A., et al., *SopE and SopE2 from Salmonella typhimurium activate different sets of RhoGTPases of the host cell.* Journal of Biological Chemistry, 2001. **276**(36): p. 34035-34040.

209. Zhang, L., et al., *Type III effector VopC mediates invasion for Vibrio species.* Cell reports, 2012. **1**(5): p. 453-460.

210. Kodama, T., et al., *Identification and characterization of VopT, a novel ADP‐ribosyltransferase effector protein secreted via the Vibrio parahaemolyticus type III secretion system 2.* Cellular microbiology, 2007. **9**(11): p. 2598-2609.

211. Hiyoshi, H., et al., *VopV, an F-actin-binding type III secretion effector, is required for Vibrio parahaemolyticus-induced enterotoxicity.* Cell host & microbe, 2011. **10**(4): p. 401-409.

212. Zhou, X., et al., *A Vibrio parahaemolyticus T3SS effector mediates pathogenesis by independently enabling intestinal colonization and inhibiting TAK1 activation.* Cell reports, 2013. **3**(5): p. 1690-1702.

213. Shirai, H., et al., *Molecular epidemiologic evidence for association of thermostable direct hemolysin (TDH) and TDH-related hemolysin of Vibrio parahaemolyticus with*

:

gastroenteritis. Infection and immunity, 1990. **58**(11): p. 3568-3573.

214. Honda, T. and T. Iida, *The pathogenicity of Vibrio parahaemolyticus and the role of the thermostable direct haemolysin and related haemolysins.* Reviews in Medical Microbiology, 1993. **4**(2): p. 106-113.

215. Letchumanan, V., K.-G. Chan, and L.-H. Lee, *Vibrio parahaemolyticus: a review on the pathogenesis, prevalence, and advance molecular identification techniques.* Frontiers in microbiology, 2014. **5**: p. 705.

216. Wang, R., et al., *The pathogenesis, detection, and prevention of Vibrio parahaemolyticus.* Frontiers in microbiology, 2015. **6**: p. 144.

217. Raghunath, P., *Roles of thermostable direct hemolysin (TDH) and TDH-related hemolysin (TRH) in Vibrio parahaemolyticus.* Frontiers in microbiology, 2015. **5**: p. 805.

218. Hamada, D., et al., *Tetrameric structure of thermostable direct hemolysin from Vibrio parahaemolyticus revealed by ultracentrifugation, small-angle X-ray scattering and electron microscopy.* Journal of molecular biology, 2007. **365**(1): p. 187-195.

219. Honda, T., et al., *The thermostable direct hemolysin of Vibrio parahaemolyticus is a pore-forming toxin.* Canadian journal of microbiology, 1992. **38**(11): p. 1175-1180.

220. Kundu, N., et al., *Disulphide bond restrains the C-terminal region of thermostable direct hemolysin during folding to promote oligomerization.* Biochemical Journal, 2017. **474**(2): p. 317-331.

221. Takeda, Y., et al., *Inactivation of the biological activities of the thermostable direct hemolysin of Vibrio parahaemolyticus by ganglioside Gt1*. Infection and immunity, 1976. **14**(1): p. 1-5.

222. Douet, J., et al., *Study of the haemolytic process and receptors of thermostable direct haemolysin from Vibrio parahaemolyticus.* Research in microbiology, 1996. **147**(9): p. 687-696.

223. Arrhenius, S. and A. Finkelstein, *Immunochemie: Anwendungen der physikalischen Chemie auf die Lehre von den physiologischen Antikörpern*. 1907: Akademische Verlagsgesellschaft.

224. Vasil, M., P. Liu, and B. Iglewski, *Temperature-dependent inactivating factor of*

:

Pseudomonas aeruginosa exotoxin A. Infection and immunity, 1976. **13**(5): p. 1467-1472.

225. Coolbaugh, J.C. and R.P. Williams, *Production and characterization of two hemolysins of Bacillus cereus.* Canadian journal of microbiology, 1978. **24**(11): p. 1289-1295.
226. Albesa, I., et al., *A thiol-activated hemolysin in gram-negative bacteria.* Canadian journal of microbiology, 1985. **31**(3): p. 297-300.
227. Sakurai, J., et al., *Interaction of thermostable direct hemolysin of Vibrio parahaemolyticus with human erythrocytes.* Biken journal, 1975. **18**(4): p. 187-192.
228. Schuck, P., et al., *Size-distribution analysis of proteins by analytical ultracentrifugation: strategies and application to model systems.* Biophysical journal, 2002. **82**(2): p. 1096-1111.
229. Tang, G.-Q., et al., *A mutant toxin of Vibrio parahaemolyticus thermostable direct hemolysin which has lost hemolytic activity but retains ability to bind to erythrocytes.* Infection and immunity, 1994. **62**(8): p. 3299-3304.
230. Emsley, P., et al., *Features and development of Coot.* Acta Crystallographica Section D: Biological Crystallography, 2010. **66**(4): p. 486-501.
231. Dal Peraro, M. and F.G. Van Der Goot, *Pore-forming toxins: ancient, but never really out of fashion.* Nature reviews microbiology, 2016. **14**(2): p. 77.
232. Yanagihara, I., et al., *Structure and functional characterization of Vibrio parahaemolyticus thermostable direct hemolysin*. J Biol Chem, 2010. **285**(21): p. 16267-74.
233. Walsh, I., et al., *PASTA 2.0: an improved server for protein aggregation prediction.* Nucleic Acids Res, 2014. **42**(Web Server issue): p. W301-7.
234. Lata, K. and K. Chattopadhyay, *Helicobacter pylori TlyA forms amyloid-like aggregates with potent cytotoxic activity.* Biochemistry, 2015. **54**(23): p. 3649-3659.
235. Naiki, H., et al., *Fluorometric determination of amyloid fibrils in vitro using the fluorescent dye, thioflavine T.* Analytical biochemistry, 1989. **177**(2): p. 244-249.
236. Fukui, T., et al., *Thermostable direct hemolysin of Vibrio parahaemolyticus is a bacterial reversible amyloid toxin.* Biochemistry, 2005. **44**(29): p. 9825-32.

:

237. Hawe, A., M. Sutter, and W. Jiskoot, *Extrinsic fluorescent dyes as tools for protein characterization.* Pharmaceutical research, 2008. **25**(7): p. 1487-1499.

238. Stryer, L., *The interaction of a naphthalene dye with apomyoglobin and apohemoglobin: a fluorescent probe of non-polar binding sites.* Journal of molecular biology, 1965. **13**(2): p. 482-495.

239. Sengupta, D., et al., *Toroidal pores formed by antimicrobial peptides show significant disorder.* Biochimica et Biophysica Acta (BBA)-Biomembranes, 2008. **1778**(10): p. 2308-2317.

:

Synopsis

:

Structure-function studies on *Vibrio parahaemolyticus* thermostable direct hemolysin

The plasma membrane of a cell acts as a selective permeable barrier and protects the cellular environment from the extracellular milieu [1, 2]. Many bacterial pathogens employ virulence factors that act by disrupting the cellular membrane integrity [3, 4]. Pore-forming toxins (PFTs) are the largest class of bacterial protein toxins which are known to destroy the plasma membrane integrity [5]. PFTs are secretory protein toxins and form pores/channels in the target host cell membranes, leading to the colloid-osmotic lysis of the cells. The general mechanism of pore-formation by bacterial PFTs involves following step: (i) secretion of the PFT as a water-soluble monomeric molecule, (ii) binding of the toxin to the membranes of the target cells, (iii) oligomerization of the toxin onto the target cell membranes, and (iv) membrane insertion of the designated structural motif(s) of the toxin molecule to form transmembrane pores [3, 5, 6].

Thermostable direct hemolysin (TDH) is the major virulence factor of the bacterial pathogen *Vibrio parahaemolyticus*, and it is known to show biological activities like cardiotoxicity, enterotoxicity, and hemolytic activity [7, 8]. TDH is an atypical pore-forming toxin that deviates from the general scheme of pore-formation mechanism of the PFTs. TDH exists as a tetramer in solution, and as an oligomer it binds to the target cell membranes to exert its membrane-damaging pore-forming activity. Unlike other PFTs, the oligomerization process of TDH is independent of the membrane-binding event [9-11]. Tetramer formation in solution appears to be important for the membrane-damaging activity of TDH. Analysis of the crystal structure of TDH shows that the toxin adopts a β-sandwich core structure [12]. A previous study has identified two key residues (Arg46 and Tyr140) present in the core β-sandwich domain that are implicated in the oligomerization of the toxin [12]. Another unique feature of TDH is that, being a bacterial PFT, it has high structural similarity with the members of the eukaryotic actinoporin family of PFTs that include Equinatoxin II, Sticholysin II and Fragaceatoxin C [9, 12]. Actinoporins also contain a conserved β-sandwich domain,

similar to that present in TDH [13-15]. Despite having high structural similarities, the mechanism of action of TDH is different from the actinoporins. Unlike TDH, actinoporins exist as monomer in solution, and oligomerize on the membranes of the target cells. There are additional unique structural features, which are limited to TDH, but not present in the actinoporins. For example, (i) presence of an extended C-terminal region (CTR), which is absent in the actinoporins, (ii) presence of cysteine residues (Cys151 and Cys161), which allow formation of an intra-protomer disulfide bond to tether the CTR against the core β-sandwich domain. Analysis of the crystal structure also shows that the extended CTR of TDH is positioned at the inter-protomer interface in the tetrameric assembly of the toxin. Also, a number of residues within this CTR appear to participate in polar and/or hydrophobic interactions with the residues from the neighboring protomer. We, therefore, speculated that the CTR of TDH may potentially contribute to the oligomerization process of the toxin. In the present research work, we have examined the implications of the CTR in the oligomerization mechanism of TDH, and have also explored the functional implications of this unique structural motif in the mode of action of the toxin.

Another distinct feature of TDH is the presence of 11-amino acid residue long, N-terminal region (NTR). The NTR of TDH could not be modeled in the crystal structure of the protein, presumably due to high degree of conformational/structural fluctuations of this motif, or possibly due to the tendency of the NTR to adopt multiple conformations [12]. The NTRs of the actinoporins are significantly longer (consist of ~30 amino acid residues), which adopt an α-helical structure, and forms the transmembrane region in the final pore structure upon encountering the target membranes [13-15]. Till date, no information is available regarding the structural or functional characterization of the flexible NTR of TDH in the mode of action of the toxin. The present study unravels the implications of the NTR in the structure-function mechanism of TDH.

Part I: C-terminal region (CTR) regulates the oligomerization mechanism of TDH thereby facilitating the membrane-damaging activity of the toxin

Analysis of the crystal structure of TDH suggested that the CTR of TDH is positioned at the protomer:protomer interface. Also, a number of residues within the CTR appear to make several polar/hydrophobic interactions with the neighboring protomer. In order to understand the role of the CTR in the oligomerization mechanism of TDH, a truncated mutant lacking the CTR was generated (TDH-ΔCTR$^{157–165}$). The mutant lacking the CTR displayed significant decrease in the functional pore-forming activity. Also, the ability to form oligomeric assembly in solution was compromised for the truncated mutant; TDH-ΔCTR$^{157–165}$ existed exclusively as monomer in solution. The binding ability of TDH-ΔCTR$^{157–165}$ toward the target cell membranes was also found to be compromised as compared to the wild type TDH. To explore further the mechanistic basis of CTR-mediated regulation of TDH oligomerization, point mutations were also introduced within the CTR to determine the key residues involved in the inter-protomer. Our data showed that the residue Gln164, when mutated to Ala, resulted into significantly reduced pore-forming activity; the mutant existed exclusively as monomer in solution. This data indicated that Gln164, present within the CTR, plays a critical role in the oligomerization mechanism of the toxin. As mentioned earlier, TDH harbors single intra-protomer disulfide bond (between Cys151 and Cys161 residues), which appears to tether the CTR at the oligomeric interface of the protein. Mutations of the cysteine residues to serine (C151S-C161S-TDH) resulted in the disruption of the oligomerization ability of TDH, and the mutant existed as monomer in solution with drastically reduced activity. Our study further showed that the intra-protomer disulphide bond presumably acts to restrain the conformational fluctuation of the CTR during the folding and assembly process of TDH, and thus mediates spatial locking of the CTR at the inter-protomer interface, thereby facilitating the oligomerization mechanism of TDH. Altogether, the present study provides novel insights regarding the regulation of the oligomerization mechanism of TDH in the bacterial PFT family. Such mechanism is not commonly documented in the structurally related members in the PFT family.

Part II: Flexible and intrinsically disordered N-terminal region (NTR) of TDH plays critical roles in the membrane-damaging cytolytic/cytotoxic activity of the toxin

The N-terminal region (^{1}FELPSVPFPAP^{11}; NTR) of TDH could not be modelled in the crystal structure of TDH, presumably due to high structural/conformational flexibility of the region. Analysis of the NTR also suggested that the motif would be intrinsically disordered. The NTR of TDH is also unusual in that it is populated with a number of aromatic/hydrophobic residues, as well as a number of proline residues. However, no information is available at present regarding the role of the NTR in the structure-function mechanism of TDH. Second part of the present thesis work has, therefore, aimed to explore the role of the NTR in the physicochemical properties, as well as in the membrane-damaging cell-killing activities of TDH. In order to examine the significance of the NTR in the mode of action of TDH, a truncated mutant lacking the NTR (NTR-deleted; NTD-TDH) was generated. Deletion of the NTR resulted into prominent changes in the physicochemical properties of TDH, without causing any global overall change in the secondary and tertiary structural organization of the protein. For example, deletion of the NTR was found to cause marked reduction in the amyloidogenic property of TDH. Presence of the NTR was also found to allow binding of hydrophobic dye, ANS (1-anilinonaphthalene-8-sulfonic acid) to TDH, while deletion of the NTR abolished the ANS-binding ability of the truncated protein. This was consistent with the increased aromatic/hydrophobic residue-content within the NTR of TDH. Presence of the NTR was also found to enhance the ability of TDH to bind to the amphipathic phase of the membrane lipid bilayer of liposomes. The mutant variant NTD-TDH showed significantly reduced cytolytic and cytotoxic activity against the multiple target eukaryotic cells that include human erythrocytes, T84 human intestinal epithelial cells, and THP-1 human monocytic cells. Our data also showed that the deletion of the NTR also compromised the binding ability toward the target cells to a prominent extent. Mutations of the aromatic/hydrophobic residues within the NTR also led to the compromised membrane-damaging cytolytic/cytotoxic activity of TDH. More interestingly, restraining of the structural/conformational flexibility of the NTR of TDH, via engineered disulfide locking

of the NTR against the β-sandwich domain, also disrupted the functionality of the toxin. Overall, these data showed that the NTR of TDH, with its intrinsically disordered structural/conformational flexibility, plays a critical role in the membrane-damaging cytolytic/cytotoxic activity of the toxin.

Publication:

Kundu, N., Tichkule, S., Pandit, S. B., & Chattopadhyay, K. (2017). Disulphide bond restrains the C-terminal region of thermostable direct hemolysin during folding to promote oligomerization. *Biochemical Journal*, *474*(2), 317-331.

References:

1. Davidson, J., *Selective permeability and the plasmamembrane.* The Plant World, 1916. **19**(11): p. 331-349.
2. Ek-Vitorin, J.F. and J.M. Burt, *Structural basis for the selective permeability of channels made of communicating junction proteins.* Biochimica et Biophysica Acta (BBA)-Biomembranes, 2013. **1828**(1): p. 51-68.
3. Iacovache, I., F.G. van der Goot, and L. Pernot, *Pore formation: an ancient yet complex form of attack.* Biochimica et Biophysica Acta (BBA)-Biomembranes, 2008. **1778**(7-8): p. 1611-1623.
4. Valeva, A., et al., *Evidence that clustered phosphocholine head groups serve as sites for binding and assembly of an oligomeric protein pore.* Journal of Biological Chemistry, 2006. **281**(36): p. 26014-26021.
5. Gonzalez, M., et al., *Bacterial pore-forming toxins: the (w) hole story?* Cellular and molecular life sciences, 2008. **65**(3): p. 493-507.
6. Parker, M.W. and S.C. Feil, *Pore-forming protein toxins: from structure to function.* Progress in biophysics and molecular biology, 2005. **88**(1): p. 91-142.
7. Honda, T. and T. Iida, *The pathogenicity of Vibrio parahaemolyticus and the role of the thermostable direct haemolysin and related haemolysins.* Reviews in Medical Microbiology, 1993. **4**(2): p. 106-113.

8. Shirai, H., et al., *Molecular epidemiologic evidence for association of thermostable direct hemolysin (TDH) and TDH-related hemolysin of Vibrio parahaemolyticus with gastroenteritis.* Infection and immunity, 1990. **58**(11): p. 3568-3573.
9. Kundu, N., et al., *Disulphide bond restrains the C-terminal region of thermostable direct hemolysin during folding to promote oligomerization.* Biochemical Journal, 2017. **474**(2): p. 317-331.
10. Honda, T., et al., *The thermostable direct hemolysin of Vibrio parahaemolyticus is a pore-forming toxin.* Canadian journal of microbiology, 1992. **38**(11): p. 1175-1180.
11. Hamada, D., et al., *Tetrameric structure of thermostable direct hemolysin from Vibrio parahaemolyticus revealed by ultracentrifugation, small-angle X-ray scattering and electron microscopy.* Journal of molecular biology, 2007. **365**(1): p. 187-195.
12. Yanagihara, I., et al., *Structure and functional characterization of Vibrio parahaemolyticus thermostable direct hemolysin.* Journal of Biological Chemistry, 2010. **285**(21): p. 16267-16274.
13. Athanasiadis, A., et al., *Crystal structure of the soluble form of equinatoxin II, a pore-forming toxin from the sea anemone Actinia equina.* Structure, 2001. **9**(4): p. 341-346.
14. Mancheno, J.M., et al., *Crystal and electron microscopy structures of sticholysin II actinoporin reveal insights into the mechanism of membrane pore formation.* Structure, 2003. **11**(11): p. 1319-1328.
15. Tanaka, K., et al., *Structural basis for self-assembly of a cytolytic pore lined by protein and lipid.* Nature communications, 2015. **6**: p. 6337.